STUDIES ON THE SURFACE PROPERTIES AND CATALYTIC ACTIVITY OF METAL CHROMITES ON THERMAL DECOMPOSITION OF AMMONIUM PERCHLORATE

Thesis submitted to the

Cochin University of Science and Technology

in partial fulfillment of the requirements for the degree of

DOCTOR OF PHILOSOPHY

(in Chemistry)

Under The Faculty of Science

by

BOLIE THERATTIL

Department of Applied Chemistry

Cochin University of Science and Technology

Cochin-682 022, Kerala, India.

May 2010

Studies on the Surface Properties and Catalytic Activity of Metal Chromites on Thermal Decomposition of Ammonium Perchlorate

Ph.D Thesis in the field of Catalysis

Author:

Bolie Therattil

Research Fellow
Department of Applied Chemistry
Cochin University of Science and Technology
Kochi, Kerala, India-682022
email: btherattil@cusat.ac.in,therattilbolie@gmail.com

Research Advisor:

Dr.S.Sugunan

Professor in Physical Chemistry
Department of Applied Chemistry
Cochin University of Science and Technology
Kochi, Kerala, India-682022
email: ssg@cusat.ac.in

Department of Applied Chemistry

Cochin University of Science and Technology

Kochi, Kerala, India-682022

May 2010

CERTIFICATE

This is to certify that the thesis herewith is an authentic record of research work carried out by Ms. Bolie Therattil under my supervision, in partial fulfillment of the requirements for the degree of Doctor of Philosophy of Cochin University of Science and Technology, and further that no part thereof has been presented before for any other degree.

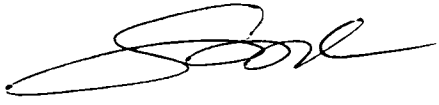

Kochi-682022
12-05-2010

Dr.S.Sugunan
(Supervising Guide)
Professor in Physical Chemistry
Department of Applied Chemistry
Cochin University of Science and Technology
Kochin-682022

DECLARATION

I hereby declare that the thesis entitled **"Studies on the Surface Properties and Catalytic Activity of Metal Chromites on Thermal Decomposition of Ammonium Perchlorate"** is the bonafide report of the original work carried out by me under the supervision of Dr. S. Sugunan at the Department of Applied Chemistry, Cochin University of Science and Technology, and no part thereof has been included in any other thesis submitted previously for the award of any degree.

12-05-2010 Bolie Therattil

Cochin-22

Acknowledgement

I express my deep gratitude and respects to my guide Prof. (Dr.) S. Sugunan, Department of Applied Chemistry for his keen interest, valuable guidance, strong motivation and constant encouragement during the course of my work. I thank him for his constructive criticism and useful suggestions apart from invaluable guidance given to me. He boosted me to explore this vast topic in an organized manner and provided me with all the ideas of research-oriented venture.

I am grateful to Prof. (Dr.). K. Girish Kumar, Head, Department of Applied Chemistry and to Prof. (Dr.). M.R. Prathapachandra. Kurup, former Head of the Department, for providing me the necessary facilities.

I am indebted to Dr. B. Viswanathan, Head, National Centre for Catalysis (NCCR) IIT Madras for the interesting discussions, motivation and inspiration that triggered me for this thesis work. I am thankful to Dr .B. Sreedhar, (Scientist IICT Hyderabad), friends of IISc Bangalore and NCL Pune for TEM-SAED, TG-MS, XPS, SEM, and XRF studies. I am grateful to former Head of Chemistry Department, Kerala University Prof. (Dr.). P. Indrasenan and his crew for initial TG-DTG analysis and for kinetic simulations. I extend my special thanks to my friends in STIC, CUSAT for their timely help in providing analysis results.

I take this opportunity to thank all the teaching and non-teaching staff of the Department of Applied Chemistry for their help and goodwill on all occasions. I take this opportunity to convey my hearty admiration to all my teachers from my school days to post graduation level.

All my lab buddies at the Physical Chemistry Laboratory made it a convivial place to work. I am deeply indebted and profoundly grateful to Dr. Ramanathan, who has been my senior, for his immense assistance and valuable suggestion during the initial stages of my research work. In particular, I would like to thank Reshmi for her friendship and help in the past four years. All other folks had inspired me in research and life through our interactions during the long hours in the lab. I also thank all my friends in the department and in CUSAT for their help and support in one way or other, which made my work much easier.

Many other people provided valuable remarks, invited me to give presentations, or asked me to join program committees or otherwise help to organize workshops and conferences. Among these are Dr.V.R.Nair, Dr.K.K.A.Rashid, Dr.P.Unnikrsihnan and Dr.V.Babu.

My deepest gratitude goes to my family for their unflagging love and support throughout my life; this dissertation is simply impossible without them. I am indebted to my father, for his care and love. I cannot ask for more from my mother, as she is simply perfect. I have no suitable word that can fully describe her everlasting love to me. I feel proud of my brother, for his talents. He had been a role model for me to follow unconsciously and has always been one of my best counselors. Words fail me to express my appreciation to my husband Mr. Joseph Thomas whose dedication, love and persistent confidence in me, has taken the load off my shoulder.

Be assured that those that were not mentioned are not the lesser, because amongst them is also the greatest.

The financial support granted by CSIR, New Delhi is gratefully acknowledged.

Last but not least, thanks are to God for my life through all tests in the past four years. You have made my life more bountiful. May your name be exalted, honored, and glorified.

Bolie Therattil

PREFACE

In recent years considerable advances have been achieved in the study of the surface structure and mechanism of action of heterogeneous catalysts. Results of catalytic studies are nowadays playing a more and more important role in design of new industrial catalysts, catalytic processes and in the optimization of existing industrial catalytic processes. Spinel chromites are known for a long time now as a kind of versatile functional materials due to their wide commercial application as catalysts for chemical reactions of hydrogenation, dehydrogenation, oxidation, alkylation, and so on. In addition to the aforementioned various commercial applications, the Cu-Cr-O composites have in recent years find great promising application as burning rate catalysts (ballistic modifier) for solid propellants used in defense (ballistic missiles) and space vehicles (rocket propellants). In spite of this development in the technology of spinel chromites, the scientists now prefer to examine the structure, transport studies and catalytic activities of these materials in a methodological mode to evolve the correlations between them.

This thesis is the final work of my Ph.D. study at the Department of Applied Chemistry, Cochin University of Science and Technology. It serves as documentation of my work during the study, which has been made from 2006 until 2010. The Council of Scientific and Industrial have funded the study. Solely the authors have made the thesis; most of the text, however, is based on the research of others, and we have done our best to provide references to these sources.

The thesis consists of six chapters. First chapter comprised of a thorough literature survey on spinels, their preparation, thermal analysis,

thermal decomposition and kinetics of ammonium perchlorate. The objectives of the present investigation are also described at the end of this chapter. The experimental procedures and the techniques employed in this investigation are described in second chapter. Third chapter presents the results and discussion regarding the characterization. Results of activity studies towards thermal decomposition of ammonium perchlorate and the kinetics of thermal decomposition of ammonium perchlorate were presented in the subsequent two chapters. The last chapter comprehends the summary and conclusion of the results observed in the previous chapters.

CONTENTS

CHAPTER 1

INTRODUCTION AND LITERATURE SURVEY

Abstract

Catalysis is a fascinating science for those who are actively involved in it, but perhaps even more so for those who know only a little about it. Chemical reactions, for which one would expect half-life times as long as centuries, can be accomplished in minutes to hours with the magic power of a mysterious black box containing a catalyst. Catalysis is of crucial importance for the chemical industry, the number of catalysts applied in industry is very large and catalysts come in many different forms, from heterogeneous catalysts in the form of porous solids over homogeneous catalysts dissolved in the liquid reaction mixture to biological catalysts in the form of enzymes. Catalysis research is central to the science of modern chemical processing, fuel technologies and environmental control. Heterogeneous catalysis has shaped our past and will shape our future. The increase in the rate of reactions catalyzed by quaternary ammonium salts is often proportional to the concentration of the catalyst used.

1.1 THE PHENOMENON CATALYSIS

The phenomenon of catalysis is so intricately woven into the fabric of chemistry, and the recognition of its nature and importance is so intimately associated with the pioneering of the founders of modern chemistry and physics – Berzelius, Davy, Faraday, Nernst, Kirchhoff and Ostwald [1]. The term "catalysis" was introduced as early as 1836 by Berzelius in order to explain various decomposition and transformation reactions. He concluded that besides 'affinity' a new force is operative, the 'Catalytic Force'. The word 'catalysis' stems from the Greek: it has the sense of 'down' and 'loosen'. A definition that is still valid today is due to Ostwald (1895): "a catalyst accelerates a chemical reaction without affecting the position of the equilibrium" [2]. Catalysis is a multidisciplinary science. It is a combination of fundamental and applied science with major contributions from chemistry, physics and material science. The importance of catalysis in the chemical industry is shown by the fact that 90 % of all chemicals are produced with the aid of catalysts; in newly developed processes. Its technological importance lies in the tremendous achievements of this science to give humanity some cheap, highly convenient and outstanding materials [3]. Catalysis - as a tool for carrying out reactions-had already been exploited much earlier. It has been applied for thousands of years in processes such as fermentation [4-9].

Catalysts come in a multitude of forms, varying from atoms and molecules to large structures such as zeolites or enzymes. The main classes of materials employed as catalysts are metals (generally transition and noble metals),

oxides (including transition-metal oxides), transition-metal sulfides and zeolites. Oxides commonly studied as catalytic materials belong to the structural classes of corundum, rocksalt, wurtzite, spinel, perovskite, rutile, and layer structure. In addition they may be employed in various surroundings: in liquids, gases or at the surface of solids [5].

It is customary to distinguish the following three sub-disciplines in catalysis: homogeneous, heterogeneous and bio catalysis. In homogeneous catalysis, both the catalyst and the reactants are in the same phase, i.e. all are molecules in the gas phase, or, more commonly, in the liquid phase. Heterogeneous catalysis covers all the cases where the catalyst and the substrate are in different phases. Biocatalysis is a rather special case, somewhere between homogeneous and heterogeneous catalysis. In most cases, the biocatalyst is an enzyme – a complex protein that catalyzes the reactions in living cells [10].

1.2 SPINELS

Spinels have a general formula AB_2O_4 and in the unit cell there are 32 oxygen ions with eight of the 64 tetrahedral and 16 of the 32 octahedral sites occupied. When the A ions are all housed by the tetrahedral sites and all the B ions are in the octahedral ones we talk of 'normal spinels'. However, in certain other spinels, the eight tetrahedral positions are occupied, not by the eight A, but by one-half of the B ions, the rest of which, together with the A ions, are arranged at random in the 16 octahedral positions. These inverse spinels are

therefore formulated B (AB) O_4. In 'intermediate' or 'random' spinels both the divalent and trivalent ions are randomly distributed in tetrahedral and octahedral sites [11-12]. It is convenient to describe different modes of distribution by a parameter η, which gives the fraction of divalent metal ions in octahedral sites. Thus, for the normal spinel η=0; for the inverse spinel η =1; and for randomly distributed situation η =0.67 [1].

There are several ways in which defective spinels can arise, the most common being those in which, by appropriate change of cation valence, vacancies occur in the cation sublattices, both tetrahedral and octahedral. Replacement of the ions present in the original (normal or inverse) spinel by foreign ions can be effected, thereby offering abundant scope for the design of multi-component, spinel-based catalysts.

1.3 SPINELS AS CATALYTS

The ample diversity of properties that the spinel compounds exhibit is derived from the fact that the possibility of synthesis of multicomponent spinels by partial substitution of cations in position A and B giving rise to compounds of formula $(A_xA'_{1-x})(ByB'_{2-y})$ O_4. This accounts for the variety of reactions in which they have been used as catalyst. Moreover, partial substitution of A and B ions giving rise to complex oxides is possible while keeping the spinel structure.

Chromites, which are molecular compounds with the ACr_2O_4 formula, have a normal type spinel structure [13, 14], i.e., the tetrahedra of oxygen atoms surround divalent metal ions and the octahedra of oxygen surround chromium ions [15]. Chromites are considered as a significant spinel system with numerous potential applications. One particular chromite, iron chromite ($FeCr_2O_4$), is known to occur due to different industrial processes.

$CuCr_2O_4$, which undergoes a phase transition at 853 K, is a p-type semiconductor in which conduction takes place by the hopping of charge carriers between the octahedral site cations and shows considerable changes in its electrical transport properties near the tetragonal 3 cubic phase transition temperature. Copper chromites, has wide commercial application as catalyst for chemical reactions such as hydrogenation, dehydrogenation, oxidation, alkylation, etc. Multimetallic oxide structures may also be multifunctional. In addition to versatile commercial applications as a catalyst, copper chromite finds application as a ballistic modifier [16] for solid propellants used in defense (ballistic missiles) and space vehicles (rocket propellants). Therefore, copper chromite is an important material of great demand.

1.4 PREPARATION OF SOLID CATALYSTS: BLACK MAGIC REVEALED

The complex and diverse synthesis protocols of solid catalysts sometimes give the impression of alchemy, instead of 21st-century chemistry. The final catalytic properties depend strongly on every step of the preparation, as well as

on the purity (and impurity) of the starting materials. Small changes in drying temperatures, aging times, solvent compositions, or stirring rates can affect the catalyst performance [1]. Methods of catalyst preparation are very diverse and each catalyst may be produced via different routes [17].

Generally, the catalysts may be classified according to the preparation procedure as: (i) bulk catalysts or supports and (ii) impregnated catalysts. On this basis the relative preparation methods are: (i) the catalytic active phase is generated as a new solid phase and (ii) the active phase is introduced or fixed on a pre-existing solid by a process which intrinsically depends on the support surface [18].

Several techniques such as sol–gel [19], self-propagating combustion [20], precipitation [21-32] and emulsion drying [33] have been adopted for the synthesis of nano-crystalline materials. Among these, self-propagating combustion synthesis is the most widely used method. Nevertheless, this method has the drawback of producing highly agglomerated particles. To remove this drawback, a low-temperature Pechini method [34] has been introduced and yields a phase-pure product with controlled stoichiometricy. In the Pechini method, a mixture of hydroxycarboxylic acid (citric acid) and hydroxyl alcohol (ethylene glycol) is used, in which citric acid plays the role of distributing the cations atomistically throughout the polymeric structure. All these steps are tedious and must be performed carefully. The process includes the removal of excess of ethylene glycol under reduced pressure to cause polymerization.

Hence, this investigation, reports a sol–gel thermolysis method (an alternative method where only hydroxyl alcohol was used without the aid of hrdroxycarboxylic acid) that is quite suitable for the larger-scale synthesis of well-dispersed nano-crystalline metal oxide powder of high purity. This sol–gel thermolysis is a novel and unique combination of a thermal process and a chemical gelation process. In this hydroxyl alcohol-assisted method, hydroxyl alcohol (poly vinyl alcohol – PVA) just dissolves in water and wraps the cations to form sols, instead of being dissociated in water [35]. Therefore, the sol-gel mechanism is essentially different from the sol-gel processes. PVA helps the homogeneous distribution of the metal ions in its polymeric network structure and inhibits their segregation or precipitation from the solution. In PVA-assisted sol-gel method that the hydroxyl polar ligands on the long chains of PVA can adsorb the metal ions in the solution and partially prevent them from meeting with each other. When the optimal amount of PVA is added, PVA plays a role of wrapping and covering the metal ions will not grow in size and will not be precipitated, resulting in the formation of a cocoon-like structure in the PVA's polymeric structure. If the amount of PVA added is too large, the metal ions may be covered by several layers of the polymer and the dehydration process becomes difficult because of the wrapping of water by PVA. This cocoon-like structure could inhibit precipitation of the metal ions from the solution. The molecular weight of PVA affected the precipitation of the metal ions because when the molecular chains of the polymer were too short, the metal ions could not be completely covered by the polymer. The organic polymer(s) not only acts as an excellent fuel, but also controls the size during the formation of the sol–gel and prevents the particles from aggregating

during the thermolysis of dry gel due to its long chain structure. The method investigated has may; however, provide a wider scope for tailorability, and for precise control of the particle-size and morphology of nano-crystalline powders [36].

1.5 THERMAL ANALYSIS

The following formal definition of Thermal Analysis was originally provided by the International Conferedaration for Thermal Analysis and Calorimetry (ICTAC). Thermal Analysis (TA) refers to a group of techniques in which a property of a sample is monitored against time or temperature in while the temperature of the sample, in a specified atmosphere, is programmed. A recent discussion of the above ICTAC definition by Hemminger and Serge [37,38] points out some of the difficulties and suggests some modification to: Thermal Analysis (TA) means the analysis of a change in a property of a sample, which is related to an imposed temperature alteration.

1.5.2 REACTIONS OF SOLIDS

As a solid is heated, the amplitude of the vibrations of the lattice constituents are increased and eventually a temperature will be reached where one (or more) of the following changes will occur, (i) Phase transition: a new arrangement of constituents may become more stable than the original [39,40], (ii) Melting: When sufficient energy becomes available, the forces of attraction

between constituents become insufficient to maintain the ordered arrangement of the solid and the system relaxes to the more disordered arrangement of constituents in a liquid [41], (iii) Sublimation: When the kinetic energy of the constituents increases rapidly, direct transition to the disordered arrangement of a gas may occur, without the intermediate formation of a liquid phase, (iv) Thermal decomposition: When the bonding forces within constituent molecules or ions are weaker than those between the atoms constituting these units, increasing the temperature may result in bond redistribution and the formation of products chemically different from the reactant. Such chemical processes are referred to as thermal decomposition (or crystolysis) [42].

1.5.2 THERMAL DECOMPOSITION OF AMMONIUM PERCHLORATE

The number of works on various aspects of the kinetics and mechanism of the thermal decomposition of ammonium perchlorate (AP) exceeds the number of studies of the thermal decomposition of all other onium salts. This is because: (i) AP is the main oxidizer in solid rocket propellants (ii) AP is a convenient model for decomposition studies of ionic solids [43].

Ammonium perchlorate (AP) is a white crystalline solid which undergoes a reversible crystallographic transition from the low-temperature orthorhombic structure to a cubic structure around 240° [44, 45]. This polymorphic change is attributable to the onset of free rotation of the perchlorate anions [46]. The

phase transition is endothermic and is accompanied by a significant amount of decomposition with concomitant heat generation.

AP is stable at room temperature but decomposes at measurable rates at temperatures greater than about 150°C. At decomposition temperatures below approximately 300°C, AP undergoes an autocatalytic reaction, which ceases after about 30% decomposition. This is usually called the low-temperature reaction. The residue is quite stable at these temperatures unless rejuvenated by sublimation, recrystallization, or mechanical disturbance [47-52]. At temperatures above 350°C, the high-temperature decomposition occurs; this reaction is not autocatalytic and decomposition is complete. Concurrently with these decomposition reactions, AP also undergoes dissociative sublimation [47, 49, 50].

1.6 THERMOGRAVIMETRIC ANALYSIS

The thermal analysis technique of thermogravimetry (TG) is one in which the change in sample mass is recorded as a function of temperature. Three modes of TG may be described: (a) *isothermal or static thermogravimetry*, in which the sample is recorded as a function of time at constant temperature; (b) *quasistatic thermogravimetry*, in which the sample is heated to constant mass at each of a series of increasing temperatures; and (c) *dynamic thermogravimetry*, in which the sample is heated in an environment whose temperature is changing in a predetermined manner, preferably at a linear rate [53].

1.7 DIFFERENTIAL THERMAL ANALYSIS

Differential thermal analysis (DTA) is a thermal technique of recording the difference in temperature between a substance and a reference material as the two specimens are subjected to identical temperature regims in an environment heated or cooled at a controlled rate. The record obtained is called the differential thermal or DTA curve and, provided the substance is thermally active in the temperature range used, shows a series of peaks, the position of which is determined by the chemical composition and crystal structure of the substance and the area of which is related to the energy involved in the reaction occurring [54]. Temperature changes in the sample are due to endothermic or exothermic enthalpic transitions or reactions. Generally speaking, phase transitions, dehydration, reduction, and some decomposition reactions produce endothermic effects, whereas crystallization, oxidation, and some decomposition reactions produce exothermic effects.

1.8 KINETICS OF SOLID STATE REACTION

One of the major reasons for carrying out kinetic studies is to investigate reaction mechanisms. One of the fundamental tenets of chemical kinetics is that no reaction mechanism can ever be proved on the basis of kinetic data alone; at best, one may demonstrate that a proposed mechanism is consistent with the kinetic data. Furthermore, kinetic analysis may not be the most efficient means of determining a reaction mechanism [55]; however, it is extremely useful for drawing reasonable mechanistic conclusions [56,57]. The

most common experimental techniques employed to study kinetics of thermally activated reactions are thermogravimetry (TG), differential scanning calorimetry (DSC), and differential thermal analysis (DTA). These techniques are widely applicable to many types of reactions but are not chemically specific in their means of detection. These techniques are universally applicable to kinetic analysis because all reactions involve changes in enthalpy. However, the techniques by themselves do not provide any information about the nature of the reaction. For this reason, thermal analysis techniques are sometimes combined with chemically specific detection methods such as Fourier transform infrared (FTIR) spectroscopy, mass spectrometry (MS), and gas chromatography (GC) to analyze gaseous products. X-ray diffractometry (XRD) as well as FTIR and electron paramagnetic resonance (EPR) spectroscopy are also used as complementary techniques to analyze solid reaction products. Whereas TG, DSC, and DTA can provide important measures of the overall (global) kinetics of thermally stimulated reactions, the aforementioned complementary techniques permit a deeper insight into the mechanism of solid state reactions. The data obtained by the chemically specific techniques are sometimes subjected to kinetic analysis, the results of which are helpful in elucidating the overall kinetic scheme [58-61].

The kinetics of thermally stimulated reactions is normally studied under the conditions of isothermal and/or non-isothermal (usually linear) heating. A major problem of the isothermal experiment is that a sample requires some time to reach the experimental temperature. During this period of non-isothermal heating, the sample undergoes some transformations that are likely

to affect the results of the following kinetic analysis. The situation is especially aggravated by the fact that under isothermal conditions, a typical solid-state process has its maximum reaction rate at the beginning of the transformation. This especially restricts the use of high temperatures. Non-isothermal heating resolves these problems and has therefore become more popular in the field of solid-state kinetics than the classic isothermal experiment. However, the advantages of the non-isothermal experimental technique are at least partially offset by serious computational difficulties associated with the kinetic analysis.

1.9 COATS-REDFERN METHOD

In the past few decades, determination of the mechanism function and calculation of the kinetic parameters from non-isothermal TG, DTA and DSC data have been subjects of considerable interest. Consequently, a considerable number of methods have been suggested whereby kinetic parameters can be evaluated from the data of non-isothermal experiments.

In 1964, Coats and Redfern presented an integral method [62], which has since become one of the most widely used methods in non-isothermal kinetic analysis.

This method is an integral method that assumes various orders of reaction and compares the linearity in each case to select the correct order [63]. The equations are given below.

By plotting the appropriate left-hand side of the below equations versus 1/T, the slope equals (-E/2.303R).

$$\log\left[\frac{1-(1-\alpha)^{1-n}}{T^2(1-n)}\right] = \log\frac{AR}{\beta E}\left[1-\frac{2RT}{E}\right] - \frac{E}{2.303RT} \qquad for \quad n \neq 1$$

$$\log\left[\frac{-\log(1-\alpha)}{T^2}\right] = \log\frac{AR}{\beta E}\left[1-\frac{2RT}{E}\right] - \frac{E}{2.303RT} \qquad for \quad n = 1$$

E and A values can be calculated from these equations.

1.10 OBJECTIVES OF THE PRESENT WORK

The main objectives of the present work can be summarized as follows:

- Preparation of a series of spinel systems with composition $CuCr_{2-x}Fe_xO_4$ (x=0.5,1.0,1.5,2.0) and $Cu_{1-x}M_xCr_2O_4$ (M is a transition metal cation like Ni, Co, Mn and x=0,0.25,0.5,0.75 and 1.0) by sol gel thermolysis route.

- Characterization of the systems by physicochemical and spectroscopic methods such as XRD, XRF, SEM, Surface area (by N_2 adsorption), TG-DTA, TPD, XPS, TEM etc.

- Most important were the evaluation of the catalytic activity and various parameter effects of the systems for thermal decomposition of ammonium perchlorate by TG-DTA, TG-MS and post characterization of the spent catalysts by XRD and SEM.

- To perform kinetic analysis using Coats-Redfern non-isothermal method to get kinetic triplets.

- To propose the mechanism of thermal decomposition of uncatalyzed and catalyzed ammonium perchlorate.

REFERENCES

[1] J.M. Thomas and W.J. Thomas, "Principles and Practice of Heterogeneous Catalysis", VCH Verlagsgesellschaft mbH, Weinheim, (1997) p.1

[2] Jens Hagen, "Industrial Catalysis: A Practical Approach", WILEY- VCH Verlag GmbH & Co. KGaA, Weinheim (2006).

[3] P.L. Gai, E.D. Boyes, "Electron Microscopy in Heterogeneous Catalysis", IOP Publishing Ltd.(2003),London

[4] R. A. Santen, J. A. Moulijn, van Leeuwen Piet W. N , B. A. Averill, "Catalysis: An Integrated Approach", 2nd Edition, Elsevier Science & Technology Books (1999).

[5] I. Chorkendorff, J.W. Niemantsverdriet, "Concepts of Modern Catalysis and Kinetics" WILEY-VCH Verlag GmbH & Co.KGaA,Weinheim (2003).

[6] Gabor.A.Somorjai, "Introduction to Surface Chemistry and Catalysis", John Wiley & Sons, Inc.(1994).

[7] István T. Horváth, "Encyclopaedia of Catalysis, Volume 1", John Wiley & Sons,Inc.(2003)

[8] B. Cornils, Wolfgang A. Hermann, Robert Schlogl, Chi-Huey Wang, "Catalysis from A to Z:- A Concise Encyclopedia" (2000) 902

[9] G.C. Bond, "Heterogeneous Catalysis: Principles and Applications", Clarendon Press, Oxford (1987).

[10] Gadi Rothenberg, "Catalysis Concepts and Green Applications", WILEY-VCH Verlag GmbH & Co.KGaA,Weinheim (2008).

[11] Romeijn, F.C., 1953, *Philips Reserve Report*, Vol. 8, pp. 304.

[12] Miyahara, S., and Ohnishi, H., 1956, *Journal of the Physical Society of Japan*, Vol.11, pp. 1296.

[13] Sawaoka, A., Saito, S., Inoue, K., and Asada, T., 1971, "Effect of High Pressure on the Lattice Constants of Chromites Having The Spinel Structure," *Material Review Bulletin*, Vol. 6, No. 2, pp. 97-102.

[14] R. Rao, A. Dandekar, R.T.K. Baker, M.A. Vannice, J. Catal. 171 (1997) 406.

[15] G.S. Pearson, Combust. Flame 14 (1970) 73.

[16] P. W. M. Jacobs and H. M. Whitehead. *Chem. Rev.* 69, 551 (1969).

[17] R.K. Datta and K. Roy, *Nature*, 191(1961)169.

[18] S. Hafner and F. Laves,*Z.Krist.*,115(1961)321.

[19] J. Haber, J.H. Block and B. Delmon, *Pure & Appl. Chem.*, Vol. 67, Nos 8/9, pp. 1257-1306, 1995.

[20] M. Campanati, G. Fornasari and A. Vaccari, *Catalysis Today* 77(2003)301.

[21] B.J. Hwang, R. Santhanam, D.G. Liu, J. Power Sources 101 (2001) 86.

[22] D. Kovacheva, H. Gadjov, K. Petrov, S. Mandel, J. Mater. Chem. 12 (2002)1184.

[23] K.M. Shaju, G.V. Subba Rao, B.V.R. Chowdari, J. Electrochim. Acta 48 (2002) 145.

[24] Ph. Courty, Ch. Marcilly, in: G. Poncelet, P. Grange, P.A. Jacobs (Eds.), Preparation of Catalysts III, Studies in Surface Science and Catalysis, vol. 16, Elsevier, Amsterdam, 1983, p. 485.

[25] C. Perego, P.L. Villa, Catal. Today 34 (1997) 281

[26] A. Vaccari, Catal. Today 41 (1998) 53.

[27] J.-F. Le Page, J. Cosyns, P. Courty, E. Freund, J.-P. Franck, Y. Jacquin, B. Juguin, C. Marcilly, G. Martino, J. Miquel, R. Montarnal, A. Sugier, H. Van Landeghem, Applied Heterogeneous Catalysis: Design, Manufacture, Use of Solid Catalysts, Technip, Paris, 1987.

[28] J.T. Richardson, Principles of Catalyst Development, Plenum Press, New York, 1989.

[29] M.V. Twigg (Ed.), Catalyst Handbook, 2nd ed., Wolfe, London, 1989.

[30] F. Schüth, K. Unger, in: G. Ertl, H. Knözinger, J. Weitkamp (Eds.), Handbook of Heterogeneous Catalysis, vol. 1, Wiley/VCH, New York/Weinheim, 1997, p. 72.

[31] F. Cavani, F. Trifirò, A. Vaccari, Catal. Today 11 (1991) 173.

[32] F. Trifirò, A. Vaccari, in: J.L. Atwood, J.E.D. Davies, D.D. MacNicol, F. Vögtle (Eds.), Comprehensive Supramolecular Chemistry, vol. 7, Pergamon Press, Oxford, 1996, p. 251.

[33] S.J. Yoon, S.H. Lee, K.H. Kim, K.S. Ahn, *Mater.Chem.Phys.*73(2002)330.

[34] Z.Wang ,S.K.Saxena,P.Lazor,H.S.C.O Neil , J. Phys. Chem. Solids 64 (2003) 425.

[35] Yang-Kook Sun, In-Hwan Oh, *Ind.Eng.Chem.Res.*,35 (1996),4296.

[36] S.T. Myung, H.T. Chung, S. Komaba, N. Kumagai, H.-B. Gu, *J. Power Sources* 90 (2003) 103.

[37] W. Liu, G.C. Farrington, F. Chaput, B. Dunn, *J. Electrochem. Soc.* 143 (1996) 879.

[38] A. Subramania , N. Angayarkanni, T. Vasudevan, *Journal of Power Sources* 158 (2006) 1410–1413

[39] W. Hemminger and S.M. Sarge, "Handbook of Thermal Analysis and Calorimetry", Vol.1,(Ed. M.E. Brown), Elsevier, Amsterdam, 1998,Ch.1.

[40] W. Hemminger, Recommendations of the ICTAC Nomenclature Committee, ICTAC NEWS, December 1998,p.106-122.

[41] C.N.R. Rao and K.J. Rao, "Phase Transitions in Solids", McGraw-Hill, New York, 1978.

[42] J.W. Christian, "Transformations in Metals and Alloys", Pergamon, Oxford, 1965; Vol.1, 2nd Edn. 1975.

[43] A.R. Ubbelobde, "Melting and Crystal Structure", Clarendon, Oxford, 1965; "The Molten State of Matter", Interscience, New York, 1978.

[44] A.K. Galwey and M.E. Brown, "Thermal Decomposition of Ionic Solids", Elsevier, Amsterdam, 1999.

[45] G.B. Manelis, G.M. Nazin, Yu.I. Rubtsov and V.A. Strunin, "Thermal Decomposition and Combustion of Explosives and Propellants", Taylor and Francis, 2003.

[46] W. Hueckel, "Structural Chemistry of Inorganic Compounds", Vol. 11, Elsevier Publishing Co., Amsterdam, 1951, pp 667-670

[47] D. Vorlaender and E. Kaascht, *Ber.,* 56B, 1157 (1923).

[48] C. Finbak and 0. Hassel, *2. Physik. Chem.,* B32, 130.(1936).

[49] L. L. Bircumshaw and B. H. Newman, *Proc. Roy. SOC.* (London), A227,115 (1954).

[50] L. L. Bircumshaw and B. H. Newman, *ibid.,* A227, 228 (1955).

[51] L. L. Bircumshaw and B. H. Newman, "The Thermal Decomposition of Ammonium Perchlorate," ERDE Report No. 8/EMR/50, 1951.

[52] A. K. Galwey and P. W. M. Jacobs, *Proc. Roy. SOC.* (London), A254,455 (1960).

[53] Wesley WM. Wendlandt, "Thermal Methods of Analysis", John Wiley & Sons, Toronto,1974.

[54] R.C.Mackenzie, "Differential Thermal Analysis", Vol.1, Academic Press Inc., London, 1970.

[55] Maciejewski M, Reller A. 1987. *Thermochim. Acta* 110:145–52

[56] Vyazovkin S. 1996. *Int. J. Chem. Kinet.* 28:95–101.

[57] Sviridov VV, Lesnikovich AI, Lecvhik SV, Kovalenko KK, Guslev VG. 1984. *Thermochim. Acta* 77:341–56.

[58] Vyazovkin S, Goryachko V, Bogdanova V, Guslev V. 1993. *Thermochim. Acta* 215:325–28

[59] Ravindran PV, Dhami PS, Rajagopalan KV, Sundaresan M. 1992. *Thermochim. Acta* 197:91–99
[60] Kinoshita R, Teramoto Y, Yoshida H. 1993. *Thermochim. Acta* 222:45–52
[61] Forster KM, Formica JP, Richardson JT, Luss D. 1994. *J. Solid State Chem.* 108:152–57
[62] A. W. Coats and J. P. Redfern, Nature, 201 (1964) 68.
[63] Yalcin Tonbul , Kadir Yurdakoc, *Turk J Chem.*, 25 (2001) , 333 -339

CHAPTER 2

EXPERIMENTAL METHODOLOGY

Abstract

The preparation of catalysts is frequently described as an art, and a catalyst recipe may specify detailed and arcane procedures that appear to be necessary in order to achieve reproducibility and the desired products. The process chosen for the preparation of catalyst represents a balance between the cost of preparation and the degree to which the ideal chemical and physical properties are achieved. Most practical catalysts are highly complex materials, and a basic problem is how to correlate catalyst behaviour with physical and chemical structure. During the past decade several ingenious ways of establishing the compositions, crystallographic structures and electronic properties of the last few layers of adsorbents and catalysts – or sub-monolayer amounts of adsorbed species-have been devised thanks largely to the arrival of new techniques such as photoelectron and Auger spectroscopy, and the extension of more traditional ones such as infrared spectroscopy.

In this chapter, we will encounter different chemicals used; methods of preparation and various techniques adopted for structural characterization of catalysts and discuss its capabilities and limitations.

2.1 INTRODUCTION

The majority of heterogeneous catalysts are highly complex composites, usually poorly characterized and not readily characterizable. A mixture of inspiration, science, technology and empiricism is used in their design and development. Their purpose is to bring about, as rapidly as possible, a desired conversion of the reactants, while minimizing the rates at which these substances undergo other reactions, yet in most cases the mechanisms of the desired and unwanted reactions are understood in broad outline only [1]. Characterization is a central aspect of catalyst development [2, 3]. The elucidation of the structures, compositions, and chemical properties of both the solids used in heterogeneous catalysis and the adsorbates and intermediates present on the surfaces of the catalysts during reaction is vital for a better understanding of the relationship between catalyst properties and catalytic performance. This knowledge is essential to develop more active, selective, and durable catalysts, and also to optimize reaction conditions [4]. In this chapter, we come upon some techniques for characterizing catalysts and discuss their capabilities and limitations. These techniques can be broadly grouped according to the nature of the probes employed for excitation, including photons, electrons, ions, and neutrons, or, alternatively, according to the type of information they provide. Here we have chosen to group the main catalyst characterization techniques by using a combination of both criteria into structural, thermal, optical, and surface-sensitive techniques.

2.2 CHEMICALS FOR CATALYST PREPARATION

The chemicals used for the preparation of catalysts are listed below in Table 2.1.

Table 2.1: Chemicals used for the preparation of catalysts

Sl. No.	Chemicals	Company
1.	$Cr(NO_3)_3.9H_2O$	Merck
2.	$Mn(NO_3)_2.4H_2O$	Merck
3.	$Fe(NO_3)_3.9H_2O$	Merck
4.	$Co(NO_3)_2.6H_2O$	Merck
5.	$Ni(NO_3)_2.6H_2O$	Merck
6.	$Cu(NO_3)_2.3H_2O$	Merck
7.	Polyvinyl alcohol	Merck
8.	Sucrose	Merck
9.	Conc. HNO_3	Merck

2.3 CATALYST PREPARATION

Sol-Gel Thermolysis

A novel sol–gel thermolysis process using sucrose as the fuel for combustion process and PVA as the protecting agent as well as secondary fuel synthesized the nano-crystalline spinel type chromites [5]. In a typical synthesis procedure, stoichiometric amounts of desired metal were dissolved in 100 mL distilled water to obtain a mixed metal nitrate solution. The pH of the mixture was adjusted to 1 by adding nitric acid. Then a mixture of PVA

(polyvinyl alcohol) and sucrose (4 mol per unit mole of metal ion) were added to the previous solution under hot conditions to compose the homogeneous precursor solution and the molar ratio of PVA to the total metal ions was fixed to be 2:1. The molecular weight of the PVA used was 1, 25,000. The PVA – sucrose mixture just wraps the metal ions to form the sol. After stirring for 30 min, the solution was heated with constant stirring at 80°C for 6 hours to evaporate the water solvent to produce dark transparent viscous gels. The gels were then dried at 150°C for 2 h to obtain the foamy dark precursor powders of the corresponding chromites. The metal ions formed clusters with the oxide ions and remained embedded in the resulting matrix of the mesoporous carbonaceous material. After grinding, the precursors were successively heated at 550°C for 5 h in a muffle furnace to eliminate the organic contents and the final polycrystalline chromites were obtained.

Role of sucrose and PVA in the preparation route

Only PVA could fulfil the purpose, but due to its graphitization tendency, it was partially replaced by sucrose [5]. The aqueous sucrose (always in excess) solution in presence of nitric acid is oxidized to saccharic acid. The saccharic acid is a very good chelating agent for metal ions. PVA (10–20 mol %) in presence of saccharic acid at ambient temperature (~200°C) undergoes polycondensation (polyesterification) reaction [6]. A schematic representation of this reaction is shown in Fig. 2.1. During heating at 200°C, polycondensation reaction occurs and most of the water molecules are removed, resulting in a high viscous polymeric resin. The utility of the polymeric approach comes from the chemical bonding (complexation) of the

cations in to the polymeric chains and ensures the atomistic distribution of the cations throughout the polymeric network. Further heat-treatment of the polymeric resin (at 200°C) causes charring. It is assumed that the metal ions are homogeneously distributed into the charred mass and oxidized at low external temperatures (480–600°) to the corresponding nano-crystalline oxides [7].

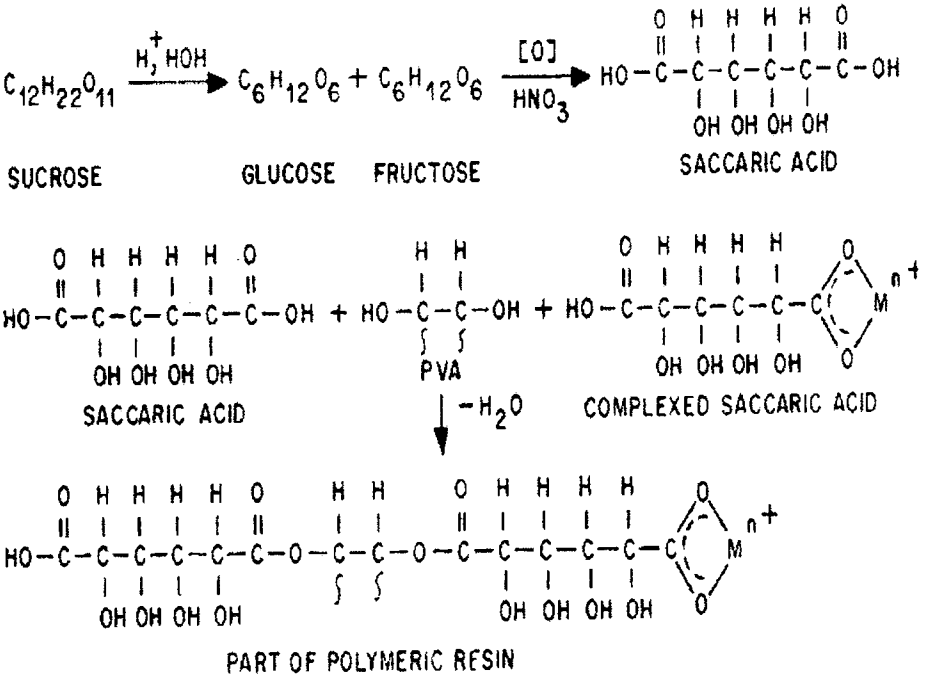

Fig: 2.1 Chemistry of sucrose process

2.4 CATALYSTS PREPARED

The catalysts prepared for the present work with its symbols are listed in Table 2.2.

Table 2.2 Notations of the catalysts prepared

Sl. No.	Catalyst	Symbol
1.	$CuCr_2O_4$	CCr
2.	$Cu_{0.75}Co_{0.25}Cr_2O_4$	CCoCr-1
3.	$Cu_{0.5}Co_{0.5}Cr_2O_4$	CCoCr-2
4.	$Cu_{0.25}Co_{0.75}Cr_2O_4$	CCoCr-3
5.	$CoCr_2O_4$	CoCr
6.	$CuFe_{0.5}Cr_{1.5}O_4$	CFCr-1
7.	$CuFeCrO_4$	CFCr-2
8.	$CuFe_{1.5}Cr_{0.5}O_4$	CFCr-3
9.	$CuFe_2O_4$	CF
10.	$Cu_{0.75}Mn_{0.25}Cr_2O_4$	CMCr-1
11.	$Cu_{0.5}Mn_{0.5}Cr_2O_4$	CMCr-2
12.	$Cu_{0.25}Mn_{0.75}Cr_2O_4$	CMCr-3
13.	$MnCr_2O_4$	MCr
14.	$Cu_{0.75}Ni_{0.25}Cr_2O_4$	CNCr-1
15.	$Cu_{0.5}Ni_{0.5}Cr_2O_4$	CNCr-2
16.	$Cu_{0.25}Ni_{0.75}Cr_2O_4$	CNCr-3
17.	$NiCr_2O_4$	NCr
18.	$FeCr_2O_4$	FCr

2.5 CHARACTERIZATION TECHNIQUES

Catalyst characterization is a lively and highly relevant discipline in catalysis. The ultimate goal of catalyst characterization is to look at the surface

atom by atom, and under reaction conditions. The industrial view on catalyst characterization emphasizes on developing an active, selective, stable and mechanical robust catalyst [8]. Numerous tools are available to explore fundamental relations between the state of a catalyst and its catalytic properties.

Several spectroscopic, microscopic and diffraction techniques are used to investigate catalysts. As Fig. 2.2 illustrates, such techniques are based on some type of excitation (in-going arrows in Fig. 2.2) to which the catalyst responds (symbolized by the outgoing arrows) [9].

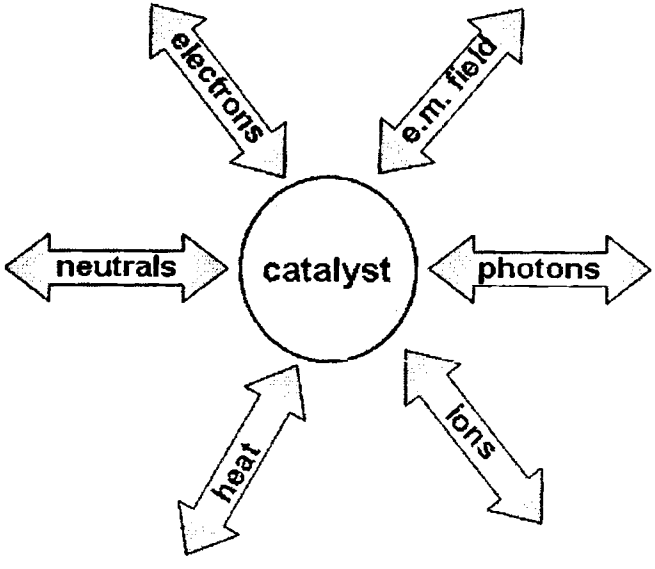

Fig. 2.2. Catalyst characterization techniques: The circle represents the sample under study, the inward arrows denote excitation processes, and the outward arrows indicate how the information should be extracted.

2.6 STRUCTURAL TECHNIQUES

2.6.1 Powder X-ray diffraction

X-ray diffraction is one of the oldest and most frequently applied techniques in catalyst characterization. Powder X-ray diffraction (XRD) is a standard method for the characterization of polycrystalline solids to identify crystalline phases inside catalysts by means of lattice structural parameters, and to obtain an indication of particle size. In catalyst characterization, diffraction patterns are mainly used to identify the crystallographic phases that are present in the catalyst [9]. Monochromatic X-rays, incident on a polycrystalline sample, are diffracted in all possible directions (as governed by the Bragg equation) simultaneously. Each lattice spacing in the crystal gives rise to a cone of diffraction. Each cone is a set of closely spaced dots, where each dot represents diffraction from a single crystallite within the sample. With a large number of crystallites, these join together form a continuous cone [10].

For a maximum to occur in the diffraction pattern at a particular angle of incidence θ (with respect to lattice planes (hkl), the Bragg equation must be satisfied:

$$n\lambda = 2\, d_{hkl} \sin \theta_{hkl}$$

where d_{hkl} -interplanar distance between (hkl) planes, n-order of diffraction and λ = wavelength of incident X-rays

X-ray diffraction can also be used to estimate the average crystallite or grain size of catalysts and become broader for crystallite sizes below about 100

nm. Average particle sizes below about 60 nm can be roughly estimated by applying the Scherrer equation,

$$L = (0.9\lambda\ 180)/(\pi\ \beta_{hkl} \cos\theta)$$

where β_{hkl} is the full width at half-maximum of an *hkl* peak at θ value.

The XRD peaks are intense and sharp only if the sample has sufficient long-range order. The strength of XRD for catalyst characterization is that it gives clear and unequivocal structure information on particles that are sufficiently large, along with an estimate of their size, and it can reveal this information under reaction conditions. The limitation of XRD is that it can not detect particles that are either too small or amorphous. Hence, one can never be sure that there is no other phases present than the ones detected with XRD. In particular, the surface, where catalytic activity resides, is invisible in standard XRD [9].

Powder X-ray diffraction data were recorded using Bruker AXS D8 Advance X-ray Diffractometer Ni filtered Cu Kα radiation source (λ=1.5406Å) by recording θ in the range of 5-80° at a scan rate of 2 °C/min.

2.6.2 Scanning electron microscopy

In scanning electron microscopy (SEM), the yield of either secondary or back-scattered electrons is recorded as a function of the position of the

primary electron beam, and the contrast of the signal used to determine the morphology of the surface: the parts facing the detector appear brighter than those pointing away from the detector [11]. SEM can be used to image over a very large magnification range from 1μm to 100μm, allowing examination of the topology of catalyst surfaces and the morphology of particles and crystals [10,12].

Secondary electron images were obtained on JSM-840 A (Oxford Instruments) scanning electron microscope connected to a 4-quadrant backscattered electron detector under a resolution of 1.38 eV coated with a layer of gold to minimum charge effects.

2.6.3 Energy dispersive X-ray analysis

The elemental analysis of catalysts was determined using energy dispersive X-ray analyzer (EDX). This technique is used in conjunction with SEM. An electron beam strikes the surface of a conducting sample. The energy of the beam is typically in the range 10-20 k eV. This causes X-rays to be emitted from the point of the material. The energy of the X-rays emitted depends on the material under examination. The X-rays are generated in a region about 2 microns in depth. By moving the electron beam across the material an image of each element in the sample can be acquired. The detector used in EDX is the Lithium drifted Silicon detector. This detector must be operated at liquid nitrogen temperature. When an X-ray strikes the detector, it will generate a photoelectron within the body of the Si, as this photoelectron travels through the Si, it generates electron-hole pairs. The electrons and holes

are attracted to opposite ends of the detector with the aid of a strong electric field. The size of the current pulse thus generated depends on the number of electron-hole pairs created, which in turn depends on the energy of the incoming X-ray. Thus, an X-ray spectrum can be acquired giving information on the elemental composition of the material under examination. A Beryllium window often protects the Si-Li detector. The absorption of the soft X-rays by Be precludes the detection of elements below an atomic number of 11 (Na). In windowless systems, elements with as low atomic number as 4 (Be) have been detected, but the problems involved get progressively worse as the atomic number is reduced [13]. The chemical compositions of catalysts were obtained from Stereoscan 440 Cambridge, UK energy dispersive X-ray analyzer used in conjunction with SEM.

2.6.4 Transmission Electron Microscopy

The current literature on TEM in catalysis is vast, and forms a rich source of inspiration for many investigators in the field [14-18]. The transmission electron microscope (TEM) has become the premier tool for the microstructural characterization of materials [19]. Transmission electron microscopy (TEM) resembles optical microscopy, except that electromagnetic instead of optical lenses are used to focus an electron beam on the sample. In TEM, a primary electron beam of high energy and high intensity passes through a condenser to produce parallel rays, which impinge on the sample. As the attenuation of the beam depends on the density and the thickness, the transmitted electrons form a two-dimensional projection of the sample mass,

which is subsequently magnified by the electron optics to produce a so-called bright-field image. The dark-field image is obtained from the diffracted electron beams, which are slightly off-angle from the transmitted beam. Very useful results often follow from simple bright field and dark field images without detailed interpretation of image contrast [1]. A combination of topographic and crystallographic information, including particle size distributions, can be obtained in this way. TEM belongs to the most often-used techniques for the characterization of catalysts. The determination of particle sizes or of distributions therein has become a matter of routine, although the results rest of course on the assumption that the size of the imaged particle is truly proportional to the size of the actual particle, and that the detection probability is the same for all particles, independent of their dimensions [8].

A great advantage of the transmission electron microscope is in the capability to observe, by adjusting the electron lenses, both electron microscope images (information in real space) and diffraction patterns (information in reciprocal space) for the same region. By inserting a selected area aperture and using the parallel incident beam illumination, we get a diffraction pattern from a specific area as small as 100 nm in diameter. Because a selected area diffraction pattern can be recorded from almost every grain in a polycrystalline material, reciprocal lattices (=crystal structures) and mutual crystal orientation relationships can be easily obtained [20].

To study the surface morphology, particle size, and selected area electron diffraction (SAED) of the sol-gel thermolysed samples, transmission

electron microscopy (TEM) (model Phillips Technai-12, FEI, Netherlands) was employed with acceleration voltage 120 kV in bright field mode.

2.6.5 X-ray Fluorescence Analysis

X-ray fluorescence (XRF) analysis is a powerful analytical tool for the spectrochemical determination of almost all the elements present in a sample. XRF radiation is induced when photons of sufficiently high energy, emitted from an X-ray source, impinge on a material. These primary X-rays undergo interaction processes with the analyte atoms. High-energy photons induce ionization of inner shell electrons by the photoelectric effect and thus electron vacancies in inner shells (K, L, M ...) are created. The prompt transition of outer shell electrons into these vacancies within some 100 fs can cause the emission of characteristic fluorescence radiation. Not all transitions from outer shells or subshells are allowed, only those obeying the selection rules for electric dipole radiation. The creation of a vacancy in a particular shell results in a cascade of electron transitions, all correlated with the emission of photons with a well-defined energy corresponding to the difference in energy between the atomic shells involved. The family of characteristic X-rays from each element including all transitions allows the identification of the element. Next to this radiative form of relaxation, a competing process can take place: the emission of Auger electrons. Both processes have *Z*-dependent probabilities that are complementary: the Auger yield is high for light elements and the fluorescence yield is high for heavy elements.

The working principle of XRF analysis is the measurement of wavelength or energy and intensity of the characteristic photons emitted from the sample. This allows the identification of the elements present in the analyte and the determination of their mass or concentration. All the information for the analysis is stored in the measured spectrum, which is a line spectrum with all characteristic lines superimposed above a certain fluctuating background. Other interaction processes, mainly the elastic and inelastic scattering of the primary radiation on sample and substrate, induce the background.

The most striking feature of XRF analysis is that this technique allows the qualitative and quantitative analysis of almost all the elements (Be-U) in an unknown sample. The analysis is, in principle, non-destructive, has high precision and accuracy, has simultaneous multi-element capacity and requires only a short irradiation time so that a high sample throughput is possible; on-line analysis is also possible and the running costs are low. The technique is extremely versatile for applications in many fields of science, research and quality control, has low detection limits and a large dynamic range of concentrations covering up to 9 orders of magnitude.

In contrast to all these attractive properties there are some disadvantages. The absorption effects of the primary radiation and the fluorescence radiation created in the analyte result in a shallow layer a few tenths of a millimeter deep that provides information on its composition [21].

The solid samples were simply placed into the sample holder and analysed semi quantitatively using a MiniPal 2 EDXRF (Energy Disperse XRF) Spectrometer.

2.7 ADSORPTION–DESORPTION AND THERMAL TECHNIQUES

2.7.1 BET surface area

Brunauer Emmett and Teller developed the famous BET equation for the determination of the surface area of a solid [22]. The method is based on non-specific physisorption of a gas (N_2 or Ar) onto a solid close to the condensation temperature of the adsorbing gas. Adsorption is characterized by an isotherm, which represents the equilibrium amount of gas adsorbed on a solid at a given temperature as a function of pressure. The BET equation extends the Langmuir isotherm to multilayer adsorption,

$$P/V\,(P_0 - P) = 1/V_mC + (C\text{-}1)P/CV_m\,P_0)$$

where V:the volume, reduced standard conditions (STP) of gas adsorbed per unit mass of adsorbent at a given pressure, P and constant temperature, P_0: the saturation pressure at the measurement temperature, V_m: volume of gas adsorbed at STP per unit mass of adsorbent, when the surface is covered by a unimolecular layer of adsorbate, and C: a constant, related to the free energy of adsorption.

According to this equation, a plot of P/V (P_0 – P) versus P/P_0 should yield a straight line. The surface area is then calculated using:

$$S_{BET} = V_m A_m N_a / V_{mol}$$

where N_a: Avogadro's number (6.0238×10^{23}), V_{mol}: molar volume of absorbate gas at STP ($22.41 mol^{-1}$) and A_m: Cross sectional area of adsorbed gas, Am (N_2) = 0.162 nm^2. When nitrogen is the adsorbing gas this reduces to:

$$S_{BET} = 4.353\ V_m$$

The BET surface areas of samples were measured using Micromeritics Tristar 3000 surface area analyzer. The samples were activated at 500°C for 1h before the analysis and then degassed at 350°C for 3h under nitrogen flow.

2.7.2 Temperature programmed desorption-NH_3

Temperature-programmed desorption (TPD) – which is also referred to as thermal desorption spectroscopy (TDS) – can be used on technical catalysts, but is particularly useful in surface science, where the desorption of gases from single crystals and polycrystalline foils into vacuum is examined [23]. Temperature-programmed desorption (TPD) in particular is often employed to obtain information about specific sites in catalysts [21, 22]. The temperature at which desorption occurs indicates the strength of adsorption, whereas either the amount of gas consumed in the uptake or the amount of desorption upon

heating attests to the concentration of the surface sites. The most common molecules used in TPD are NH_3 and CO_2, which probe acidic and basic sites, respectively, but experiments with pyridine, O_2, H_2, CO, H_2O, and other molecules are often performed as well [24-26]. In this, an inert gas is passed over a catalyst bed, while the temperature is increased. A TPD profile is obtained by monitoring the gases, which are desorbed from the surface as the temperature is increased. The temperature of desorption is an indication of the strength of binding of the adsorbate [27]. The analysis of TPD spectra is a time-consuming matter, if it is to be performed correctly!

Acidity measurements were performed by temperature programmed desorption (TPD-NH_3) of ammonia using a conventional flow apparatus. In a typical experiment, about 500 mg of catalyst was activated at 773 K for 1 h and kept in a tube. The sample was pretreated by passage of nitrogen at 573 K for 1 h. Subsequently catalyst was saturated with pure anhydrous ammonia gas and the system was allowed to attain equilibrium. After 30 min, the excess and physisorbed ammonia was subsequently flushed with flowing nitrogen. TPD analysis was then carried out by desorption of ammonia from 373 to 873 (K) at a heating rate of 293 K/min in nitrogen atmosphere and trapped in H_2SO_4.The amount of ammonia desorbed is calculated by titrating against NaOH.

2.7.3 Thermal analysis

2.7.3.1 TG/DTG/DTA analysis

Changes in catalysts during preparation, which often involves thermal calcination, oxidation, and reduction, can also be followed by recording the

associated variations in sample weight, as in normal thermogravimetry (TG) or differential thermogravimetry (DTG); or in sample temperature, as in differential thermal analysis (DTA) [28-30]. Although these thermal methods are quite traditional, they are still used often in catalysis research. Thermogravimetric analysis (TGA) provides a quantitative measurement of any weight changes associated with thermally induced transitions. It can record directly the loss in weight as a function of temperature or time [31]. In TGA, the weight of sample is continuously recorded as the temperature is increased. Samples are placed in a crucible that is positioned in a furnace on a quartz beam attached to an automatic recording balance. The horizontal quartz beam is maintained in the null position by the current flowing through the transducer coil of an electromagnetic balance. Any change in the weight of the sample causes a deflection of the beam, which is sensed by one of the photodiodes connected to act as a position sensor to determine the movement of the beam. The beam is then restored to the original null position by a feedback current sent from the photodiodes to the coil of the balance and the current is proportional to the change in weight of the sample. In differential thermal analysis (DTA), the difference in temperature between the sample and a thermally inert reference material is measured as a function of temperature usually the sample temperature. Any transition that the sample undergoes results in liberation or absorption of energy by the sample with a corresponding deviation of its temperature from that of the reference. A plot of the differential temperature, ΔT, versus the programmed temperature, T, indicates the transition temperatures and whether the transition is exothermic or endothermic. When an endothermic change occurs, the sample temperature

lags behind the reference temperature because of the heat in the sample. Exothermic behaviour is associated with the decrease in enthalpy of a phase or a chemical system. DTA and thermogravimetric analyses are often run simultaneously on a single sample.

Besides the prediction of calcination temperatures during catalyst preparation, thermal analysis is also used to determine the composition of catalysts based on weight changes and thermal behaviour during thermal decomposition and reduction, to characterize the aging and deactivation mechanisms of catalysts, and to investigate the acid–base properties of solid catalysts using probe molecules. However, these techniques lack chemical specificity, and require corroboration by other characterization methods.

Thermogravimetry (TG) and differential thermal analysis (DTA) measurements were performed with a Perkin Elmer Pyris Diamond TG/DTA Analyzer under nitrogen atmosphere at heating rate of 10°C/min from room temperature to 800°C with samples mounted on a platinum sample holder.

2.7.3.2 TGA adsorption studies

The catalyst samples activated at 500°C for 2h were kept in two different desiccators saturated with pyridine, and 2,6 – dimethylpyridine (2,6-DMP) vapours respectively. For the effective and uniform adsorption the samples were kept inside the desiccator for 48 h. After this, the weight loss of the adsorbed samples was measured by thermogravimetric analysis operating

between 40 to 600°C at a rate of 20°C/minute. For the pyridine adsorbed samples, the weight loss between 100-200°C, 201-400°C and 401-600°C are considered to be measures of weak, medium and strong acid sites, respectively. Since the 2,6-DMP weakly bound to Lewis acid sites get desorbed below 300°C , the weight loss between 301-400°C, 401-500°C and 501-600°C are considered to be measures of weak, medium and strong acid sites, respectively.

2.8 OPTICAL SPECTROSCOPIES

2.8.1 FT-Infrared spectroscopy

In catalysis, infrared (IR) spectroscopy is commonly used to characterize specific adsorbates. Because of the localized nature and particular chemical specificity of molecular vibrations, IR spectra are quite rich in information, and can be used to extract or infer both structural and compositional information on the adsorbate itself as well as on its coordination on the surface of the catalyst. In some instances, IR spectroscopy is also suitable for the direct characterization of solids, especially if they can be probed in the far-IR region (10–200 cm^{-1}) [32-34]. Every chemical compound has its own characteristic IR spectrum.

Several working modes are available for IR spectroscopy studies [32-34]. The most common arrangement is transmission, where a thin solid sample is placed between the IR beam and the detector; this mode works best with weakly absorbing samples. Using the so-called transmission technique the catalyst powder is compressed and used as a self-supporting disc.

Unfortunately, the necessary high pressure can cause phase transitions within the disc and thus leads to misinterpretations. Furthermore, using discs that are too thick can result in total absorption of the IR radiation by the catalyst material. These disadvantages are overcome by diffuse reflectance infrared Fourier transform spectroscopy (DRIFTS), where pure catalyst powders can be analysed without any previous mechanical manipulation. Many substances in their natural states (eg. powders and rough surface solids) exhibit diffuse reflection, i.e. incident light is scattered in all directions as opposed to specular (mirror-like) relflection where the angle of incidence equals the angle of reflection. These spectra can exhibit both absorbance and reflectance features due to contributions from transmission, internal and specular reflectance components as well as scattering phenomena in the collected radiation.

Diffuse reflection accessories are commercially available. They collect the diffusely scattered IR radiation by means of large ellipsoid mirrors. Even the largest mirrors only permit the collection of a part of the scattered radiation; therefore the use of diffuse reflection accessories is restricted to FT-IR spectrometers (diffuse reflection in IR by FT spectrometer – DRIFT). The Kubelka-Munk transformation has to be performed in order to linearize the ordinate of the obtained spectra. Integrating spheres (so-called Ulbricht spheres) are no longer used in MIR due to the lack of non-absorbing and uniformly high-scattering coatings for the inside of the sphere.

The applications of IR spectroscopy in catalysis are many. IR can be used to directly characterize the catalysts themselves. Further catalyst

characterization can be carried out by appropriate use of selected adsorbing probes.

Owing to its great molecular specificity, good sensitivity, and high versatility, IR spectroscopy is one of the most widely used techniques for catalyst characterization. Nevertheless, IR catalytic studies do suffer from a few limitations. In particular, strong absorption of radiation by the solid often limits the vibrational energy window available for analysis. Also, the intensities of IR absorption bands are difficult to use for quantitative analysis. Finally, it is not always straightforward to interpret IR spectra, especially in cases involving complex molecules with a large number of vibrational modes.

The IR spectra were recorded through JASCO's FTIR-4000 series spectrometer in the MIR range (4000 cm^{-1} to 400 cm^{-1}) in DRIFT mode.

2.8.2 Infrared adsorption studies

The exposed cations and anions on oxide surfaces have been described as acid-base site pairs [35,36]. The oxygen anions can act as Bronsted or Lewis base sites; the metal cations are Lewis acid sites. Hydroxyl groups bound at certain oxide surfaces may exhibit considerable Bronsted acidity, but by and large we can neglect Bronsted acidity of oxide surfaces in surface science studies. Strong Bronsted acidity usually arises in mixed oxides rather than pure oxides, due to charge imbalances and/or coordination changes caused by incorporation of a second cation type [37,38].

A variety of physico chemical methods have been employed and widely applied to evaluate the strength and the amount of acid sites on catalysts. A large variety of probe molecules have been utilized to both qualitatively ascertain the acidity and provide the measure and nature of these acidic sites [39-46]. For example, pyridine was chosen as the base probe molecule to measure the acidity. When chemisorbed on a surface possessing acid properties, pyridine can interact with acidic protons, electron acceptor sites and H from neutral or weakly acidic hydroxyls [43,44].

The acid–base properties of specific surface sites can be tested by recording the ensuing vibrational perturbations and molecular symmetry lowering of either acidic (CO and CO_2) or basic (pyridine and ammonia) adsorbates. Oxidation states can also be probed by using carbon monoxide [47,48].

The catalyst samples activated at 500°C for 2h were kept in two different desiccators saturated with pyridine, and 2,6 – dimethylpyridine (2,6-DMP) vapours respectively. For the effective and uniform adsorption the samples were kept inside the desiccator for 48 h. The IR spectra were recorded through JASCO's FTIR-4000 series spectrometer in the MIR range (4000 cm^{-1} to 400 cm^{-1}) in DRIFT mode.

2.8.3 UV-vis Diffused reflectance spectroscopy

Many materials undergo electronic transitions upon heating which can be studied by UV-Vis spectroscopy. Most often, the samples studied by this method are liquids. Analysis of powders and other solids is less straightforward, unless they can be dissolved and measured as a liquid. For non-soluble solids, the only feasible methods for such analysis in the UV-Vis are specular reflectance and diffuse reflectance. The former is suitable for highly reflective materials; the latter for powders and roughened solids.

Diffuse reflectance spectroscopy (DRS) is a spectroscopic technique based on the reflection of light in the ultraviolet (UV), visible (VIS) and near-infrared (NIR) region by a powdered sample. In a DRS spectrum, the ratio of the light scattered from an "infinitely thick" closely packed catalyst layer and the scattered light from an infinitely thick layer of an ideal non-absorbing (white) reference sample is measured as a function of the wavelength λ. The scattered radiation, emanating from the sample, is collected in an integration sphere and detected.

The main drawback of the use of UV–Vis spectroscopy for catalyst characterization is that the data commonly show broad and overlapping absorption bands with little chemical specificity. Also, it is often quite difficult to properly interpret the resulting spectra.

UV-vis DR spectra for the initial determination of the oxidation state of the transition metals were taken in the range 200-900nm on a Spectro UV-VIS DOUBLE BEAM UVD-500 spectrometer. The spectra were recorded at room temperature using MgO as a reference. Prior to measurement, the samples were pretreated for 1h at the calcinations temperature.

2.9 SURFACE-SENSITIVE SPECTROSCOPY

2.9.1 X-ray Photoelectron Spectroscopy (XPS)

(XPS), also known as *electron spectroscopy for chemical analysis* (ESCA), is one of the most powerful and common chemical analysis techniques. XPS is based on the photoelectric effect in which the binding energy (E_B) of a core level electron is overcome by the energy ($h\nu$) of an impinging soft X-ray photon, and the core-level electron is excited and ejected from the analyte. The kinetic energies of the ejected photoelectrons, E_K, are measured by an electron spectrometer whose work function is φ. Invoking conservation of energy, the following relationship is obtained:

$$E_B = h\nu - E_K - \varphi$$

The binding energy of the photoelectron is characteristic of the orbital from which the photoelectron originates. The binding energy of the ejected photoelectron depends on the final state configuration after photoemission. The final state is characterized by full relaxation of all atomic orbitals towards the hole in the core level [37].

Shake-up peaks may occur when the outgoing photoelectron simultaneously interacts with a valence electron and excites it (shakes it up) to a higher-energy level. The kinetic energy of the core electron is then slightly reduced giving a satellite structure a few eV below (above on the binding energy scale) the core level position [38].

A general ingredient of core level spectroscopies is the core hole spin-orbit splitting. The coupling of the orbit and spin angular momenta is given by the spin-orbit interaction, which is essentially a relativistic effect. The spin-orbit interaction is very large for core holes and in general two peaks or structures will be visible in the spectrum, separated by the core hole spin-orbit splitting. The intensity ratio of $2p_{1/2}$ versus $2p_{3/2}$ peak is 1:2. and that of $3d_{3/2}$ to $3d_{5/2}$ peak is 2:3. This rule breaks down if there are other interactions, which are able to mix the spin-orbit split states. The charge-transfer effect plays a major role in XPS. More drastic charge-transfer effects were observed in f and d electron systems where charge transfer occurs from conduction (or valence) band states to the f or d electron states in order to screen the core-hole potential. This causes a splitting of the XPS spectra into well-screened and poorly screened final states. The multiplet coupling effect plays a minor role in the XPS process compared to that of the charge-transfer effect [39].

The measurement is carried out in an UHV chamber. Monochromatic X-ray photons, typically from an Al-Kα (1486.6 eV) or Mg-Kα (1253.6 eV) X-ray source, are shone at the sample to eject photoelectrons. These electrons have energies ranging from 0 eV up to almost the same energy as the incident photons but most are emitted at a few discrete energies that are characteristic

of the elements present in the sample. The photoelectrons are collected by an electron energy analyser such as a hemispherical mirror analyser (HMA) to produce a spectrum of the number of electrons vs. their kinetic energy. Analysis of this spectrum provides quantitative information about the composition of the near surface region of the sample [16].

The XPS were performed on Kratos Axis 165 X-ray photoelectron spectrometer equipped with dual Al-Mg anodes interfaced with the necessary data handling software. For all catalysts prepared the spectra were recorded under ultrahigh vacuum conditions (10^{-9} Torr), using Al Kα primary radiation (15 kV, 5 mA) operated at 150W. Each analysis started with a survey scan from 0 to 1200 eV with a dwell time of 100 milliseconds, pass energy of 160 eV at steps of 1eV with one sweep. For the high-resolution analysis, the number of sweeps was increased, the pass energy was lowered to 80eV at steps of 100 meV and the dwell time was changed to 250 milliseconds. The spectra were charge corrected using the advantageous C 1s signal at 284.6 eV. The relative intensities of the surface composition of different elements were corrected with their corresponding atomic sensitivity factors using the vision two software in unix system. Prior to the XPS studies, all the catalysts were reduced in 6% H_2 balance He flow at 523K for 4 h, followed by passivation in N_2 atmosphere.

REFERENCES

[1] J.M Thomas and R.M. Lambert, "Characterisation of Catalysts", John Wiley & Sons (1980) p-76.

[2] J.M. Thomas, W.J. Thomas, "Principles and Practice of Heterogeneous Catalysis", VCH, Weinheim, 1997.

[3] R.A. van Santen, P.W.N.M van Leeuwen, J.A. Moulijn, B.A. Averill (Eds.), "Catalysis: An Integrated Approach", (2nd ed.), Elsevier, Amsterdam, 1999.

[4] Ryan Richards, "Surface and Nanomolecular Catalysis", CRC Press, Taylor and Francis Group, 2006.

[5] A. Sen and P. Pramanik, *Journal of Materials Synthesis and Processing*, Vol. 10, No. 3, May 2002.

[6] P.A. Lessing, *Ceram. Bull.* 68 (1989) 1002.

[7] R.N. Das, *Materials Letters,* 47 (2001) 349.

[8] J.W. Niemantsverdriet, "Spectroscopy in Catalysis: An Introduction", VCH Publisher, New York (1995) 165.

[9] I. Chorkendorff, J.W. Niemantsverdriet, "Concepts of Modern Catalysis and Kinetics", WILEY-VCH Verlag GmbH & Co. KGaA, Weinheim, 2003.

[10] Sandra E.Dann, "Reactions and Characterization of Solids", The Royal Society of Chemistry, 2000.

[11] J. Goldstein, D.E. Newbury, D.C. Joy, C.E. Lyman, P. Echlin, E. Lifshin, L.C. Sawyer, J.R. Michael, "Scanning Electron Microscopy and X-Ray Microanalysis" (3rd ed.), Kluwer Academic Publishers, New York, 2003.

[12] Charles N.Satterfield, "Heterogeneous Catalysis in Industrial Practice",(2nd ed.),McGraw-Hill International Editions,1993.

[13] J. Matta, D. Courcot, E. Abi-Aad, A. Aboukais, *Chem. Mater.* 14 (2002) 4118.

[14] M. Jose´-Yacama´n and M. Avalos-Borja, *Catal. Rev. – Sci. Eng.* 34 (1992) 55.

[15] A.K. Datye and D.J. Smith, *Catal. Rev. – Sci. Eng.* 34 (1992) 129.

[16] J.M. Thomas and P.L. Gai, *Adv. Catal.* 48 (2004) 171.

[17] P.L. Hansen, S. Helveg, and A.K. Datye, *Adv. Catal.* 50 (2006) 77.

[18] J. Liu, *J. Electron Microsc.* 54 (2005) 251.

[19] Brent Fultz and James Howe, "Transmission Electron Microscopy and Diffractometry of Materials", 3 rd Edn, Springer-Verlag Berlin Heidelberg (2008).

[20] Leonid A. Bendersky and Frank W. Gayle , J. *Res. Natl. Inst. Stand. Technol.* 106, 997–1012 (2001)

[21] G. Gauglitz and T. Vo-Dinh, "Handbook of Spectroscopy", WILEY-VCH Verlag GmbH & Co. KGaA, Weinheim 2003.

[22] B.K Hodnett, "Heterogeneous Catalytic Oxidation: Fundamental and

Technological Aspects of the Selective and Total Oxidation of Organic Compounds", John Wiley, New York (2000).
[23] J.L. Falconer and J.A. Schwartz, *Catal. Rev. – Sci. Eng.* 25 (1983) 141.
[24] R.J. Cvetanovic', Y. Amenomiya, *Catal. Rev.* 6 (1972) 21.
[25] S. Bhatia, J. Beltramini, D.D. Do, *Catal. Today* 7 (1990) 309.
[26] R.J. Gorte, *Catal. Today* 28 (1996) 405.
[27] M. Niwa, Y. Habuta, K. Okumura, N. Katada, *Catal. Today* 87 (2003) 213.
[28] W.M. Wendlandt, "Thermal Methods of Analysis" (2nd ed.), Wiley, New York, 1974.
[29] J.W. Dodd, K.H. Tonge, "Thermal Methods: Analytical Chemistry by Open Learning", Wiley, Chichester, 1987.
[30] M. Maciejewski, A. Baiker, *J. Therm. Anal.* 48 (1997) 611.
[31] H.H. Willlared, L.L. Merrit Jr., J.A. Dean, F.A. Settle Jr., "Instrumental Methods of Analysis" ,7th edn., CBS Publishers, New Delhi (1986).
[32] P.R. Griffiths, J.A. de Haseth, "Fourier Transform Infrared Spectroscopy", Wiley, New York, 1986.
[33] F. Zaera, in "Encyclopedia of Chemical Physics and Physical Chemistry", Vol. 2, J.H. Moore, N.D.Spencer (Eds.), IOP Publishing, Philadelphia, PA, 2001, p. 1563.
[34] J. Ryczkowski, *Catal. Today* 68 (2001) 263.
[35] R. J. Kokes, *Intra-Sci. Chem. Rep.*, 6 (1972) 77.
[36] R. L. Burwell, G. L. Haller, K. C. Taylor and J. F. Read, *Adv. Catal.*, 29 (1969) 1.
[37] K. Tanabe, "Solid Acids and Bases", Academic Press, New York, 1970
[38] H. H. Kung, *J. Solid state chem.*, 52 (1984) 191.
[39] M.C. Kung and H.H. Kung, *Catal. Rev. – Sci. Eng.*, 27 (1985) 425.
[40] P. Berteau and B. Delmon, *Catal. Today*, 5 (1989) 121.
[41] G. Busca, *Catal. Today*, 27 (1996) 323.
[42] J.A. Lercher, C. Grundling and G. Edermirth, *Catal. Today*, 27 (1996) 353.
[43] G. Busca, *Catal. Today*, 41 (1998) 191.
[44] J.C. Lavalley, *Catal. Today*, 27 (1996) 377
[45] G. Ramis, G. Busca and V. Lorenzelli, *Mat. Chem. Phys.*, 29 (1991) 425.
[46] R. Philipp and K. Fujimoto, *J. Phys. Chem.*, 96 (1992) 9035.
[47] A. Zecchina, D. Scarano, S. Bordiga, G. Ricchiardi, G. Spoto, F. Geobaldo, *Catal. Today* 27 (1996) 403.
[48] K.I. Hadjiivanov, G.N. Vayssilov, *Adv. Catal.* 47 (2002) 307.

CHAPTER 3

SURFACE AND CHEMICAL CHARACTERIZATION

Abstract

Characterization is a central aspect of catalyst development, which gives insight into the relation between physical and chemical properties of the catalyst and its activity. The catalyst characterization in industrial research deals with the materials science of catalysts on a more or less mesoscopic scale, whereas the ultimate goal of fundamental catalytic research is to characterize the surface of a catalyst at the microscopic level – that is, on the atomic scale. Spectroscopy, microscopy, diffraction and methods based on adsorption and desorption or bulk reactions (reduction, oxidation) all offer tools to investigate the nature of an active catalyst. One key parameter is the surface area, which is mainly determined by the size of the particles. Quantitative determination of the composition and structure on the atomic scale is one of the major thrusts in surface studies.

This chapter presents the results and discussion pertaining to the structural characteristics of the catalyst systems by various spectroscopic and non-spectroscopic techniques.

3.1 POWDER X-RAY DIFFRACTION

In catalyst characterization, diffraction patterns are mainly used to identify the crystallographic phases that are present in the catalyst [1]. Every crystalline substance has a unique X-ray pattern because the line position depends on unit cell size, and the line intensity depends on the type of the atoms present and their arrangement in the crystal [2]. The X-Ray diffraction patterns of the powdered samples were recorded using a Bruker AXS D8 Advance X-ray Diffractometer using Ni filtered CuK_{α} radiation source (λ=1.5406Å) and are presented in Fig.3.1.1-3.1.5. Fig.3.1.1 shows the influence of calcination tempertature on the XRD pattern of $CuCr_2O_4$. It can be seen that the intensity of the peak turns out to be sharper with increase in calcination temperature and this suggests the growth of the particle size and increase in crystallinity at higher calcination temperatures. The uncalcined CCr was found to be amorphous from the X-ray diffraction pattern. At 175°C the XRD pattern is broader, indicative of the gradual but incomplete formation of spinel phase [3]. It was observed that only at a calcination temperature of 550°C, the spinel phase was formed and hence it was taken as the optimum calcination temperature for the prepared chromites. Most of the intermediate products disappeared, and a single phase of CCr was formed when the materials was calcined at 550°C for 5 h. The use of PVA greatly suppresses the formation of precipitates from which the heterogeneity stems. Thereby, the fine mixture state of calcined materials in the homogeneous composition makes it possible to form a single phase of CCr under mild condition. This may be ascribed to the fact that the materials derived from the sol are of atomic

scale and homogeneously mixed with each other and thus have high sinterability. The theoretical (from JCPDS Card Data) and experimental d_{hkl} values for spinels such as $CuCr_2O_4$, $CoCr_2O_4$, $FeCr_2O_4$, $CuFe_2O_4$, $MnCr_2O_4$, $NiCr_2O_4$ and $Ni_{0.5}Cu_{0.5}Cr_2O_4$ are presented in Table 3.1.1. It can be seen that the experimental data are well coordinated with the theoretical data. Interestingly, it was also observed that the mixed chromites of the Co-Cu, Fe-Cu, Mn-Cu and Ni-Cu series gave much identical XRD patterns with those of the corresponding simple chromites. In the systems studied, the compositional differences are due to the different proportions of the atoms Co, Fe, Mn and Ni in pure $CuCr_2O_4$. These atoms have close atomic numbers and so, much alike XRD patterns. No peaks of any impurities (metal oxides or other impurities) are observed in the XRD pattern. These results indicate that the product is a highly pure crystal with a cubic structure for Co-Cu and Mn-Cu series; tetragonal structure for Fe-Cu and Ni-Cu series, and also confirm the effectiveness of the preparation of high purity metal oxides particles.

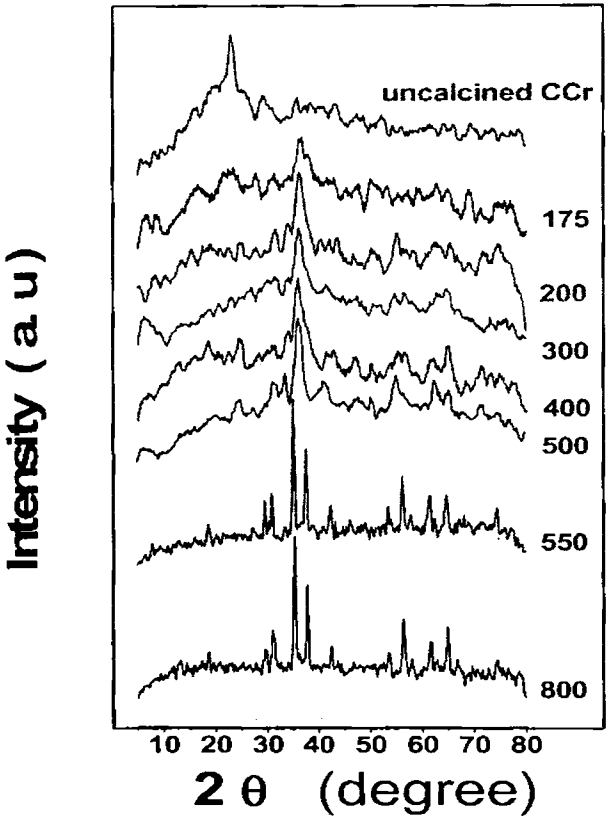

Fig. 3.1.1 XRD pattern of $CuCr_2O_4$ calcined at different temperatures.

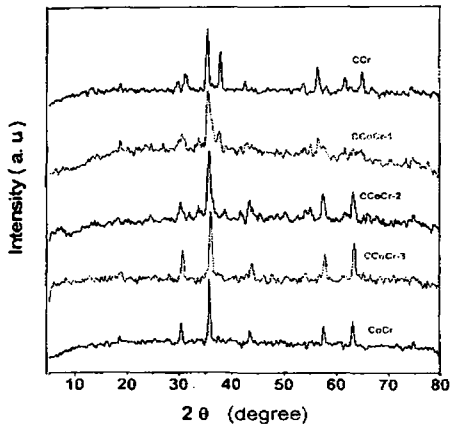

Fig. 3.1.2 XRD pattern of Co-Cu chromites.

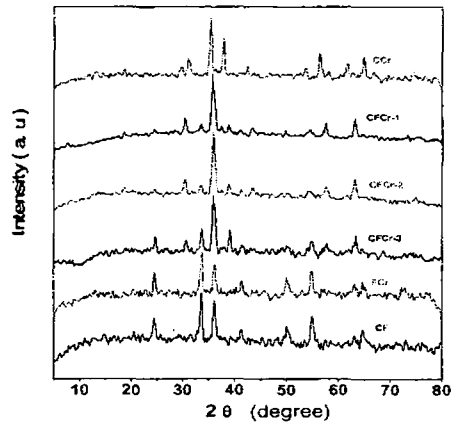

Fig. 3.1.3 XRD pattern of Fe-Cu chromites.

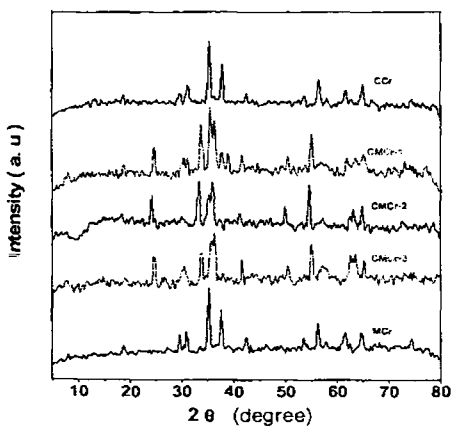

Fig. 3.1.4 XRD pattern of Mn-Cu chromites.

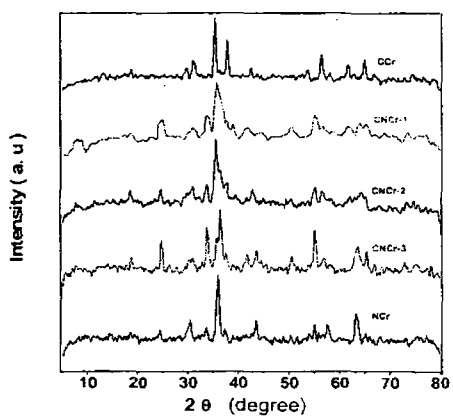

Fig. 3.1.5 XRD pattern of Ni-Cu chromites.

Table 3.1.1. XRD data, average crystallite size and BET surface area.

Sample	System	BET Surface area (m^2/g)	Average Crystallite size (nm)	Experimental data (theoretic		
				2θ	d_{hkl} (Å)	hk
CCr	Tetragonal	10	29.7	35.2 (35.2)	2.55	21
CFCr-1	Tetragonal	26	18.1	35.7	2.51	31
CFCr-2	Tetragonal	11	28.7	35.8	2.51	31
CFCr-3	Tetragonal	10	29.5	35.9	2.50	31
CF	Tetragonal	4	33.9	35.5 (35.5)	2.51	31
FCr	Tetragonal	13	27.3	33.7	2.65	31
CMCr-1	Cubic	18	23.2	35.4	2.53	31
CMCr-2	Cubic	17	24.4	35.9	2.50	31
CMCr-3	Cubic	18	23.0	36.5	2.47	31
MCr	Cubic	24	20.3	35.4(35.2)	2.68	31
CCoCr-1	Cubic	15	26.3	35.4	2.53	31
CCoCr-2	Cubic	15	26.4	35.7	2.51	31
CCoCr-3	Cubic	37	15.4	35.9	2.52	31
CoCr	Cubic	66	10.1	35.7(35.7)	2.52	31
CNCr-1	Tetragonal	20	22.0	35.5	2.53	21
CNCr-2	Tetragonal	26	18.2	35.4(35.2)	2.53	21
CNCr-3	Tetragonal	35	16.2	36.4	2.46	21
NCr	Tetragonal	45	13.5	36.0 (36.0)	2.65	21

X-ray line broadening provides a quick but not always reliable estimate of the particle size [4]. Crystallite size is a measure of the size of a coherently diffracting domain. Due to the presence of polycrystalline aggregates crystallite size is not generally the same thing as particle size. The average crystallite size of the samples can be determined from the Scherrer equation:

$$L = (0.9\lambda\ 180)/(\pi\ FWHM_{hkl} \cos\theta)$$

where; L is the average particle size, λ is wavelength of the X-ray used, $FWHM_{hkl}$ is the full width at half-maximum of an *hkl* peak at θ (glancing angle) value. The crystallite size of $CuCr_2O_4$ at different heat treatments is presented in Table 3.1.2. It can be seen that the crystallite size of the sample is increased with increase in calcination temperature. The crystallite size of the prepared catalysts is presented in Table 3.1.1. No significant observations can be attained from the crystallite size with refernce to the various metal cation incorporation into the copper chromite spinel.

Table 3.1.2. Heat Treatment schedules, surface area and crystallite size values of $CuCr_2O_4$.

Heat treatment schedule	Surface area (m^2/g)	Crystallite size (nm)
Dried at 150°C/2h	110	6.4
Calcined at 175°C/5h	61	11.1
Calcined at 200°C/5h	44	12.9
Calcined at 300°C/5h	26	17.8

Calcined at 400°C/5h	21	22.3
Calcined at 500°C/5h	11	28.5
Calcined at 550°C/5h	10	29.7
Calcined at 800°C/5h	6	31.5

It is very difficult to establish uniquely the distribution of cations among octahedral and tetragonal sites in the Co-Cu, Fe-Cu, Mn-Cu and Ni-Cu series from the intensity consideration of various hkl planes of spinel phase, since there are three kinds of cations distributed between the A and B sites, and all of the three cations have nearly equal scattering powers. The compound $CuCr_2O_4$, $MnCr_2O_4$, $CoCr_2O_4$ and $NiCr_2O_4$ are normal spinels. The compound $CuFe_2O_4$ is reported to be an inverse spinel or a partly inverse spinel. However, most frequently spinel structures are only partially normal or inverse, with significant disorder in cation distribution.

The substitution of tetrahedral Cu^{2+} ions from $CuCr_2O_4$ by any bivalent cation does not affect the distribution of cations in the substituted spinel oxides [5,6]. Site preference energy for oxide spinels indicate that Ni^{2+} and Cr^{3+} occupy octahedral sites, although Cr^{3+} is also capable of forcing Ni^{2+} into tetrahedral positions [5].

3.2 SCANNING ELECTRON MICROSCOPY

The scanning electron micrograph of the representative samples shown in the Figure 3.2 suggest that sol-gel thermolyzed CCr and CF resulted in a

tetragonal- shaped crystals and the rest of the samples resulted in an agglomerated crystalline powder morphology. Thus the crystalline nature of the material, as revealed from the XRD data, is supported by SEM images.

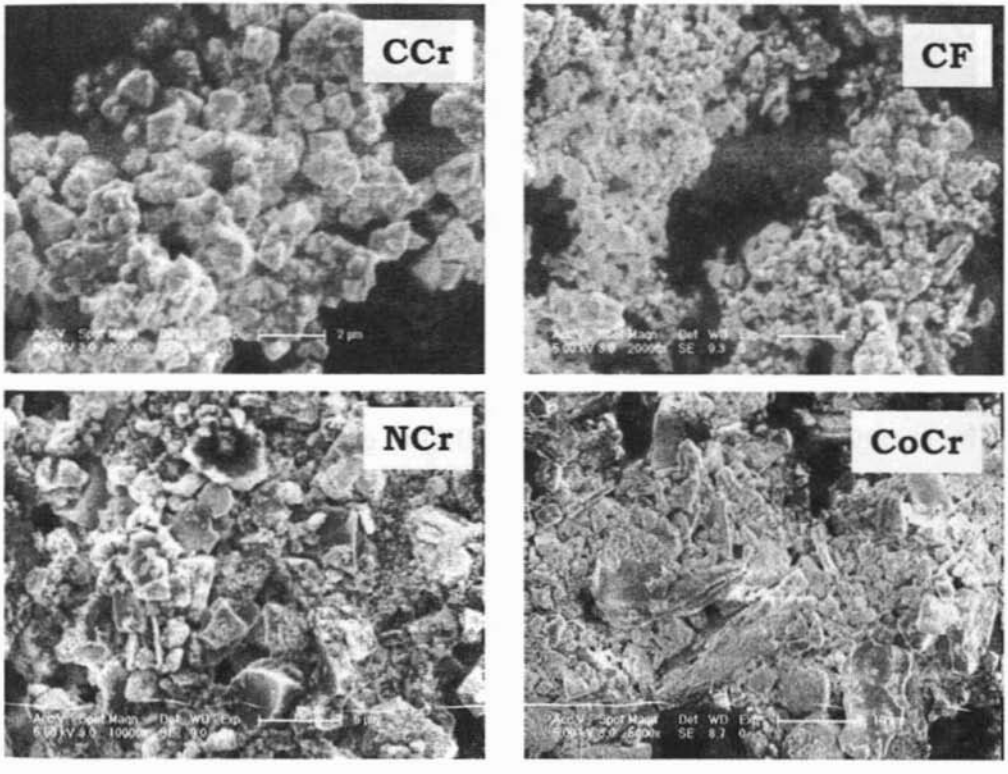

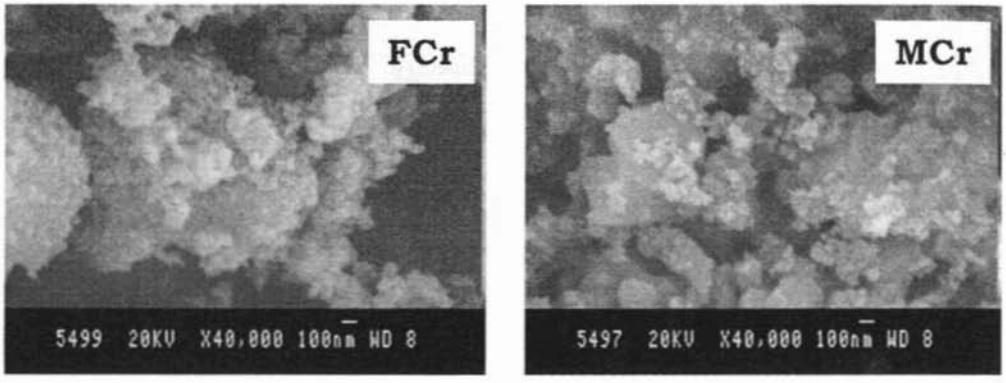

Fig. 3.2 SEM micrograph of some of the representative spinels.

3.3 ENERGY DISPERSIVE X-RAY ANALYSIS

A detailed analysis of all catalysts after calcination has been performed by energy dispersive X-ray analysis (EDX) to get the amount of each species present in the prepared catalysts. The EDX spectra obtained for $CuCr_2O_4$ is shown in Figure 3.3.

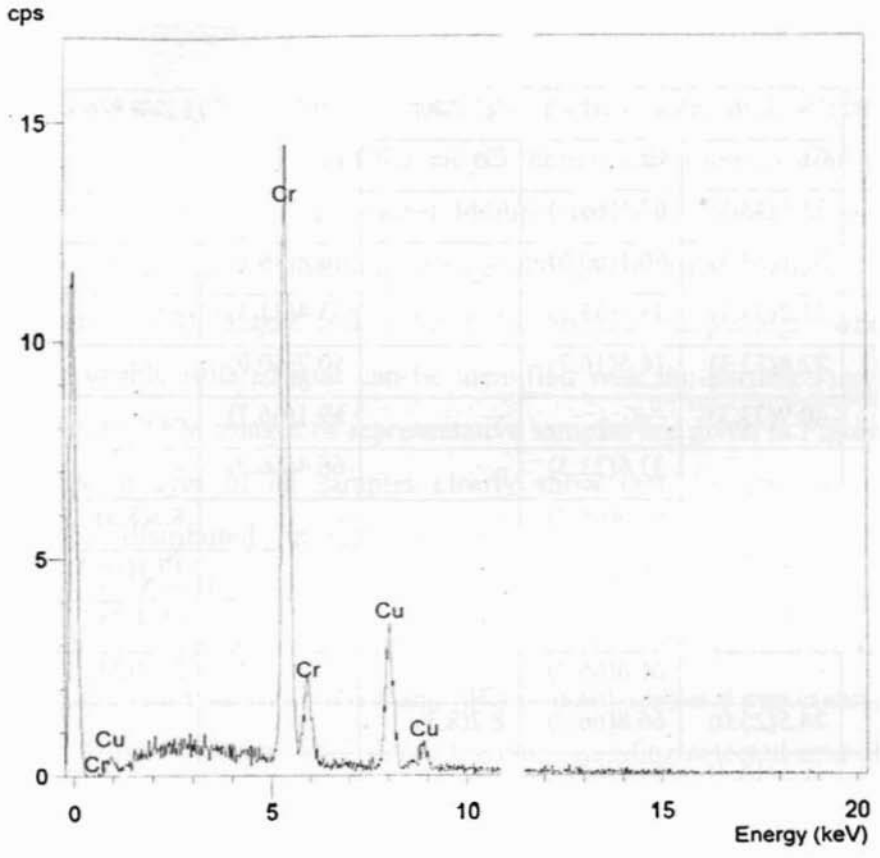

Fig. 3.3 EDX spectra of CCr sample.

The EDX analysis performed on the catalysts clearly reveals the occurance of various elements. Intensity of the spectra correlates to the amount of element (%) present. The elemental composition as atom % of catalysts is presented in Table 3.3.

Table 3.3: Atom percentage from EDX analysis

Sample ID	Atom Percentage (theoretical)*					
	Cu	Cr	Co	Fe	Mn	Ni
CCr	32.5(33.3)*	67.5(66.7)	-	-	-	-
CFCr-1	33.1(33.3)	50.1(50.0)	-	16.8(16.7)	-	-
CFCr-2	33.2(33.3)	33.4(33.3)	-	33.4(33.3)	-	-
CFCr-3	32.8(33.3)	16.5(16.7)	-	50.7(50.0)	-	-
CF	40.9(33.3)	-	-	59.1(66.7)	-	-
FCr	-	33.6(33.3)	-	66.4(66.7)	-	-
CMCr-1	25.1(25.0)	66.6(66.7)	-	-	8.3(8.3)	-
CMCr-2	16.5(16.7)	66.4(66.7)	-	-	17.1(16.7)	-
CMCr-3	8.1(8.3)	66.5(66.7)	-	-	25.4(25.0)	-
MCr	-	66.6(66.7)	-	-	33.4(33.3)	-
CCoCr-1	24.5(25.0)	66.8(66.7)	8.7(8.3)			-
CCoCr-2	16.5(16.7)	67.0(66.7)	16.5(16.7)	-	-	-
CCoCr-3	8.1(8.3)	67.1(66.7)	24.8(25.0)	-	-	-
CoCr	-	67.2(66.7)	32.8(33.3)	-	-	-
CNCr-1	24.5(25.0)	68.0(66.7)	-	-	-	7.5(8.3)
CNCr-2	16.5(16.7)	68.2(66.7)	-	-	-	15.3(16.7)
CNCr-3	8.0(8.3)	68.5(66.7)	-	-	-	23.5(33.3)
NCr	-	69.2(66.7)	-	30.8(33.3)	-	-

The chemical compositions of catalysts were obtained from Stereoscan 440 Cambridge, UK energy dispersive X-ray analyzer used in conjunction with SEM.

3.4 TRANSMISSION ELECTRON MICROSCOPY

To study the surface morphology, particle size, and selected area electron diffraction (SAED) of the sol-gel thermolysed samples, transmission electron microscopy (TEM) (model Phillips Technai-12, FEI, Netherlands) was employed with acceleration voltage 120 kV in bright field mode. The bright field TEM images reflect the basic powder morphology, where the smallest visible isolated spot can be identified with the particle / crystallite agglomerate. TEM images of representative samples are given in Figure 3.4.1. The TEM images of all samples clearly show that the nanoparticles are uniformly distributed through out the matrix with almost spherical morphology. The particle size Gaussian histographs were obtained and are shown in Fig.3.4.3. and the values in Table 3.4.1. It reveals that the average particle size is minimum for NCr and MCr (~ 5.0/1 nm) and maximum for CF and FCr (15.3/4). Figure 3.4.2 shows the corresponding selected area electron diffraction (SAED) pattern. Tropism of the particles at random and small particles causes the widening of diffraction rings that made up of many diffraction spots, which indicate that the nanoparticles are polycrystalline structure. Electron diffraction reveals that each particle is composed of many small crystal nuclei, which is a convincing proof that the particles grow in an aggregation model.

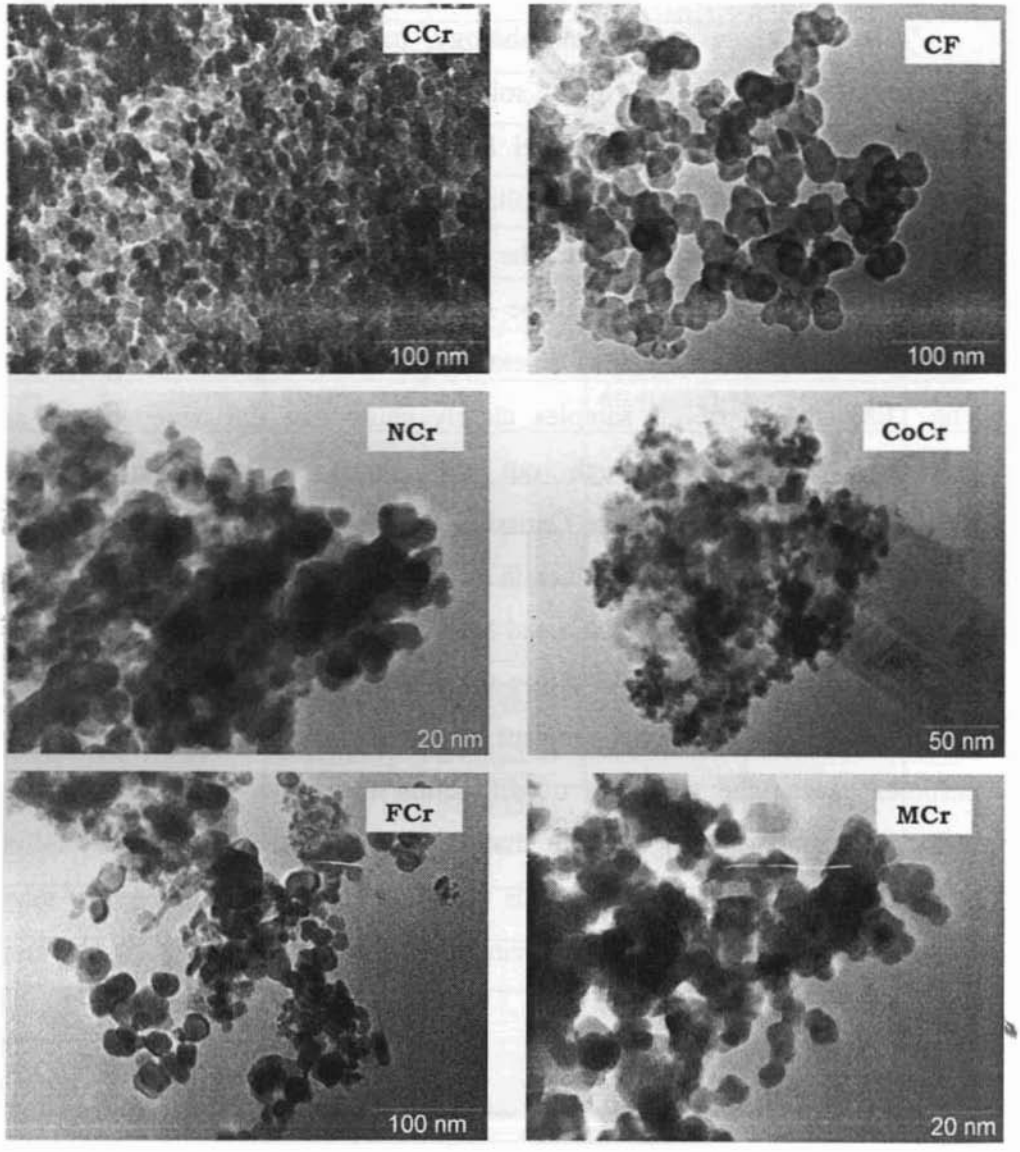

Fig. 3.4.1 TEM image of some of the representative spinels.

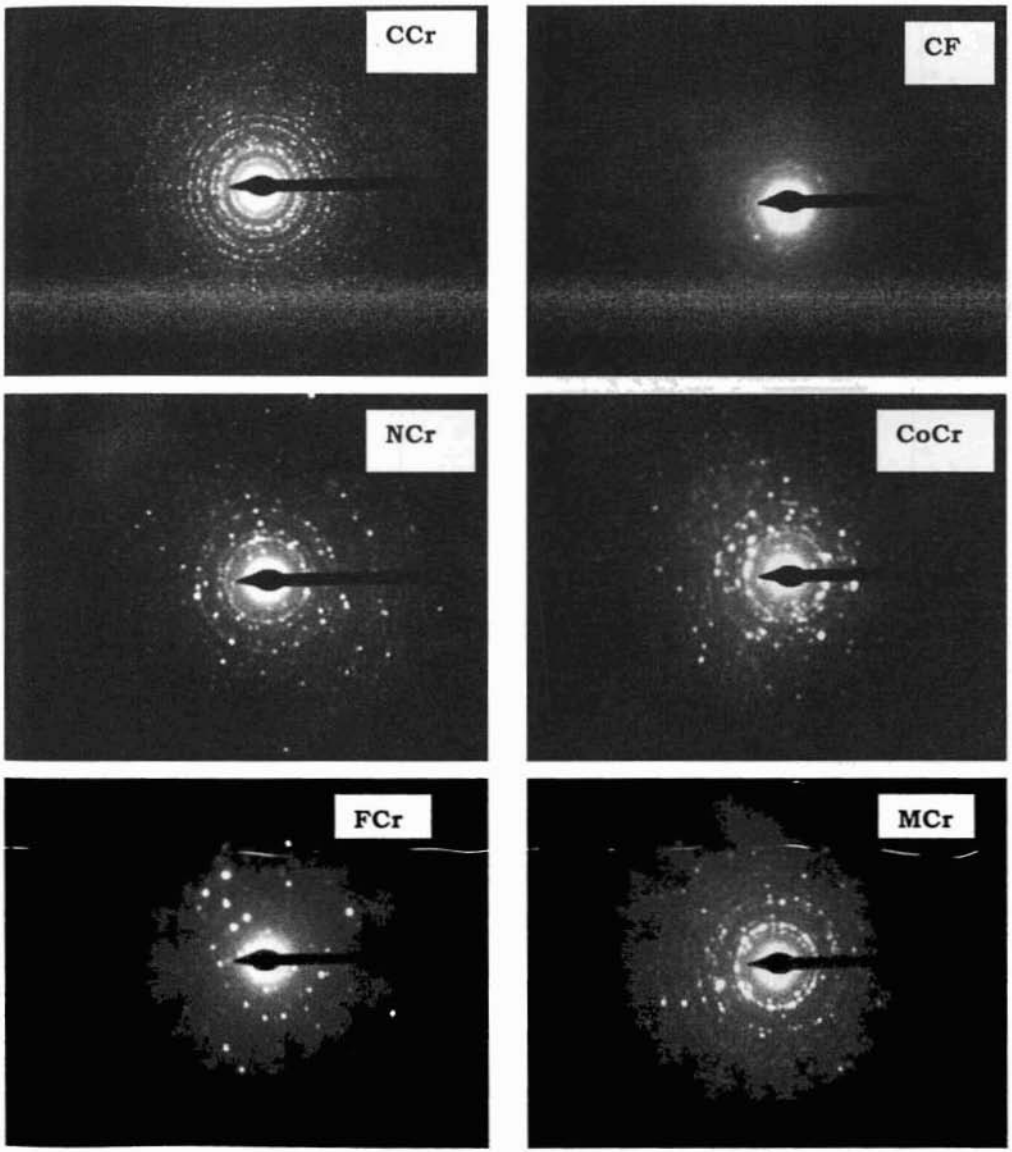

Fig. 3.4.2 SAED pattern of some of the representative spinels.

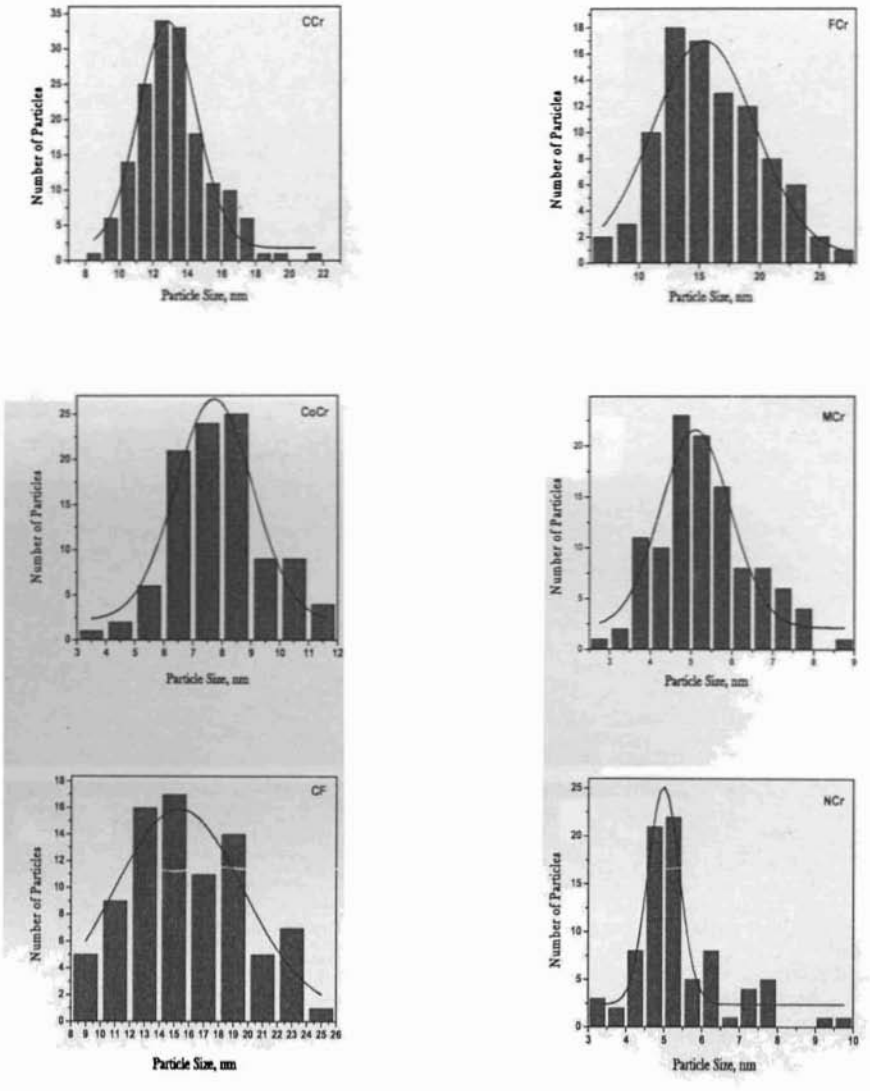

Fig. 3.4.3 Gaussian histograph for the particle size distribution of some samples.

Table 3.4.1 Average particle size of a few representative samples.

Catalysts	Particle Size (nm)
CCr	12. 8
CF	15. 3
CoCr	7. 7
FCr	15. 4
MCr	5. 1
NCr	5. 0

3.5 X-RAY FLUORESCENCE ANALYSIS

The solid samples were simply placed into the sample holder and analysed semi quantitatively using a MiniPal 2 EDXRF (Energy Disperse XRF) Spectrometer. The theoretical and experimental element concentrations [%] obtained from XRF analysis are in good agreement.

Table 3.5: Elemental percentage from XRF analysis

Sample ID	Element concentration [%] (theoretical)					
	Cu	Cr	Co	Fe	Mn	Ni
CCr	27.1(27.4)	44.7(44.9)	-	-	-	-
CFCr-1	27.1(27.2)	33.4(33.4)	-	11.8(12.0)	-	-
CFCr-2	27.2(27.0)	22.4(22.1)	-	23.9(23.7)	-	-
CFCr-3	26.7(26.8)	10.8(11.0)	-	35.5(35.3)	-	-
CF	26.3(26.6)	-	-	46.8(46.7)	-	-
FCr	-	24.8(25.0)	-	46.3(46.5)	-	-
CMCr-1	20.5(20.8)	45.3(45.4)	-	-	5.7(6.0)	-

CMCr-2	13.9(14.0)	45.7(45.8)	-	-	11.9(12.1)	-
CMCr-3	7.2(7.1)	46.4(46.2)	-	-	18.0(18.3)	-
MCr	-	46.8(46.7)	-	-	24.4(24.6)	-
CCoCr-1	20.8(20.7)	45.2(45.1)	6.2(6.4)		-	-
CCoCr-2	13.9(13.9)	45.3(45.4)	12.9(12.9)	-	-	-
CCoCr-3	7.1(7.0)	45.7(45.6)	19.1(19.4)	-	-	-
CoCr	-	45.7(45.8)	26.0(26.0)	-	-	-
CNCr-1	20.7(20.7)	45.3(45.2)	-	-	-	6.2(6.4)
CNCr-2	13.6(13.9)	45.6(45.4)	-	-	-	13.0(12.8)
CNCr-3	6.8(7.0)	45.2(45.6)	-	-	-	19.0(19.3)
NCr	-	45.7(45.9)	-		-	26.1(25.9)

3.6 BET SURFACE AREA

The BET surface areas of the samples calcined at 550°C were measured by nitrogen adsorption at liquid nitrogen temperature (Micromeritics Tristar 3000 surface area analyzer). The data are shown in Table 3.1.1. It was observed that $CuFe_2O_4$ having the lowest surface area among the studied catalysts possesses highest average crystallite size calculated from the XRD line broadening.

3.7 TEMPERATURE PROGRAMMED DESORPTION-NH_3

Acidity measurements were performed by temperature programmed desorption (TPD-NH_3) of ammonia using a conventional flow apparatus. From

the results, it was clear that the mixed chromites possessed more acidity than simple chromites.

Table 3.7.1. Surface acidity measured by ammonia TPD method.

Catalyst	Acidity distribution (mmol/g)			
	Weak (RT-200°C)	Medium (201-400°C)	Strong (401-600°C)	Total acidity
CCr	0.19	0.11	0.05	0.35
CFCr-1	0.28	0.21	0.03	0.52
CFCr-2	0.29	0.20	0.05	0.54
CFCr-3	0.27	0.21	0.06	0.54
CF	0.24	0.21	0.11	0.56
FCr	0.25	0.20	0.10	0.55
CMCr-1	0.19	0.11	0.08	0.38
CMCr-2	0.23	0.13	0.07	0.43
CMCr-3	0.26	0.23	0.01	0.50
MCr	0.20	0.12	0.04	0.36
CCoCr-1	0.27	0.11	0.02	0.40
CCoCr-2	0.28	0.13	0.02	0.43
CCoCr-3	0.25	0.18	0.05	0.48
CoCr	0.25	0.10	0.01	0.36
CNCr-1	0.26	0.13	0.02	0.41
CNCr-2	0.24	0.14	0.05	0.43
CNCr-3	0.26	0.17	0.03	0.46
NCr	0.28	0.17	0.10	0.55

3.8 TG/DTG/DTA ANALYSIS

Thermogravimetry (TG) and differential thermal analysis (DTA) measurements were performed with a Perkin Elmer Pyris Diamond TG/DTA Analyzer under nitrogen atmosphere at heating rate of 10°C/min from room temperature to 800°C with samples mounted on a platinum sample holder.

Figures 3.8.1 and 3.8.2 show the results of TG, DTG and DTA for gel precursors. According to the TG trace, the weight loss of the gel precursor 540°C and three discrete weight loss regions occurred at 50-150, 150-435 and 435-540°C, respectively. The weight loss in the temperature range of 50-150°C corresponds to the removal of water, which is accompanied by an endothermic peak at 85°C in figure 3.8.2. The weight loss in the temperature range of 150-435°C indicates the decomposition of the nitrates, which occurs with an exothermic peak at 343°C in figure 3.8.2. The decomposition of nitrates is an exothermic reaction, and, therefore, the nitrates ions act as an oxidizer, helping the decomposition of PVA [7]. After this stage, it was found that the gel precursor turned into fluffy dark brown powders. The produced gases are presumed to be NO_2 and CO_2 [8]. The weight loss in the temperature range of 435-540°C corresponds to the decomposition of organic constituents with an exothermic peak at 473°C in figure 3.8.2. Above 540°C, the weight loss of the gel precursor was not observed.

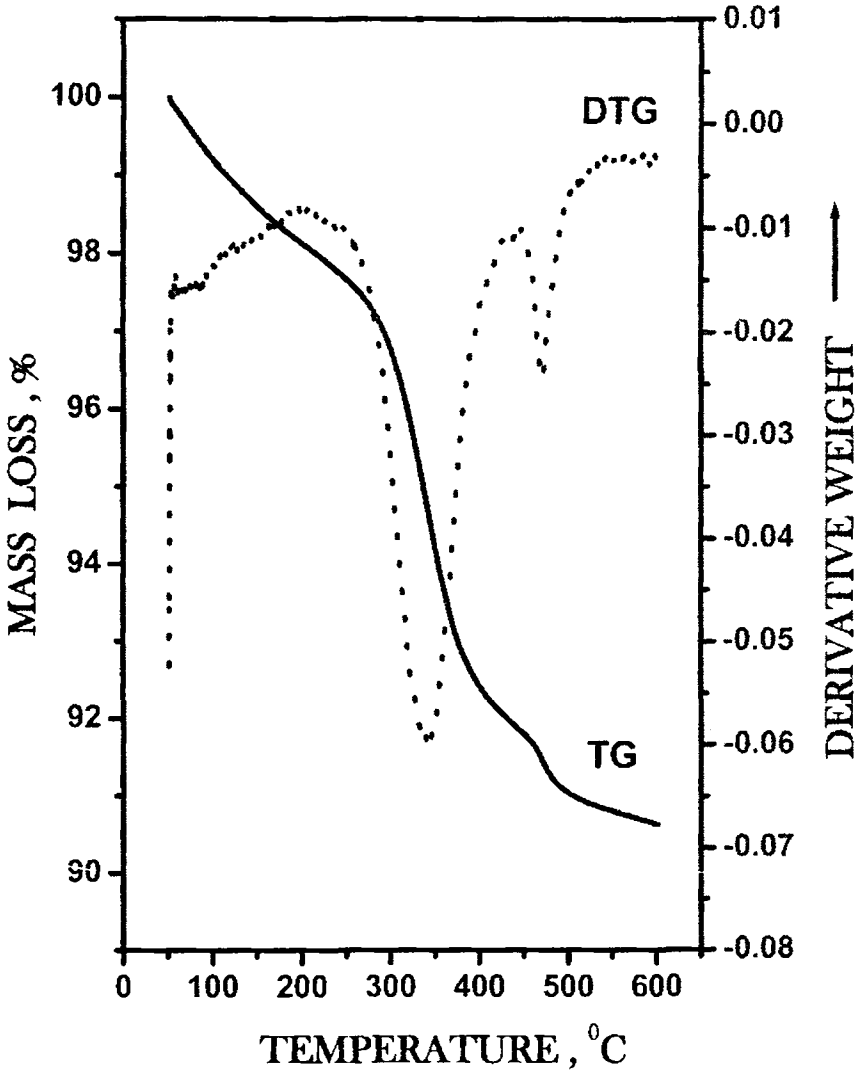

Fig.3.8.1. TG-DTG trace of the gel precursor

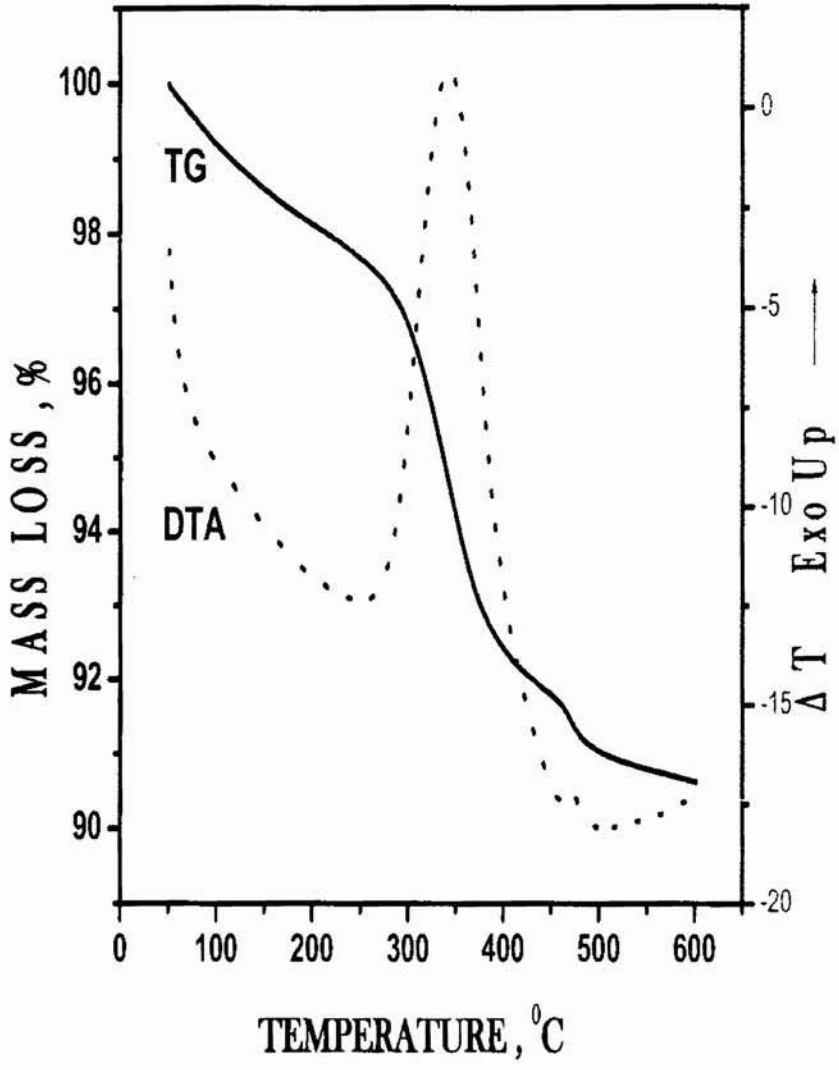

Fig.3.8.2. TG-DTA trace of the gel precursor

3.9 TGA ADSORPTION STUDIES

The potential use of pyridine and 2, 6-dimethylpyridine as probe molecules for the determination of acid strength of solid acids has recently attained increased applications. Since pyridine gets adsorbed on both Bronsted and Lewis acid sites, thermodesorption study of pyridine-adsorbed samples gives the total acid amount of the solid surface. Thus, this method can be used as a support for the results obtained from NH_3-TPD method. But 2,6-dimethylpyridine (2,6-DMP) adsorbs strongly on Bronsted acid sites and forms wesk bonds with Lewis acid sites [9]. According to Satsuma *et al.* [10] the 2, 6-DMP weakly bound to Lewis acid sites, get adsorbed below 300°C. Hence, thermodesorption study of 2, 6-DMP adsorbed samples beyond 300 °C can give the measure of Bronsted acid sites. The detection of Bronsted acid sites by 2, 6-DMP may be due to its stronger basicity (higher pKa value) than that of pyridine [10].

These methods of determining the total acidity and Bronsted acidity have been done for the prepared samples. It is confirmed that the results obtained from the thermodesorption studies of pyridine-adsorbed samples can be used as a support for the NH_3-TPD studies. The total acidity values and the acidity in the weak, medium and strong regions for catalysts obtained from TGA of pyridine-adsorbed samples are in good agreement with the data for acidity from NH_3-TPD studies.

Table 3.9.1 Acidity measurement by TG analysis of pyridine adsorbed samples.

Catalyst	Pyridine desorbed (%wt loss) 10^2 m^{-2}/g			
	Weak	Medium	Strong	Total.
CCr	0.10	0.09	0.02	0.21
CFCr-1	0.11	0.09	0.08	0.28
CFCr-2	0.13	0.08	0.08	0.29
CFCr-3	0.11	0.10	0.07	0.28
CF	0.12	0.10	0.07	0.29
FCr	0.12	0.11	0.06	0.29
CMCr-1	0.09	0.08	0.05	0.22
CMCr-2	0.09	0.08	0.07	0.23
CMCr-3	0.10	0.08	0.06	0.24
MCr	0.14	0.06	0.02	0.22
CCoCr-1	0.13	0.07	0.04	0.24
CCoCr-2	0.12	0.09	0.04	0.25
CCoCr-3	0.13	0.08	0.04	0.25
CoCr	0.12	0.08	0.03	0.23
CNCr-1	0.13	0.07	0.05	0.24
CNCr-2	0.12	0.08	0.04	0.24
CNCr-3	0.13	0.07	0.06	0.26
NCr	0.13	0.07	0.02	0.22

Table 3.9.2 Acidity measurement by TGA of 2,6-DMP adsorbed samples.

Catalyst	2,6-DMP desorbed (%wt loss)			
	Weak	Medium	Strong	Total
CCr	0.08	0.05	0.03	0.16
CFCr-1	0.11	0.09	0.03	0.23
CFCr-2	0.14	0.05	0.05	0.24
CFCr-3	0.13	0.05	0.06	0.24
CF	0.14	0.06	0.05	0.25
FCr	0.15	0.07	0.03	0.25
CMCr-1	0.08	0.06	0.04	0.18
CMCr-2	0.11	0.05	0.03	0.19
CMCr-3	0.10	0.07	0.03	0.20
MCr	0.09	0.06	0.01	0.16
CCoCr-1	0.10	0.06	0.02	0.18
CCoCr-2	0.12	0.05	0.02	0.19
CCoCr-3	0.09	0.08	0.01	0.18
CoCr	0.10	0.04	0.02	0.16
CNCr-1	0.11	0.06	0.02	0.19
CNCr-2	0.10	0.06	0.02	0.18
CNCr-3	0.10	0.06	0.03	0.19
NCr	0.09	0.07	0.01	0.17

It is assumed that the weak and medium acidity obtained from NH_3-TPD studies and TGA of pyridine-adsorbed samples are mainly due to Bronsted as well as weak Lewis acid sites.

3.10 FT-INFRARED SPECTROSCOPY

According to group theory, spinel type oxides should exhibit four bands ν_1- ν_4 [11,12]. As the high frequency bands ν_1 and ν_2 are nearly insensitive to changes in the bivalent cations [13] they should not be significantly affected when Cu^{2+} from $CuCr_2O_4$ is substituted by another bivalent cation. According to Waldron *et. al* [3] and White *et. al* [14] the high frequency band at 620cm^{-1} is due to the stretching vibration of the tetrahedral M-O bond and the low frequency band at around 500cm^{-1} is due to the vibration of the octahedral M-O bond present in the spinel structure. However, according to Tarte such interpretation is true only in special circumstances i.e when the co-ordination polyhedra round the two metal ions have very different frequencies. For majority of the spinels including chromites, the vibrational frequencies are similar in magnitude [15].

The infrared spectra of some representative samples are shown in Figure 3.10.1. A broad band around 3400 cm^{-1} which may be assigned to the stretching vibration of associated water molecules and OH groups and a medium band at ~ 1630 cm^{-1} associated with bending vibration [16,17]. The IR spectra were recorded through JASCO's FTIR-4000 series spectrometer in the MIR range (4000 cm^{-1} to 400 cm^{-1}) in DRIFT mode.

Table 3.10.1 IR frequencies and band assignments for the prepared catalysts

Sample ID	Wavenumber (cm^{-1})			
	OH stretching	OH bend	M-O bond	
			υ_1	υ_2
CCr	-	-	602	520
CFCr-1	3400	1631	619	522
CFCr-2	-	-	619	522
CFCr-3	3401	1630	618	523
CF	3400	1630	591	421
FCr	3402	1632	618	523
CMCr-1	3400	1631	622	521
CMCr-2	3400	1630	622	522
CMCr-3	-	-	621	520
MCr	3400	1630	621	520
CCoCr-1	-	-	626	525
CCoCr-2	-	-	627	524
CCoCr-3	-	-	626	524
CoCr	-	-	627	525
CNCr-1	3401	1630	618	502
CNCr-2	3400	1631	617	499
CNCr-3	3400	1632	618	501
NCr	3400	1630	617	500

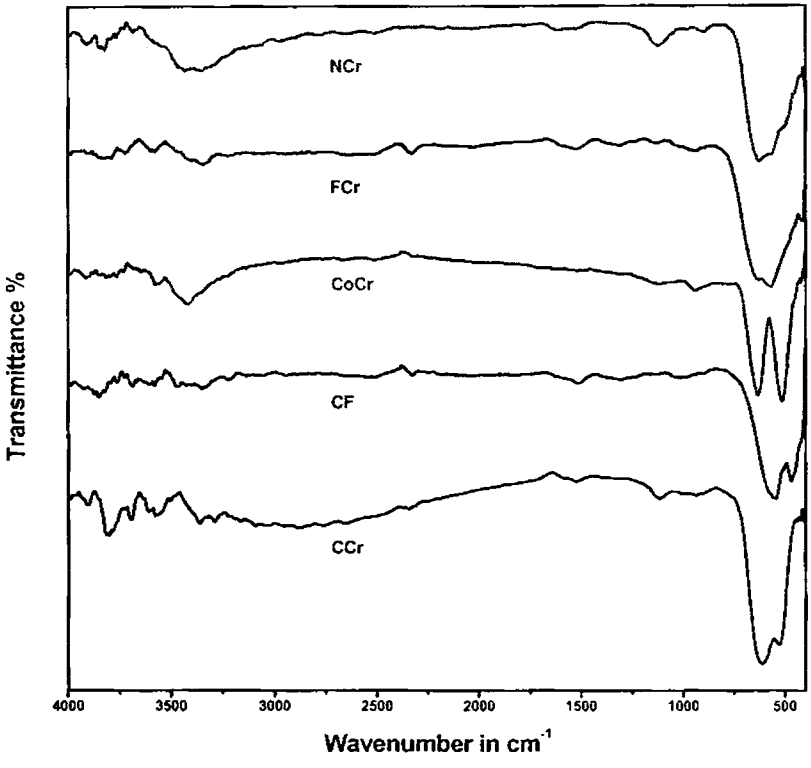

Fig.3.10.1: DRIFT spectra of a few representative samples.

3.11 INFRARED ADSORPTION STUDIES

To study the surface sites, DRIFT studies were performed on pyridine-adsorbed catalysts. All the samples were activated at 500°C for 2h and kept in a desiccator saturated with pyridine vapours.

Adsorption of pyridine has been investigated with the intention of characterizing the active acidic species present on the spinel surface. In the region from 1425 to 1635 cm^{-1}, pyridine ring modes are observed. The pyridine molecule can retained on the surface of oxides in following three different modes [18] namely, (1) interaction of the N lone pair electron and the H atom of OH group, (2) transfer of a proton from surface OH group to the pyridine forming pyridinium ion (Bronsted acidity), and (3) pyridine coordination to an electron deficient metal atom (Lewis acidity). The most sensitive vibrations are ν_{19b}, ν_{19a}, ν_{8b} and ν_{8a} [19]. According to Kline and Turkevich [20] 8a and 19a are symmetric ring vibrations and ν_{8b} and ν_{19b} are asymmetric ring vibrations to the two-fold rotational axis. The ν_{8a} and ν_{19b} are very sensitive with regard to the nature of intermolecular interactions via nitrogen lone pair of electrons [19]. The ν_{8a} and ν_{19b}, whose positions depend upon the strength of the adsorbing Lewis site, are taken as a measure of Lewis acidic strength. Among the above four vibration modes, ν_{8a} is very sensitive with respect to the oxidation state, coordination symmetry and cationic environment [21]. A broad ν_{8a} band around 1604 cm^{-1} decrease in width as we move from simple spinel oxides to mixed spinel oxides and indicates a decrease in the disorder of cation distribution in these spinels. ν_{8b} band is found to be very labile and its stability on the surface is temperature dependent [22,23]. A weak band centered at 1540 cm^{-1} is attributed to pyridinium ion [21,24].

Table 3.11.1 IR frequencies and assignments of pyridine chemisorbed on catalysts.

Catalysts	ν_{8a}	ν_{8b}	$\nu_{pyridinium\ ion}$	ν_{19a}	ν_{19b}
CCr	1604	1573	1540	1480	1443
CFCr-1	1608	1571	1541	1480	1444
CFCr-2	1608	1569	1538	1488	1454
CFCr-3	1608	1569	1537	1488	1450
CF	1606	1571	1538	1487	1451
FCr	1609	1570	1540	1489	1455
CMCr-1	1610	1569	1540	1490	1456
CMCr-2	1613	1568	1543	1486	1443
CMCr-3	1614	1575	1540	1489	1444
MCr	1612	1575	1541	1480	1445
CCoCr-1	1610	1569	1543	1488	1450
CCoCr-2	1612	1568	1542	1487	1443
CCoCr-3	1611	1569	1540	1488	1446
CoCr	1611	1568	1541	1485	1453
CNCr-1	1613	1569	1541	1490	1451
CNCr-2	1606	1569	1540	1487	1446
CNCr-3	1607	1568	1542	1487	1449
NCr	1611	1569	1540	1489	1450

3.12 UV-VIS DIFFUSED REFLECTANCE SPECTROSCOPY

The spectrum of chromite consists of five characteristic bands around 336, 422, 532, 660, 750 nm. The nature and location of these bands at 660 and 422 nm implies that they are due to spin allowed transitions of Cr^{+3} ion and assigned to $^4A_{2g}(F) \rightarrow {}^4T_{2g}(F)$ and $^4A_{2g}(F) \rightarrow {}^4T_{1g}(F)$ transitions respectively [25]. The bands at 750 and 532nm are assigned to $^6A1_g(S) \rightarrow {}^4T_{1g}(G)$ and $^6A_{1g}(S) \rightarrow {}^4T_{2g}(G)$ transitions respectively. The higher energy band at 336 nm is identified as of $^6A_{1g}(S) \rightarrow {}^4T_{2g}(P)$ transition from the electronic energy level diagram of Cr^{+3} in octahedral field. Generally, Fe^{+3} display a broad band around 900 $\{^6A_{1g}(S) \rightarrow {}^4T_{2g}(G)\}$ and 667nm and a shoulder band at 526nm $\{^6A_{1g}(S) \rightarrow {}^4T_{2g}(G)\}$ [26]. The large band detected in the range 600-900 nm is characteristic for an octahedral tetragonally distorted Cu^{2+} (d^9) ion [27]. The characteristic absorption bands of Co^{2+}, Ni^{2+}, Mn^{2+} are also near around 440, 535, 667 and 850 nm. Hence, it is difficult to differentiate the oxidation state of metal ions.

UV-vis DR spectra for the initial determination of the oxidation state of the transition metals were taken in the range 200-900nm on a Spectro UV-VIS DOUBLE BEAM UVD-500 spectrometer. The spectra were recorded at room temperature using MgO as a reference. Prior to measurement, the samples were pretreated for 1h at the calcinations temperature.

Table 3.12.1 Wavelenths of catalysts from UV-DRS analysis

Sample ID	Wavelength (nm)				
CCr	336	423	532	660	867
CFCr-1	336	422	535	666	864
CFCr-2	336	422	532	666	865
CFCr-3	336	422	532	666	864
CF	336	422	532	664	873
CMCr-1	335	423	532	666	870
CMCr-2	337	422	532	666	870
CMCr-3	335	422	532	664	870
MCr	336	422	532	666	870
CCoCr-1	336	422	532	666	863
CCoCr-2	335	423	532	666	864
CCoCr-3	335	423	532	666	865
CoCr	335	423	531	666	861
CNCr-1	335	422	532	660	864
CNCr-2	336	422	532	666	864
CNCr-3	336	422	532	666	863
NCr	336	423	531	666	862

3.13 X-RAY PHOTOELECTRON SPECTROSCOPY (XPS)

Table 3.13.1 report BE values and the full widths at half-maximum (FWHM) for $2p_{3/2}$ electrons of Cr, together with energy separations of the satellite peaks accompanying the main signal for Cr; kinetic energy values for the LMM Auger peak of chromium from the ESCA intensities are also reported.

The oxidation states of chromium were determined by comparing the binding energy of the Cr $2p_{3/2}$ peak and the valueof spin-orbit splitting Cr $2p_{1/2}$ – Cr $2p_{3/2}$ with reference and literature values [28-34]. Chromium in either the 3+ or 6+ oxidation states may be distinguished in terms of binding energy, the satellite structure, the spin-orbit intensity ratio, and the spinorbit splitting [35]. Binding energy and spin-orbit splitting data of the Cr 2p region for all the prepared catalyst materials are collected in Table 3.13.1, and smoothed, deconvoluted Cr 2p regions for the CFCr-2 and CMCr-2 catalyst are shown in Figure 3.13.2 and 3.13.3. For all catalyst materials, the Cr 2p doublet can be resolved into four individual peaks (Figure 3.13.2 and 3.13.3). The maximal peaks (Cr $2p_{3/2}$, 576 -577 eV) in all manifolds exhibit a spin-orbit splitting of 9.7-9.9 eV characteristic of a Cr^{3+} species. Analysis of the O 1s peak (see later) further supports this assignment. The peaks at a slightly higher binding energy to the maximal peaks have a spin-orbit splitting of 10.7/8 eV, which corresponds to the Cr^{3+} satellite. The binding energy positions and spin-orbit splittings for both valence states are in good agreement with literature values [36].

Table 3.13.1 Binding energies of the chromium photoelectron peaks obtained from the mixed transition metal oxides containing chromium.

Oxide	Photoelectron peak binding energy (eV) [FWHM]				assgnt.
	Cr LMMa	$2p_{3/2}$	$2p_{1/2}$	ΔE_{so}	
CCr	-	577.1 (2.1)	587.0 (2.0)	9.9	Cr^{3+}
		577.6 (2.3)	587.4 (2.2)	9.8	Cr^{3+}
CFCr-1	960.1 (2.2)	576.7 (2.2)	586.5 (2.0)	9.8	Cr^{3+}
		578.2 (2.4)	588.1 (2.4)	9.9	Cr^{3+}
CFCr-2	960.2 (3.0)	576.6 (2.5)	586.5 (2.3)	9.9	Cr^{3+}
		578.1 (2.3)	587.9 (2.4)	9.8	Cr^{3+}
CFCr-3	960.2 (2.6)	576.7 (2.1)	586.5 (2.4)	9.8	Cr^{3+}
		577.9 (3.2)	587.8 (3.1)	9.9	Cr^{3+}
FCr	-	576.2 (2.2)	586.1 (2.3)	9.9	Cr^{3+}
		578.1 (3.2)	587.9 (3.1)	9.8	Cr^{3+}
CMCr-1	960.1 (3.9)	576.2 (3.0)	586.0 (2.7)	9.8	Cr^{3+}
		579.0 (2.7)	588.9 (2.7)	9.9	Cr^{3+}
CMCr-2	960.1 (3.9)	576.0 (1.9)	585.9 (2.2)	9.9	Cr^{3+}
		577.1 (2.3)	587.9 (2.8)	10.8	Cr^{3+} sat.
CMCr-3	960.0 (4.3)	576.1 (2.0)	586.0 (2.7)	9.9	Cr^{3+}
		577.5 (2.5)	588.3 (2.7)	10.8	Cr^{3+} sat.
MCr	-	576.1 (2.3)	585.9 (1.5)	9.8	Cr^{3+}
		578.2 (2.5)	588.1 (3.0)	9.9	Cr^{3+}
CCoCr-1	-	576.6 (2.8)	586.4 (2.9)	9.8	Cr^{3+}
		578.9 (2.8)	588.8 (2.7)	9.9	Cr^{3+}

CCoCr-2	-	576.8 (2.2)	586.6 (2.2)	9.8	Cr^{3+}
		578.7 (3.2)	588.6 (2.8)	9.9	Cr^{3+}
CCoCr-3	-	576.5 (2.3)	586.4 (2.4)	9.9	Cr^{3+}
		578.4 (2.9)	588.2 (2.3)	9.8	Cr^{3+}
CoCr	-	576.6 (2.2)	586.5 (2.3)	9.9	Cr^{3+}
		578.2 (2.8)	588.0 (2.7)	9.8	Cr^{3+}
CNCr-1	960.0 (3.7)	576.3 (2.2)	586.2 (2.5)	9.9	Cr^{3+}
		578.1 (3.0)	588.0 (3.1)	9.9	Cr^{3+}
CNCr-2	960.0 (4.0))	576.1 (2.2)	585.9 (2.5)	9.8	Cr^{3+}
		577.1 (2.7)	587.9 (2.9)	10.8	Cr^{3+} sat.
CNCr-3	960.1 (3.8)	576.0 (2.1)	585.9 (2.7)	9.9	Cr^{3+}
		577.6 (2.7)	588.4 (2.7)	10.8	Cr^{3+} sat.
NCr	-	576.2 (2.2)	586.1 (2.9)	9.9	Cr^{3+}
		577.8 (2.7)	588.6 (2.3)	10.8	Cr^{3+} sat.

Data from the O 1s region (Table 3.13.2) support the observations made in the Cr 2p doublet region. Two peaks can be fitted in the O 1s peak for a few materials (Figure 3.13.2), with the maximal peak at ca. 530.4 eV corresponding to metal oxide lattice oxygen. The second peak at higher binding energy (ca. 532.9/534.1 eV) is characteristic of surface hydroxyl oxygen species (chemisorbed / physisorbed water), present on metal oxide [37]. For a few materials, three peaks (Figure 3.13.1 and 3.13.3) can be fitted into the O 1s peak with the two higher energy peaks assigned as before.The peak at lower binding energy to the metal oxide lattice oxygen peak is due to Cr (III) — O[35].

Table 3.13.2 Binding energies of the oxygen photoelectron peaks obtained from the mixed transition metal oxides.

Oxide	Photoelectron peak binding energy (eV) [FWHM]		
	O 1 s		
CCr	-	530.4 (3.3)	-
CFCr-1	529.4 (1.3)	530.3 (2.4)	532.9 (2.7)
CFCr-2	529.2 (2.6)	530.4 (2.8)	-
CFCr-3	529.3 (1.4)	530.3 (2.2)	534.1 (2.3)
CF	-	530.3 (2.5)	534.1 (2.1)
FCr	529.2 (1.5)	530.3 (1.9)	534.1 (1.8)
CMCr-1	529.1 (2.7)	530.4 (2.1)	534.1 (2.6)
CMCr-2	529.2 (1.4)	530.4 (2.0)	532.9 (2.6)
CMCr-3	529.0 (1.6)	530.4 (2.4)	-
MCr	529.3 (1.9)	530.4 (2.2)	534.1 (2.3)
CCoCr-1	-	530.3 (2.8)	-
CCoCr-2	529.1 (1.7)	530.3 (3.0)	-
CCoCr-3	529.1 (1.8)	530.4 (3.0)	-
CoCr	529.3 (1.6)	530.4 (3.2)	-
CNCr-1	529.2 (1.4)	530.3 (2.0)	534.1 (2.3)
CNCr-2	529.3 (2.2)	530.4 (2.1)	532.9 (2.2)
CNCr-3	529.2 (1.4)	530.3 (2.0)	532.9 (2.3)
NCr	529.2 (1.5)	530.3 (1.9)	532.9 (2.0)

The chemical state of the metal ions (Fe, Ni, Co, Mn) in Cu-Fe, Cu-Ni, Cu-Co and Cu-Mn series was determined by measuring the BE of Fe $2p_{3/2}$, Ni $2p_{3/2}$, Co $2p_{3/2}$ and Mn $2p_{3/2}$ associated with the electron ejection from the $2p_{3/2}$ atomic orbital of the metal ions. The bands corresponding to the bivalent oxidation state, metal (II), are rather complex because they present several satellites (shake-up due to electron-transfer ligand-metal and multiplet splitting). The main peaks of Fe $2p_{3/2}$, Ni $2p_{3/2}$, Co $2p_{3/2}$ and Mn $2p_{3/2}$ in catalysts were found around 711.3 (Fe^{3+}), 710.6 (Fe^{2+}), 855.7 (Ni^{2+}), 780.2 (Co^{2+}) and 640.6 (Mn^{2+}), respectively; these values and shape of the component spectra agree well with those reported in the literature [38,39]. Co 2p spectrum shows principally the main peaks $2p_{1/2}$ and $2p_{3/2}$, without the shake-up lines which are typical for bivalent high spin cobalt [40]. In the case of bivalent cobalt compounds it is now generally accepted that the main peak corresponds to a final state $2p^5\,3d^8\,\underline{L}$ ($\underline{L}$ means a ligand hole) and the satellite peak to a $2p^5\,3d^7$ final state. The satellite structure is a result of multiplet splitting in the $2p^53d^7$ state [41]. The Co $2p_{3/2}$ and $2p_{1/2}$ spin-orbit splitting is almost identical for all samples and equal to 15.0 eV. The experimental data from experimental work on the characterisation of Ni(II)-O chemical bonding in $NiCr_2O_4$ and Cu-Ni series oxides reveal some resemblances between copper and nickel XPS spectra in spinels (Lenglet et al 1986).

As expected, the B.E.s and spin orbit splitting of the $2p_{3/2}$, and 3d emissions from the respective first row transition metals increased with increasing *Z* and oxidation state for the same element.

Table 3.13.3 Iron core binding energies from the mixed transition metal oxides

Oxide	Photoelectron peak binding energy (eV) [FWHM]			assgnt.
	$2p_{3/2}$	$2p_{1/2}$	ΔE_{so}	
CFCr-1	711.3 (2.6)	724.4 (3.2)	13.1	Fe^{3+}
	713.8 (3.1)	726.8 (2.7)	13.0	
CFCr-2	711.2 (3.2)	724.3(3.0)	13.1	Fe^{3+}
	713.8 (3.5)	727.0 (3.9)	13.2	
CFCr-3	711.0 (3.0)	724.1 (3.5)	13.1	Fe^{3+}
	713.6 (3.4)	726.8 (3.6)	13.2	
CF	711.2 (2.8)	724.3 (2.4)	13.1	Fe^{3+}
FCr	710.6 (2.8)	723.6 (2.4)	13.0	Fe^{2+}
	713.3 (2.9)	726.3 (2.4)	13.0	

Table 3.13.4 Ni core binding energies from the mixed transition metal oxides

Oxide	Photoelectron peak binding energy (eV) [FWHM]			assgnt.
	$2p_{3/2}$	$2p_{1/2}$	ΔE_{so}	
CNCr-1	855.6 (2.6)	872.9 (2.4)	17.3	Ni^{2+}
	861.5 (2.7)	878.8 (1.8)	17.3	
CNCr-2	855.8 (2.8)	873.1 (3.4)	17.3	Ni^{2+}

	861.6 (2.9)	878.8 (3.0)	17.2	
CNCr-3	855.7 (3.1)	873.0 (3.6)	17.3	Ni^{2+}
	861.8 (3.2)	879.0 (3.4)	17.2	
NCr	855.7 (3.0)	873.0 (3.1)	17.3	Ni^{2+}
	861.7 (3.7)	879.1 (3.6)	17.4	

Table 3.13.5 Mn core binding energies from the mixed transition metal oxides

Oxide	Photoelectron peak binding energy (eV) [FWHM]				assgnt.
	Mn LMMb	$2p_{3/2}$	$2p_{1/2}$	ΔE_{so}	
CMCr-1	944.0 (4.1)	640.8 (2.6)	652.0 (2.5)	11.2	Mn^{2+}
		642.8 (2.7)	654.1 (2.4)	11.3	
CMCr-2	944.2 (2.7)	640.6 (2.3)	651.8 (2.4)	11.2	Mn^{2+}
		642.9 (2.2)	654.2 (2.4)	11.3	
CMCr-3	944.1 (3.2)	640.4 (2.6)	651.6 (2.9)	11.2	Mn^{2+}
		642.9 (3.3)	654.2 (3.1)	11.3	
MCr	-	640.7 (2.6)	651.9 (2.2)	11.2	Mn^{2+}
		643.1 (2.6)	654.3 (2.1)	11.2	

Table 3.13.6 Co core binding energies from the mixed transition metal oxides

Oxide	Photoelectron peak binding energy (eV) [FWHM]			assgnt.
	$2p_{3/2}$	$2p_{1/2}$	ΔE_{so}	
CCoCr-1	780.4 (3.5)	795.4 (3.0)	15.0	Co^{2+}
CCoCr-2	780.3 (3.0)	795.3 (3.1)	15.1	Co^{2+}
CCoCr-3	780.1 (3.4)	795.1 (3.0)	15.0	Co^{2+}
CoCr	780.2 (3.0)	795.2 (3.2)	15.0	Co^{2+}

The XPS characteristics of the Cu $2p_{3/2}$, lines in copper-based compounds of a spinel structure are reported in Table 3.13.7. The Cu $2p_{3/2}$ peak is typical of a Cu (II) species, in terms of both the BE value and the shape of its intense satellite structure; it is indeed known, and invariably confirmed by literature reports, that shake-up peaks appear in ESCA signals from copper whenever it attains the paramagnetic $3d^9$ configuration in its + 2 oxidation state [36,42]. Shake-up peaks are absent in d^{10} Cu (I) species. In the case of Cu^{2+}, the satellite peak is believed to arise from the transfer of electrons from the O 2p band into the 3d band via the 4sp band, with the transfer facilitated by core hole-induced polarization of these 3d electrons relative to those in the O 2p band [43-45].

The Cu 2p binding energies and chemical shifts for mixed Cu-Ni, Cu-Mn, Cu-Co and Cu-Fe chromites, which are identical with those of copper

chromite $CuCr_2O_4$, reveal the Cu^{2+} contribution to the crystallographic distortion [46].

Table 3.13.7 Cu core binding energies from the mixed transition metal oxides

Oxide	Photoelectron peak binding energy (eV) [FWHM]			assgnt.
	$2p_{3/2}$	$2p_{1/2}$	ΔE_{so}	
CCr	934.6 (1.5)	954.3 (2.0)	19.7	Cu^{2+}
CFCr-1	934.4 (2.5) 934.6 (2.5)	954.1 (2.0) 954.4 (1.7)	19.7 19.8	Cu^{2+}
CFCr-2	934.5 (3.4) 942.6 (4.2)	954.2 (3.1) 962.4 (3.0)	19.7 19.8	Cu^{2+}
CFCr-3	934.4 (2.7)	954.1 (2.5)	19.7	Cu^{2+}
CF	934.6 (2.9)	954.3 (2.4)	19.7	Cu^{2+}
CMCr-1	934.4 (2.6)	-	-	Cu^{2+}
CMCr-2	934.5 (2.6)	-	-	Cu^{2+}
CMCr-3	934.6 (2.4)	-	-	Cu^{2+}
CCoCr-1	934.7 (2.4)	954.4 (2.6)	19.7	Cu^{2+}
CCoCr-2	934.6 (2.2)	-	-	Cu^{2+}
CCoCr-3	934.7 (1.3)	-	-	Cu^{2+}
CNCr-1	934.5 (2.8)	-	-	Cu^{2+}
CNCr-2	934.6 (2.7)	-	-	Cu^{2+}
CNCr-3	934.6 (2.5)	-	-	Cu^{2+}

In addition to the expected photoelectron peaks, the spectrum in Fig.

3.13.2 and 3.13.3 also exhibits peaks due to Auger electrons. These originate because the atom from which the photoelectron has left is a highly excited ion, with a hole in one of its inner shells. This ion relaxes according to the scheme given on the right of Figure 3.13.4. One readily sees that Auger electrons have fixed kinetic energies that are independent of the energy that created the initial core hole. Nevertheless, Auger peaks are plotted on the binding energy scale, which has of course no physical significance. The main peak of the Cr LMMa and Mn LMMb Auger signal in Fig. 3.13.2 and 3.13.3 has a kinetic energy of about 486.4 and 542.4 eV, but appears at a binding energy of about 960.2 and 944.2 eV respectively; because the spectrum was taken with AlKa X-rays of 1486.6 eV. Auger peaks can be recognized by recording the spectrum at two different X-ray energies: XPS peaks appear at the same binding energies, while Auger peaks will shift on the binding energy scale. This is the main reason why X-ray sources often contain a dual anode of Mg and Al.

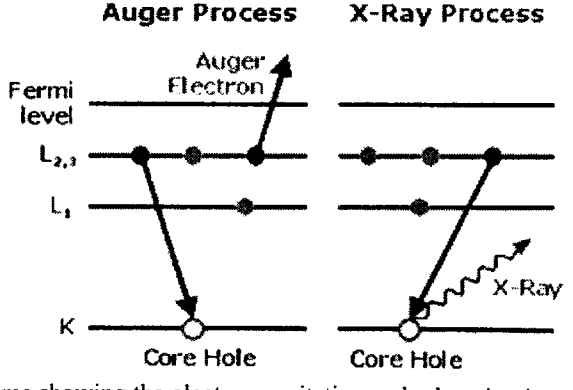

Fig.3.13.4 A scheme showing the electron excitation and relaxation in x-ray photoelectron spectroscopy (XPS) and Auger spectroscopy.

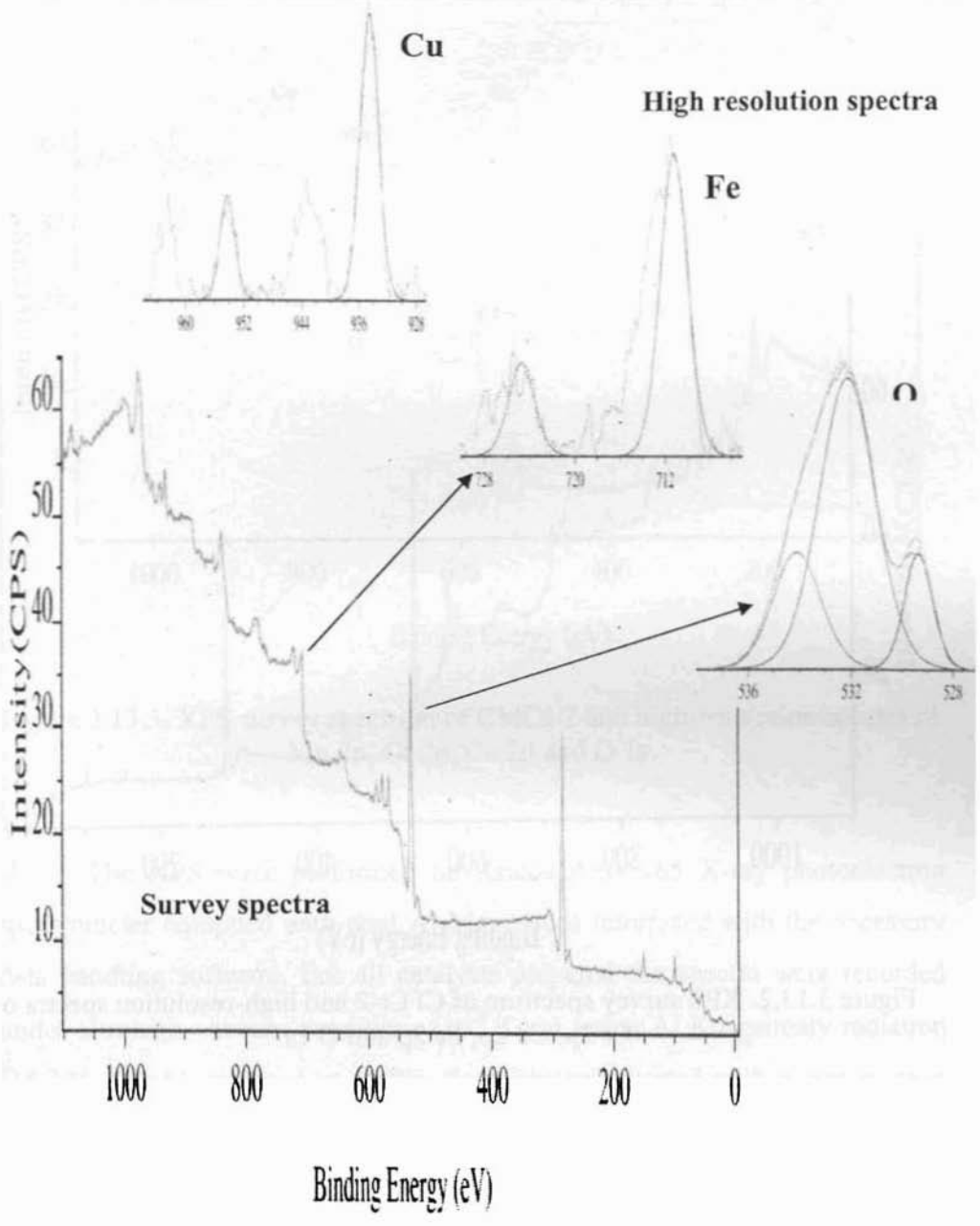

Figure 3.13.1. XPS survey spectrum of CF and high-resolution spectra of Cu2p, Fe2p and O1s.

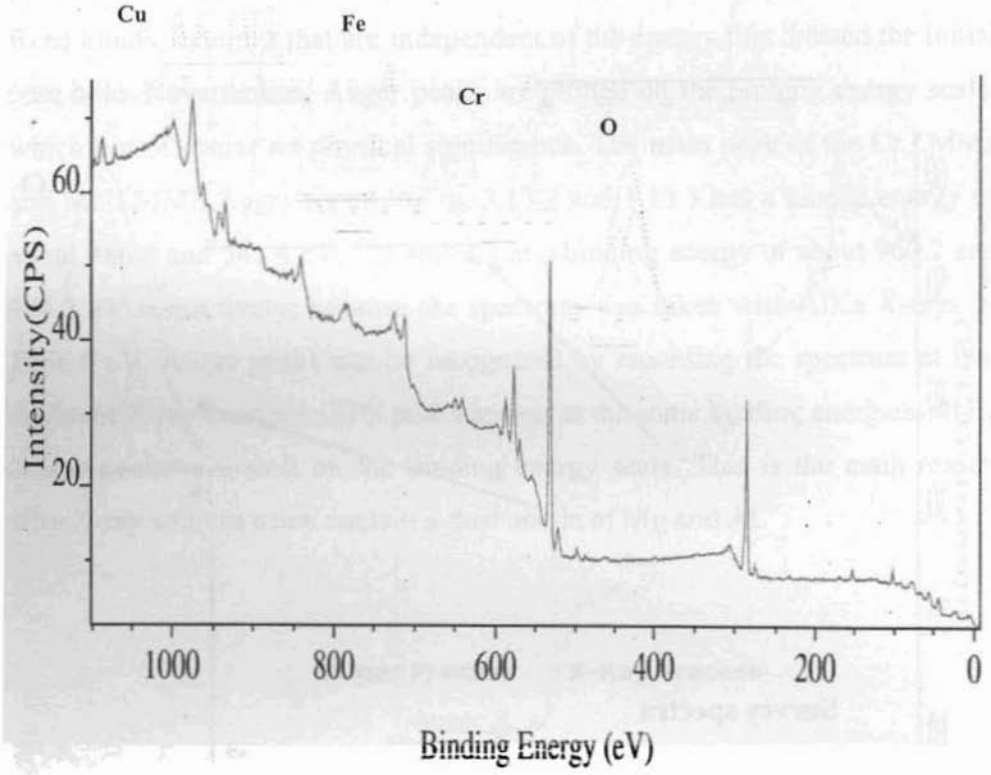

Figure 3.13.2. XPS survey spectrum of CFCr-2 and high-resolution spectra of Cr 2p, Cu 2p, Fe 2p and O 1s.

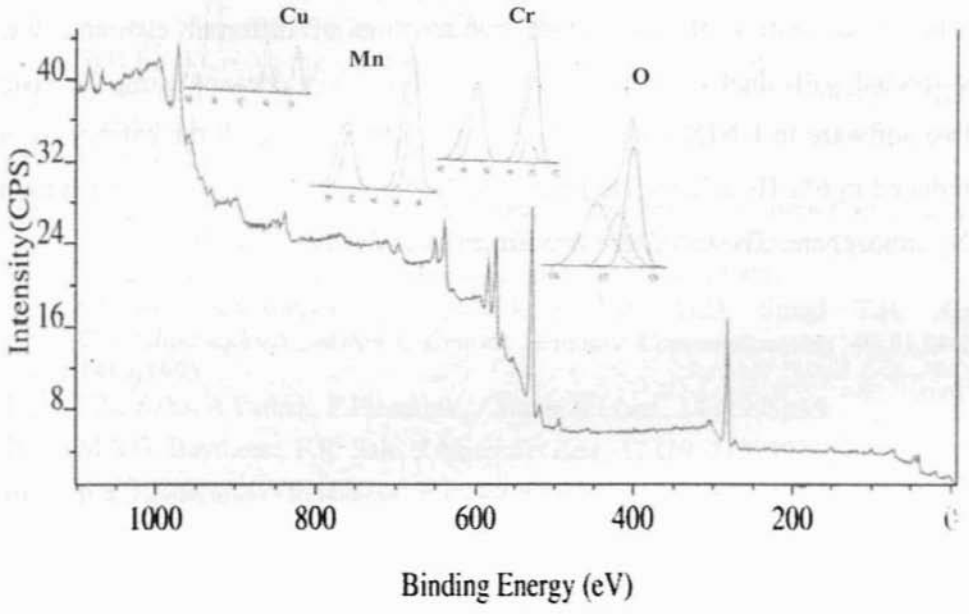

Figure 3.13.3. XPS survey spectrum of CMCr-2 and high-resolution spectra of Mn 2p, Cr 2p, Cu 2p and O 1s.

The XPS were performed on Kratos Axis 165 X-ray photoelectron spectrometer equipped with dual Al-Mg anodes interfaced with the necessary data handling software. For all catalysts prepared the spectra were recorded under ultrahigh vacuum conditions (10^{-9} Torr), using Al Kα primary radiation (15 kV, 5 mA) operated at 150W. Each analysis started with a survey scan from 0 to 1200 eV with a dwell time of 100 milliseconds, pass energy of 160 eV at steps of 1eV with one sweep. For the high-resolution analysis, the number of sweeps was increased, the pass energy was lowered to 80eV at steps of 100 meV and the dwell time was changed to 250 milliseconds. The spectra

were charge corrected using the advantageous C 1s signal at 284.6 eV. The relative intensities of the surface composition of different elements were corrected with their corresponding atomic sensitivity factors using the vision two software in UNIX system. Prior to the XPS studies, all the catalysts were reduced in 6% H_2 balance He flow at 523K for 4 h, followed by passivation in N_2 atmosphere. The estimated experimental error is (+/-) 0.2 eV.

REFERENCES

[1] J. W. Niemantsverdriet, "Spectroscopy in Catalysis: An Introduction", WILEY-VCH Verlag GmbH & Co. KGaA, Weinheim (2007).

[2] C.Whiston; "X-ray Methods", (Eds., F.E.Prichard), ACOL, Thames Polytech., London (1991).

[3] R.D. Waldron; *Phy.Rev.*, 99(1955) 1727.

[4] I. Chorkendorff, J. W. Niemantsverdriet, "Concepts of Modern Catalysis and Kinetics", WILEY-VCH Verlag GmbH & Co. KGaA, Weinheim (2003).

[5] Jendrzejewska I, *J. Alloys Compounds,* 305 (1), 90-92 (2000).

[6] Okonska Kozlowska I, Kopyczok J, Lutz H.D, Stingl T.H, *Acta Crystallographica Section C-Crystal Structure Communications,* 49(8),1448-1449(1993

[7] S.K. Saha, A.Pathak, P.Pramanik, *J.Mater.Sci.Lett.*, 14 (1995) 35.

[8] M.S.G. Baythoun, F.R. Sale, *J.Mater.Sci.Lett.*, 17 (1982) 2757.

[9] P.A.Jacobs and C.F. Heylen, *J.Catal.*,34 (1974) 2.

[10] A. Satsuma, Y.Kamiya, Y.Westi and T.Hattori, *Appl. Catal.*, 194-195 (2000) 253.

[11] Lutz H.D, Waschenbach G, Khiche G, Hacuseler H, *J. Solid State Chem.*48 (2),196-208 (1983).

[12] Basak D, Ghose J, *Spectrochimica Acta Part A: Molecular Spectroscopy,* 50(4),713-718 (1994).

[13] Preudhomme J, Tarte P, *Spectrochimica Acta Part A: Molecular Spectroscopy,*27 (90), 1817-1835 (1971).

[14] W.B.White andB.A.DeAngelis; *Spectrochemica Acta*, 23 A (1967) **985**

[15] S.D. Ross, "Inorganic infrared and Raman spectra", Mc Graw Hill, London, 1972.

[16] L.Platron et al. , Materials Research Bulletin 36 (2001)1271.

[17] Jianjun Guo et al., *Materials Letter*, 58,1920-1923 (2004).

[18] G. Busca, *Catal.Today,* 27 (1996) 323.

[19] H.Knozinger, *Adv.Catal.*25 (1976) 184.

[20] C.H.Kline, J.Turkevich, *J.Chem.Phys.12* (1944) 300.

[21] G. Busca, *Catal.Today,* 41 (1998) 191.

[22] G.Busca, V. Lorenzelli, G.Ramis and R.J. Willey, *Langmuir*, 9 (1993) 1492.

[23] G.Busca , V. Lorenzelli, V.S. Escribano and R. Guidetti, *J.Catal.*, 131 (1992) 167.

[24] S.Ghorpade, V.S.Darshane and S.G. Dixit, *Appl.Catal.A.General*, 166 (1998) 135.

[25] Miyahara, S., and Ohnishi, H., 1956, *Journal of the Physical Society of Japan*, Vol.11, pp. 1296.
[26] Sawaoka, A., Saito, S., Inoue, K., and Asada, T., *Material Review Bulletin*, Vol. 6, No. 2, pp. 97-102. (1971).
[27] A.B.P. Lever, "Inorg.Electronic Spectroscopy", Elsevier Publishing Company, 1968, pp.335.
[28] Gru¨nert, W., Shpiro, E. S., Feldhaus, R., Anders, K., Antoshin, G. V., and Minachev, Kh. M., *J. Catal.* 100, 138 (1986).
[29] Allen, G. C., and Tucker P. M., *Inorg. Chim. Acta* 16, 41 (1976).
[30] Allen, G. C., Curtis, M. T., Hooper, A. J., and Tucker, P. H., *J. Chem. Soc. Dalton Trans.* 1675 (1973).
[31] Cimino, A., De Angelis, B. A., Lucchetti, A., and Minelli, G., *J. Catal.* 45, 316 (1976).
[32] Okamoto, Y., Fuiji, M., Imanaka, T., and Teranishi, S., *Bull. Chem. Soc. Jpn.* 49, 859 (1976).
[33] Jagannathan K., Srinivasan, A., and Rao, C. N. R., *J. Catal.* 69, 418 (1981).
[34] Best, S. A., Squires, R. G., and Walton, R. A., *J. Catal.* 47, 292 (1977).
[35] Philip G. Harrison, Nicholas C. Lloyd, Wayne Daniell, Ian K. Ball, Craig Bailey, and Wan Azelee, *Chem. Mater.* 2000, *12,* 3113-3122
[36] Brooks, A. R.; Clayton, C. R.; Doss, K.; Lu, Y. C. *J. Electrochem. Soc.* 1986, *133*, 2459.
[37] J.R. Mycroft, H.W. Nesbitt and A.R. Pratt, *Geochimica et Cosmochimica Acta,* Vol. 59, No.4 (1995) pp-728.
[38] John F.Moulder *et.al,*"Handbook of X-ray Photoelectron Spectroscopy", Perkin-Elmer Corporation, USA (1992).
[39] M. Aronniemi *et al., Surface Science,* 601 (2007) 486.
[40] V A M Brabers and F van Setten, J. Phys. D: Appl. Phys., 16 (1983) L169-L172.
[41] G. Fierro, R. Dragone, G. Moretti and P. Porta, Surf. Interface Anal. 19 (1992) 565.
[42] P. E. Larson, J. Electron Spectrosc. Relat. Phenom., 4 (1974) 213.
[43] S. Hufner, "Photoelectron Spectroscopy: Principles and Applications", 3rd ed., Springer, Berlin, 2003.
[44] A. Kotani, Y. Toyozawa, J. Phys. Soc. Jpn. 37 (1974) 912.
[45] M.A. van Veenandaal, H. Eskes, G.A. Sawastsky, Phys. Rev. B 47 (1993) 11462.
[46] M Lenglett, A d'Huyssert, J Arskne, J P Bonnellez and C K Jorgensens, *J. Phys. C: Solid State Phys.* 19 (1986) L363-L368.

CHAPTER 4

THERMAL DECOMPOSITION REACTIONS

Abstract

Thermal methods provide a new means of solving existing chemical problems, as well as creating new ones. Thermal instrument can provide rapid information concerning the thermal stability, composition of pyrolysis intermediates, and composition of the final product, as a compound is heated to elevated temperatures. Ammonium perchlorate (AP) is one of the showcase examples of a thermally labile material that can undergo a decomposition process at high temperature, leading to its use in applications such as rocket propulsion. The thermal decomposition characteristics influence the combustion behavior of the propellant. The catalytic activities of transition metal oxides in the thermal decomposition of ammonium perchlorate have been done extensively. Thermogravimetric analysis (TGA) and differential thermal analysis (DTA) have been used to study the thermal decomposition of ammonium perchlorate. Because, combustion phenomena involve high reaction temperatures, this study was limited to temperatures greater than 240°C, the temperature at which AP changes crystal form from orthorhombic to cubic.

4.1 THERMAL DECOMPOSITION OF AMMONIUM PERCHLOTRATE

Perkin Elmer Pyris Diamond TG-DTA analyzer was used at a heating rate of 10°C/min in N_2 atmosphere at a flow rate of 200mL/min over the range 50–550 °C with Al_2O_3 as reference in a platinum crucible without lids. The results of the TG-DTA experiments are shown in Figs. 4.1.1 and 4.1.2. The DTA and TG results are also summarized in Table 4.1.1. The absence of yellow tinge on AP suggested the use of it without re-crystallization. TG-DTA was run with AP as such (AP bulk) and with AP that was ground mechanically and sieved to get uniform 150μm particles (AP-150 μm).

The DTA curve for AP bulk (Fig. 4.1.1) shows four events, while, the TG curve exhibits only three. The first endothermic DTA peak with a peak temperature of 237°C is accompanied with zero weight loss. This represents the transition from orthorhombic to cubic AP [1]. The first two exothermic DTA peak with a peak temperature of 320 and 361 °C corresponding 5 and 25% weight loss is attributed to the partial decomposition of AP and formation of some intermediate NH_3 and $HClO_4$ by dissociation and sublimation [2-4]. The third exothermic DTA peak with a peak temperature of 411 °C associated with 81% weight loss is caused by the complete decomposition of the intermediate to volatile products [2]. In the case of AP-150 μm the first exothermic peak occurs at 350 °C changed into a sharp one associated with only one step weight loss. The second exothermic was absent.

Moreover, as can be seen in TG trace in Fig. 4.1.1 and 4.1.2, the onset temperature of thermal decomposition of AP bulk is at 300°C and the end temperature is at 425°C.The onset temperature of thermal decomposition of AP-150 μm is at 270°C and the end temperature is at 365°C. So, the speed of thermal decomposition were found to exhibit in an order of AP-150 μm > AP bulk.

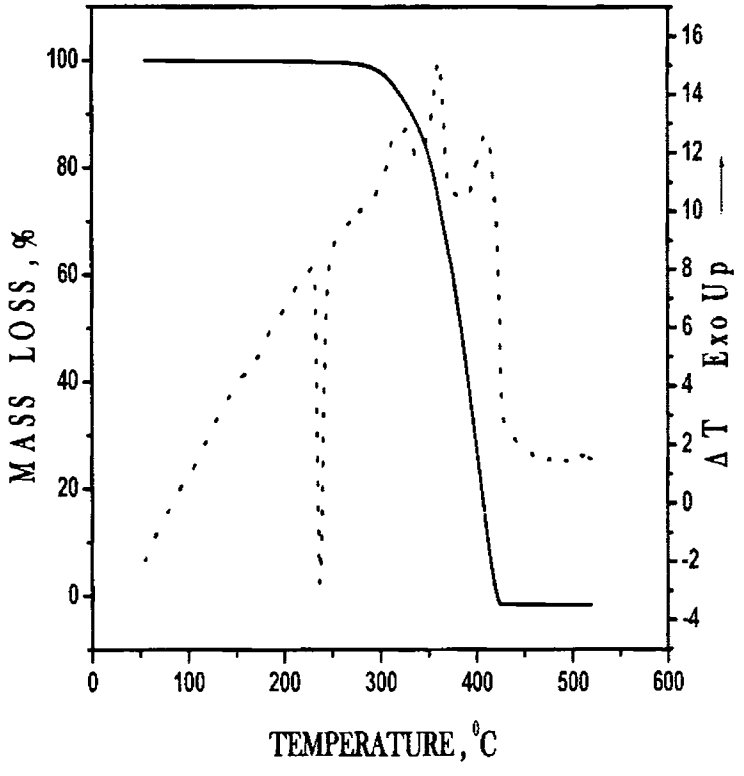

Fig.4.1.1 Solid line represents TG and dotted line represents DTA trace of bulk ammonium perchlorate.

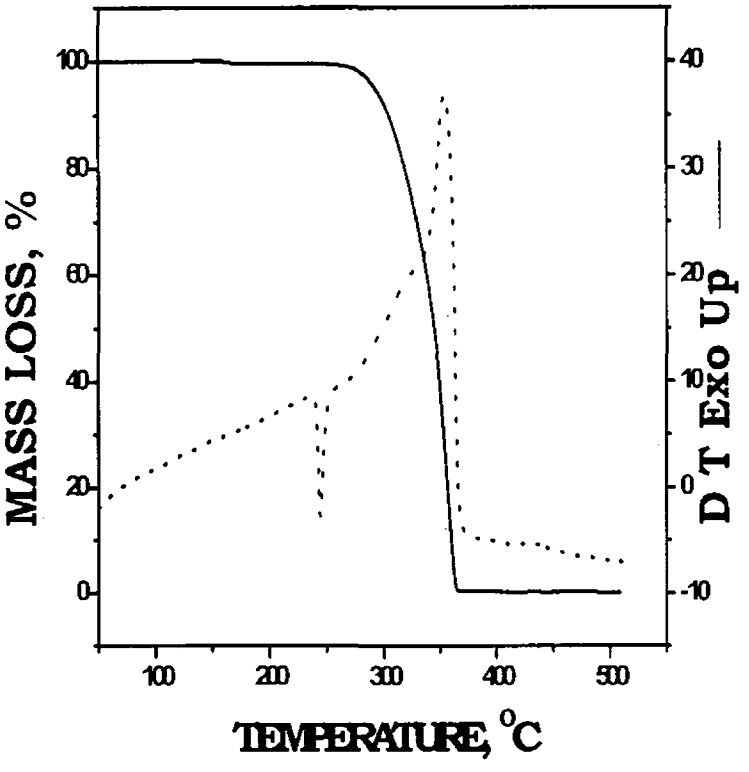

Fig.4.1.2 Solid line represents TG and dotted line represents DTA trace of ammonium perchlorate (150μm).

Table 4.1.1 Data from TG-DTA of pure AP

Sample ID	DTA peak		DTG peak	% Mass loss
	Endo	Exo		
AP- bulk	237	320	314	5
		361	360	25
		411	406	81
AP – 150μm	240	350	352	75

4.2 EFFECT OF HEATING RATE

All runs were performed on small samples (2-3mg) to minimize self-heating and cooling. In all instances, non-isothermal programs were employed with a heating cycle from 50 to 550 °C. The effect of heating rate change on the procedural decomposition temperatures of a sample has been studied under N_2 atmosphere. Experimental results of thermal analysis are markedly affected by heating rate. The initial temperature T_i, peak temperature Tp and final temperature T_f shift to the high temperature side with increasing heating rate [5]. When the thermal decomposition of AP (150μm) is measured in N_2 atmosphere at a heating rate ranging from 2.5 to 40 °C min^{-1}, T_i shifts from 255 to 315 °C and T_f from 350 to 425 °C (Figure 4.2.1). When the heating rate is high, the reaction takes place with greater speed in the higher temperature region. The reaction finishes within a narrow temperature interval, and on this account the derivative curves (DTG and DTA curves) become sharper (Figure 4.2.2). When multiple reactions are observed, individual reactions are clearly

resolved by slower heating rates for DTA curves. The inflection on the TG curve, which is observed at a high heating rate, changes into a more pronounced horizontal mass plateau at a low heating rate. When the heating rate is controlled dynamically and continuously in response to the reaction of the sample, sharper resolution can be observed, as shown in Figure 4.2.

In general slow heating rates requires a more sensitive registering system for DT to obtain comparable accuracy, whereas with fast heating rates a lower sensitivity is necessary but neighbouring peaks tend to coalesce. For normal work, rates of 8-12 °C/min are commonly used, since peaks are of satisfactory size, overlap of neighbouring peaks is not excessive and the time per determination is reasonable [6].

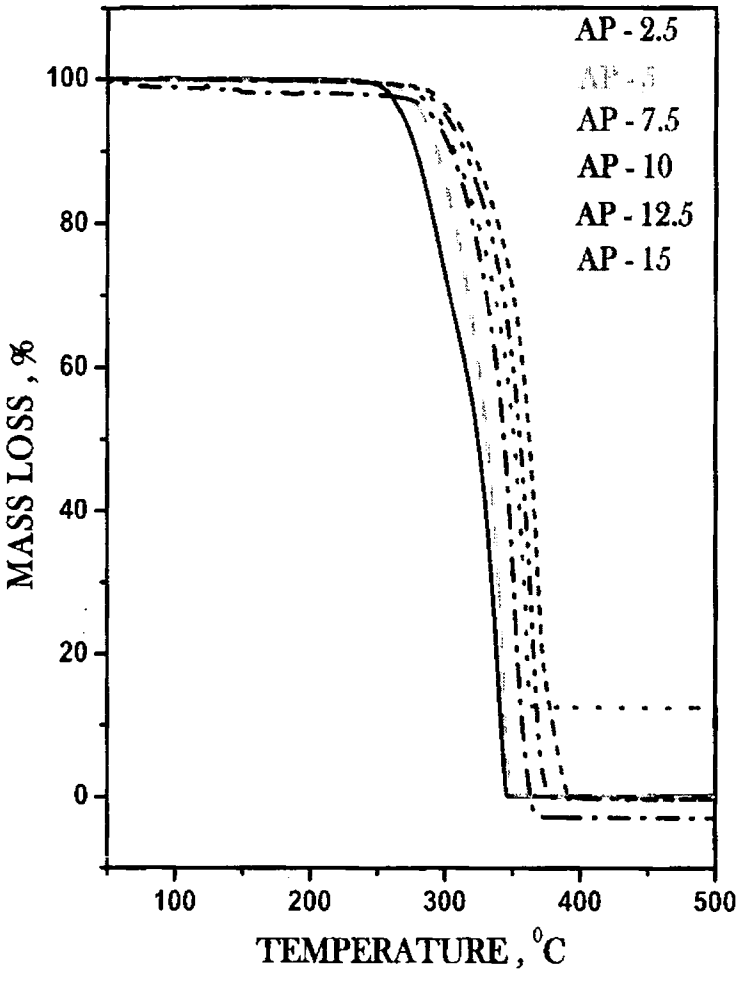

Fig.4.2.1 TG trace of AP-150μm at different heating rates

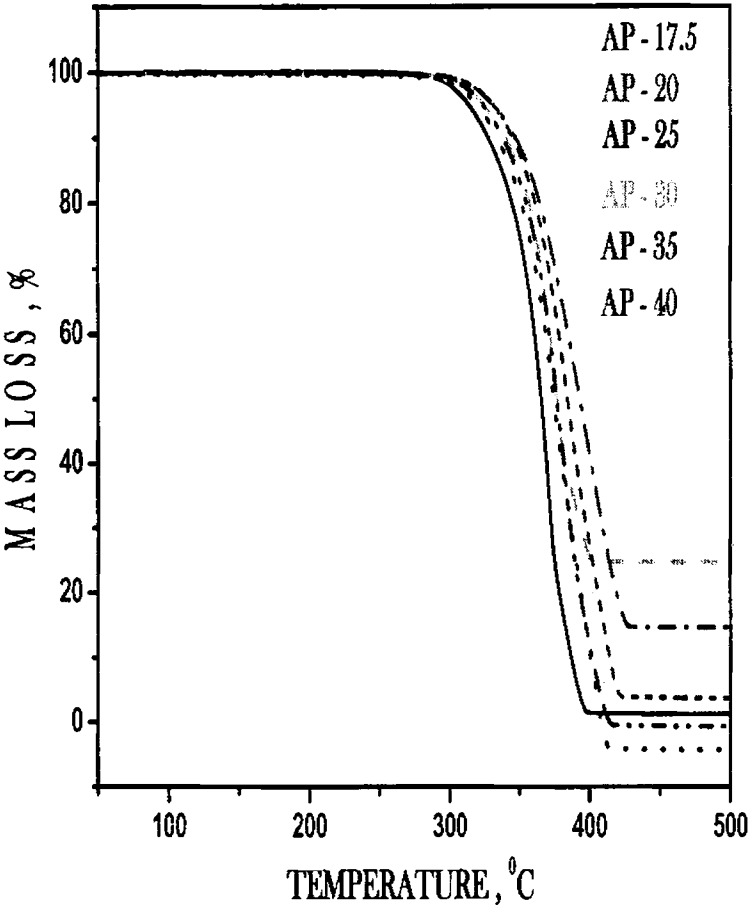

Fig.4.2.1 TG trace of AP-150μm at different heating rates

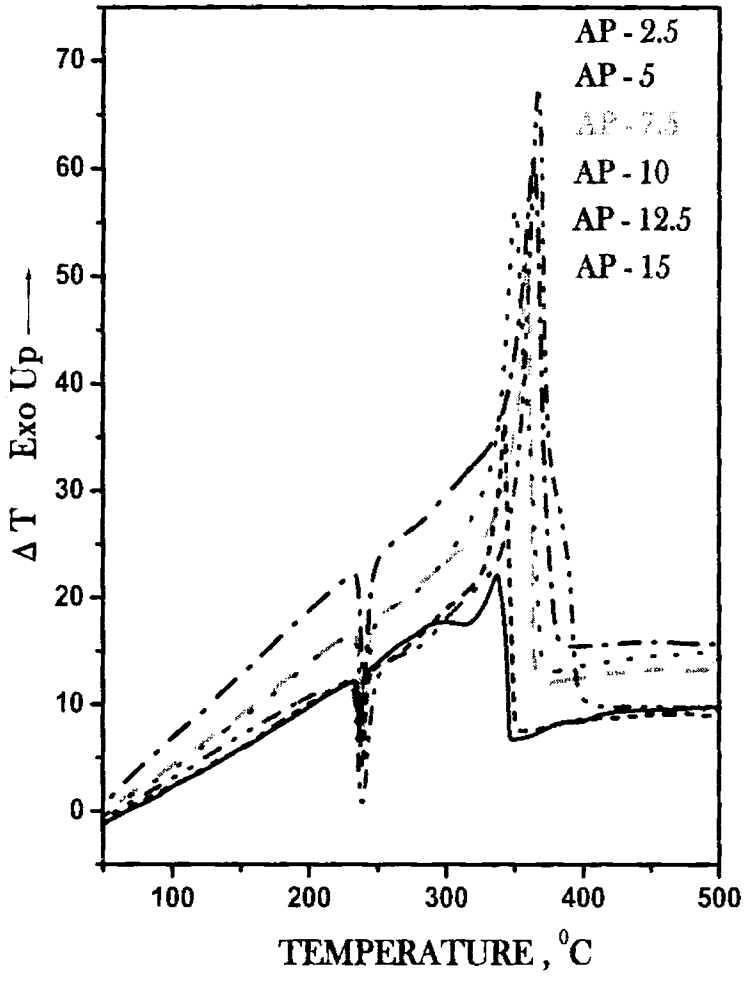

Fig.4.2.2 DTA trace of AP-150μm at different heating rates

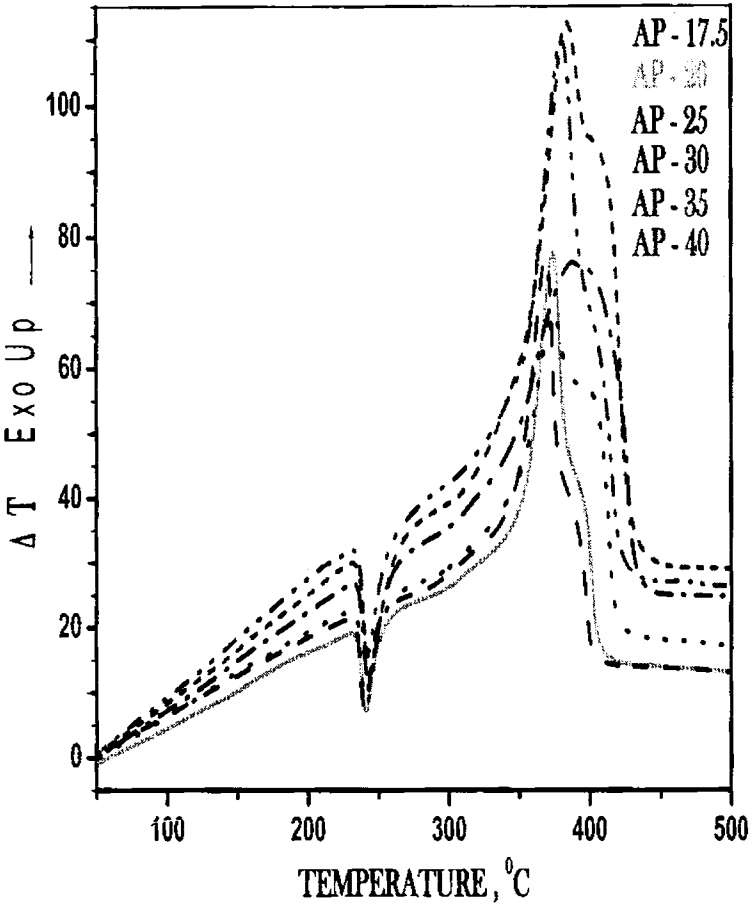

Fig.4.2.2 DTA trace of AP-150μm at different heating rates

Table 4.2.1 Data from TG-DTA of AP and AP with CCr at different heating rates.

Sl.No.	Sample ID	Heating rate	DTA peak			DTG peak	% Weight loss	DTG peak	% Weight loss
			Endothermic	Exothermic					
1	AP	2.5	237	315	338	292	20	339	82
2	AP	5	239	-	343	-	-	344	88
3	AP	7.5	239	-	359	-	-	360	52
4	AP	10	240	-	350	-	-	352	75
5	AP	12.5	240	-	364	-	-	365	78
6	AP	15	239	-	367	316 369	8 71	387	97
7	AP	17.5	240	-	369	372	69	392	95
8	AP	20	241	374	401	375	52	399	88
9	AP	25	241	374	393	376	50	397	74
10	AP	30	243	-	388			399	58
11	AP	35	242	380	403	382	62	404	93
12	AP	40	244	384	410	385	52	408	83
13	AP-CCr	5	242	273 315	327	305	34	327	82
14	AP-CCr	7.5	242	280 317	334	311	13	334	34
15	AP-CCr	10	242	324	337	317	31	341	76
16	AP-CCr	12.5	242	317	334	311	36	335	90
17	AP-CCr	15	243	324	339	315	30	341	80
18	AP-CCr	40	245	-	368	-	-	371	85

4.3 EFFECT OF MORPHOLOGY

Because of the high percentage in the propellant formulation, the performance of the propellants varies with the oxidizer properties, and in turn, the performance of the oxidizer varies with the particles' size and morphology [7]. Morphology control or morphogenesis of AP is achieved by the use of a super-molecular matrix like poly-vinyl alcohol (PVA).

An aqueous solution containing 2.5 wt% PVA (1,25,000 ml.wt) by dissolving the polymer in distilled water at 80 °C, and an AP solution of 1 M concentration was prepared by dissolving a weighed amount of AP crystals in distilled water. The salt solution was mixed with the aqueous PVA solution in various proportions [8]. Two different proportions, with the PVA-to-salt solution ratio as 1:1 (AP-PVA 1:1) and 4:1 (AP-PVA 4:1), were made and thoroughly mixed by vigorous stirring. The temperature during the mixing time was kept near 80 °C by keeping the mixture in a water bath.

After thorough mixing of the solutions, the mixture was cooled to room temperature and then kept in sealed conditions. The sample was drawn after 24h and was placed on a glass slide and dried in a desiccator. The dried samples were characterized by powder X-ray diffraction (PXRD) to study the structure of the compound. Scanning electron microscopy (SEM) images were taken to understand the morphology of the AP particles.

The crystals grown from both the mixture have rectangular wedge morphology. It is evident form the SEM micrographs. The representative SEM micrographs are depicted in the Figure 4.3.4 and 4.3.5.

The diffraction lines (Figure 4.3.3) of the AP crystals coincide with those of the ASTM card (JCPDS 43-648) but differ from one another in relative intensities, confirming that the super structure is composed of well-crystallized AP particles and that there is no change in the basic crystal structure.

The advantage of using PVA as a habit modifier is a reduced agglomeration, leading to samples containing only individual particles. Studies show that, for a chemical system in which PVA and AP molecules are involved, the PVA induces the crystallization of individual AP crystals irrespectively of the polymer-substrate concentration variations.

The performance of synthesized catalysts in the thermal decomposition of modified AP was investigated by simultaneous TG-DTA measurements. All runs were performed in small samples (3mg) in an inert atmosphere (N_2 gas) of flow rate 200mL/min in an open platinum crucible at a rate of 10 °C /min. From the TG curves (Figure 4.3.1) it is seen that in the temperature range from 50 to 550 °C, only one mass loss was observed for pure AP, modified AP (AP-PVA) and mixture of AP-PVA with catalysts. The addition of catalysts dramatically decreased the AP decomposition temperature, consistent with our DTA measurements. Figure 4.3.2 shows the DTA curves of pure AP, AP-PVA and the mixture of AP-PVA with catalyst at a 1% mass basis. Only three thermal signals were observed for AP-PVA and two for mixture of AP with catalyst, which compares to the four obvious peaks for pure AP. The first endothermic peak around 237°C in all the systems analyzed is due to the crystal transformation of AP, while the second exothermic peaks occurred at temperatures above 300°C are attributed to the AP decomposition. The thermal decomposition of pure AP, depending on the quality of crystals, usually undergoes two or more steps. From Figure 4.3.2, it is seen that, for pure AP, there are three obvious exothermic peaks centered at about 320, 361 and 411°C. The first exothermic peak corresponds to the low-temperature

decomposition (LTD) and the next two exothermic peaks to high-temperature decomposition (HTD), respectively. For AP-PVA there are two exothermic peaks at 297 (LTD) and 352°C (HTD), and for AP-PVA-catalyst there is only one exothermic peak in low-temperature decomposition range. The modification of the AP lowers the decomposition temperature of AP by 59°C. The introduction of 1% of catalysts like CCr, MCr, and CoCr lowers the decomposition temperature drastically by 94, 111 and 110°C, respectively. All the catalysts studied lowers the decomposition temperature of AP to a great extend but MCr decomposes to the maximum extend (71 % weight loss). The appreciable differences between the catalytic performances of cubic AP and rectangular wedge shaped AP indicate that the morphology of AP particles affect the catalytic reaction much.

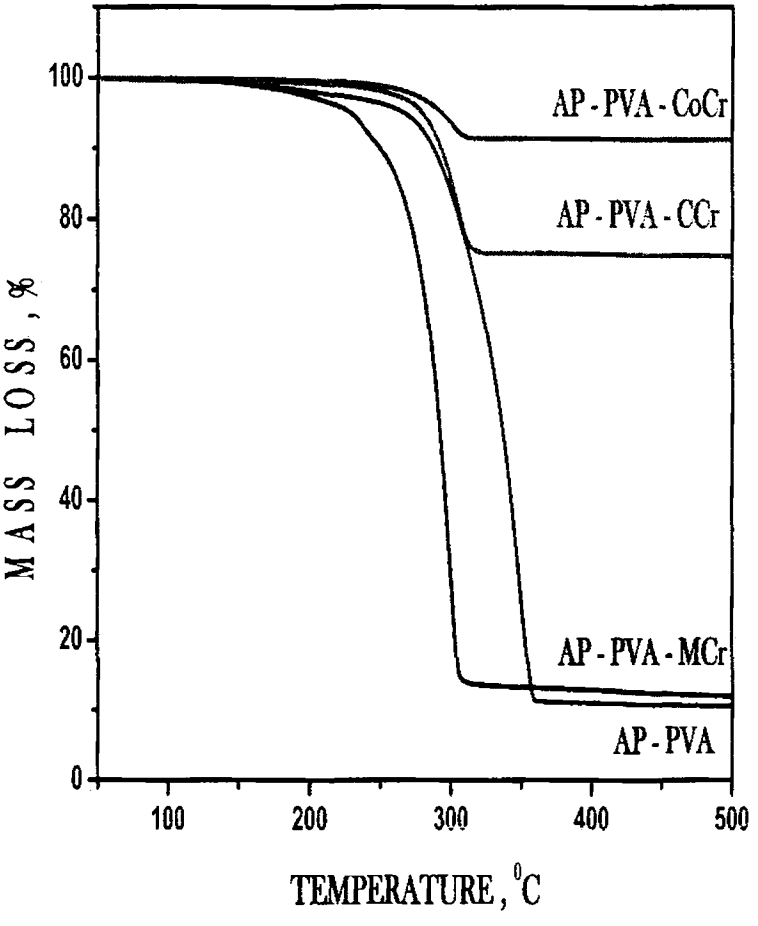

Fig. 4.3.1 TG trace of AP-PVA and AP-PVA-Catalyst.

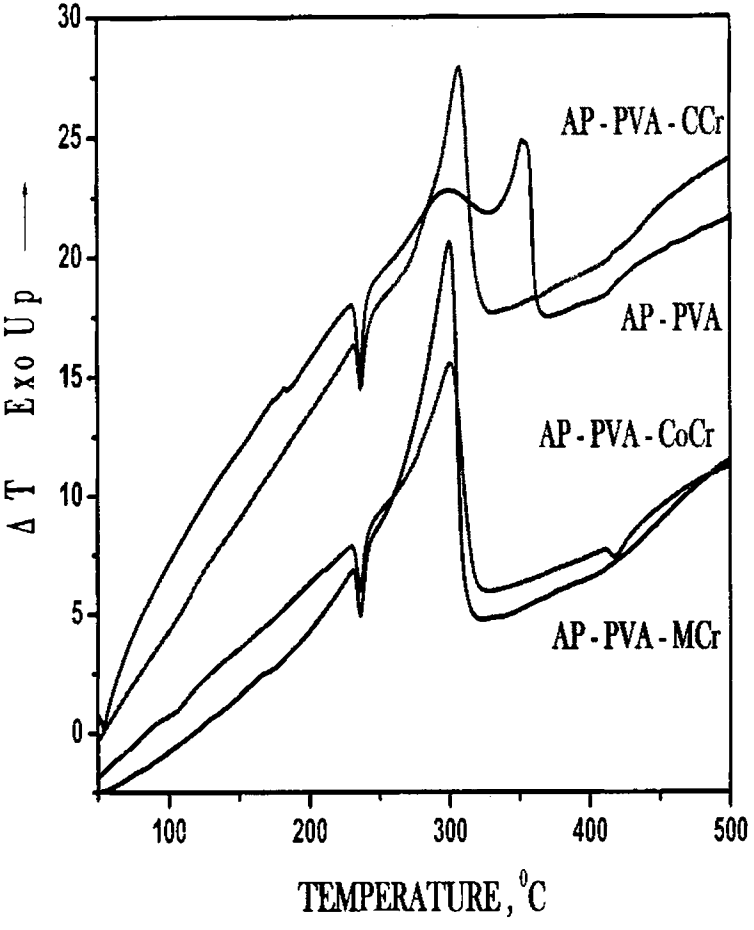

Fig.4.3.2 DTA trace of AP-PVA and AP-PVA-Catalyst.

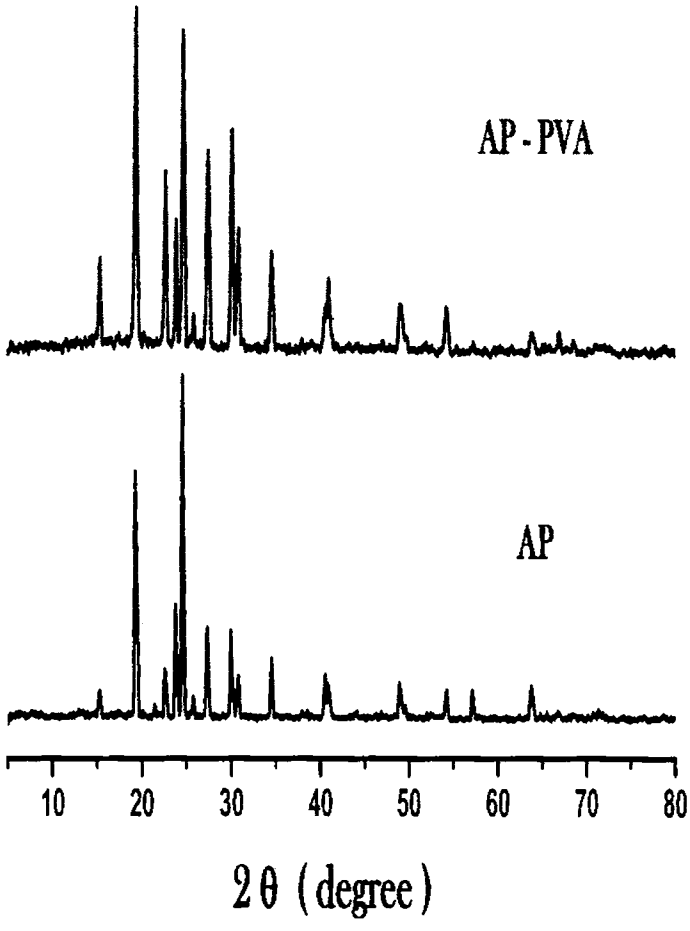

Fig. 4.3.4 XRD pattern of AP and AP-PVA

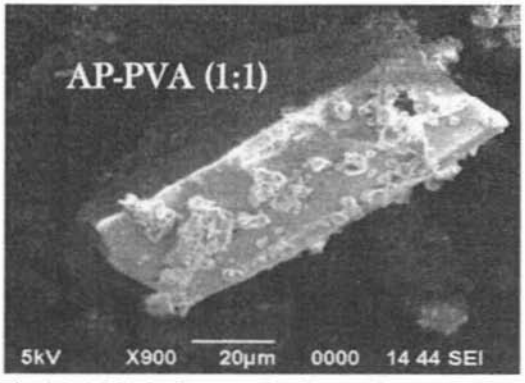

Fig.4.3.4 SEM micrograph of crystals grown from 1:1 solution of AP: PVA

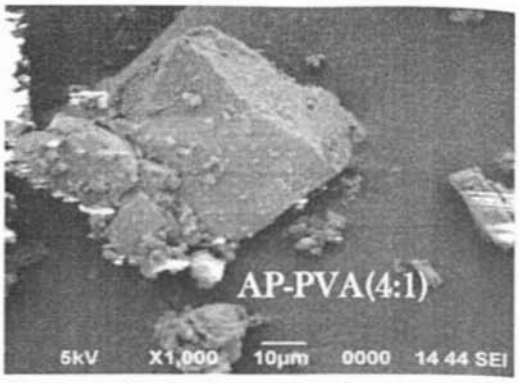

Fig. 4.3.5 SEM micrograph of crystals grown from 4:1 solution of AP: PVA

Table 4.3 TG-DTA summary of modified AP with and without 1% catalyst.

Sl.No.	Sample ID	morphology	DTA peak			DTG peak	% Weight loss	DTG peak	% Weight loss
			Endo	Exothermic					
1	AP	Cubic	237	320 361	411	314 360	5 25	406	81
2	AP-PVA	Rectangular wedge shape	237	297	352	293	12	350	75
3	AP-PVA - CCr	Rectangular wedge	236	-	307	-	-	305	18
4	AP-PVA - MCr	Rectangular wedge	235	-	300	-	-	300	71
5	AP-PVA - CoCr	Rectangular wedge	236	-	301	-	-	300	6

4.4 EFFECT OF FURNACE ATMOSPHERE

Perhaps the most widely studied instrument variable has been the effect of furnace atmosphere on the TG curve of a sample. The effect of the atmosphere on the mass-change curve depends upon (a) the type of reaction, (b) the nature of the decomposition products, and (c) the type of atmosphere

employed. All runs were performed on small samples (3mg) at a rate of 10°C/min in a platinum crucible without lid from 50 to 550°C. An inert gas (N_2) at a flow rate 200mL/min is employed to remove the gaseous decomposition products and to prevent the reaction occurring among the intermediates. If the atmosphere contains the same gas as is evolved in the reaction, only the reversible reaction will be affected and no effect will be observed on other reactions. The DTA characteristics in nitrogen do not differ significantly from those in air especially in the case of AP mixed with 1% catalyst. This is due to high oxygen balance of AP (+ 34%) that creates a similar atmosphere in an inert atmospheric condition.

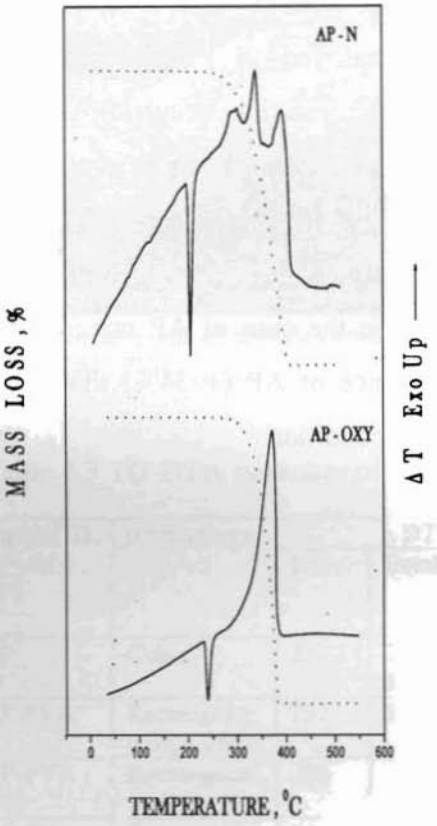

Fig 4.4.1 TG-DTA trace of AP (150μm) in nitrogen and air atmosphere.

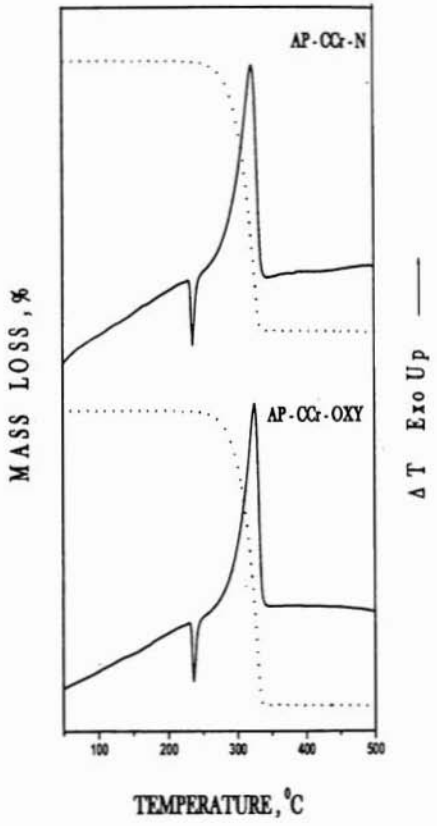

Fig 4.4.2 TG-DTA trace of AP (150μm) and 1% CCr in nitrogen and air atmosphere.

Table 4.4 TG-DTA summary of the decomposition of AP with and without 1% catalyst at different reaction atmosphere.

Sl.No.	Sample ID	atmosphere	DTA peak			DTG peak	% Weight loss	DTG peak	% Weight loss
			Endothermic	Exothermic					
1	AP-bulk	N_2	237	320 361	411	314 360	5 25	406	81
2	AP-bulk	air	240	-	373	-	-	380	99
3	AP-150μ	N_2	242	-	370	307	11	370	81
4	AP-150μ	air	239	321	348	319	28	350	90
5	AP-CCr	N_2	242	325	339	317	31	339	
6	AP-CCr	air	238	-	327	-	-	329	75
7	AP-CoCr	N_2	241	-	324	-	-	329	94
8	AP - CoCr	air	238	-	310	-	-	312	68
9	AP- CF	N_2	243	319	339	312	32	338	81
10	AP- CF	air	244	312	340	-	-	341	80
11	AP- FCr	N_2	246	-	354	-	-	354	80
12	AP- FCr	air	245	-	354	-	-	355	83
13	AP-NCr	N_2	242	326	349	307	15	351	81
14	AP-NCr	air	238	-	327	-	-	329	60
15	AP-MCr	N_2	238	-	305	-	-	306	62
16	AP-MCr	air	238	-	312	-	-	313	60

4.5 EFFECT OF RATE OF FLOW OF PURGE GAS

In all instances, non-isothermal programs were employed with a heating cycle from 50 to 550°C in an atmosphere of air at different low rate. The flow rate of the atmosphere does not appreciably affect the decomposition temperature of the sample.

Table 4.5 TG-DTA summary of the decomposition of AP with MCr at different rate of flow of purge gas in an oxidizing atmosphere.

Sample ID	DTA peak		DTG peak	% Mass loss
	Endo	Exo		
AP – MCr – OXY - 80mL	239	316	317	66
AP – MCr – OXY - 100mL	239	314	314	66
AP – MCr – OXY - 200mL	238	312	313	60

4.6 EFFECT OF PARTICLE SIZE OF AP

TG-DTA were carried out using Perkin Elmer Pyris Diamond TG-DTA computerised analyser with a heating rate of 10°C /min in a dynamic nitrogen atmosphere. α-Alumina was used as the reference material. Samples were in the form of a bimodal distribution of AP particles, i.e., coarse AP particles (150 μm) mixed with a fine AP (75μm). The decomposition of AP is independent of particle size of AP.

Table 4.6 TG-DTA summary of the decomposition of AP of different particle size.

Sample ID	DTA Peak		DTG
(75 μ : 150 μ)	Endo	Exo	
AP (1 : 1)	245	365	367
AP (1 : 2)	245	367	368
AP (1 : 4)	246	368	370
AP (1 : 5)	244	365	367

AP (2 : 1)	245	364	366
AP (4 : 1)	245	364	367
AP (5 : 1)	245	368	373

4.7 EFFECT OF CATALYST AMOUNT

The decomposition temperatures decreased as the catalyst percentage was increased. The thermal stability of the mixture decreased and spontaneous ignition occurred as the weight percentage of the catalyst in the mixture increased.

Table 4.7 TG-DTA summary of the decomposition of AP with varying amount of catalyst.

Sl.No.	Sample ID	DTA peak	
		Endothermic	Exothermic
1	AP	237	320 361 411
2	AP-CoCr-1%	242	334
3	AP-CoCr-2%	243	327
4	AP-CoCr-3%	241	326
5	AP-CoCr-4%	246	323
6	AP-CoCr-5%	242	317

4.8 EFFECT OF METAL CHROMITE CATALYST

The prepared spinel type oxides were explored as an additive to the thermal decomposition of ammonium perchlorate (AP), the key component of composite solid propellants. The performance of these spinels in the thermal

decomposition of AP was investigated by TG-DTA measurements. To reduce thermal gradients and exothermic self-heating, the experiments were performed on small (3mg) samples. Samples were placed in platinum crucible without lid and heated in a flowing atmosphere of nitrogen (200mL/min). The heating rate employed is 10°C/min.

We have examined the correlation between the catalytic activity, on the one hand, and the composition and structure, on the other, for the prepared chromite spinel oxides used as additives to ammonium perchlorate mixtures. This class of spinels was chosen because copper-chromium spinels have been found to be good combustion – rate accelerators [9], and also because the composition range from copper-chromium to copper-M (iron, cobalt, nickel, manganese) spinels allows one to determine how the position of the copper in the spinel lattice affects the catalytic activity.

The role of metal oxides in thermal decomposition of AP:

1. The oxide is generating species, which can initiate the thermal decomposition of AP.
2. It can also delay the decomposition by simple molar dilution effect.
3. The perchlorate oxide interface is the new center available for the decomposition to proceed.
4. The oxidizing power of the composite system can be different as compared to the pure AP.

As in our case all the catalysts studied are found to be accelerating and hence factor 2 is only marginal as compared to the other three factors.

The measurements of the effects of additives on the thermal decomposition of AP were made on mixtures based on AP (99 %) together with spinels (1 %), which acted as a catalyst (both AP and spinel was used as the 150 μm technical fraction).

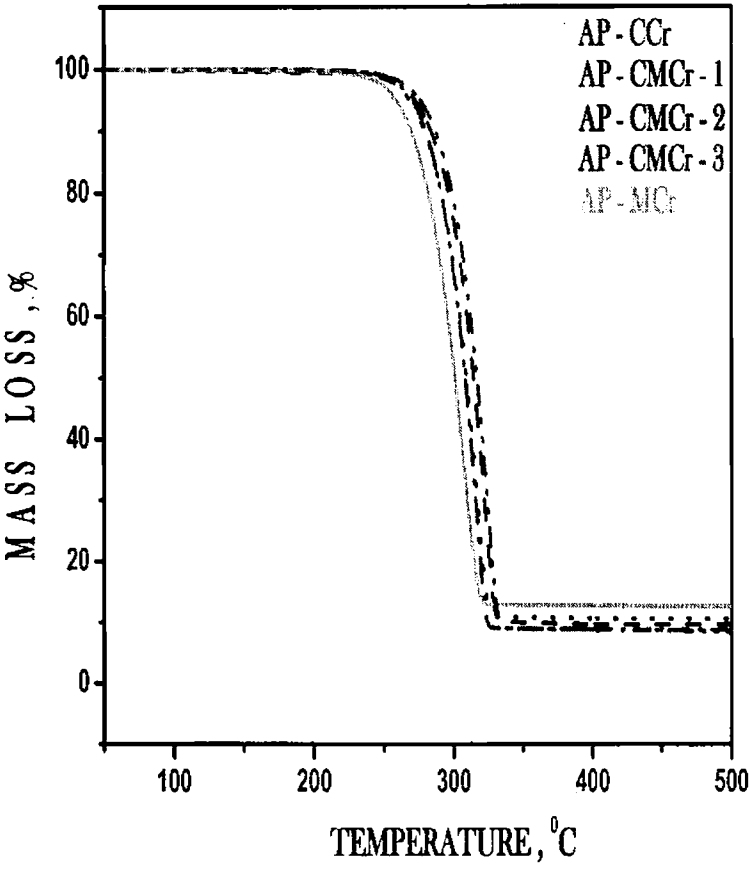

Fig. 4.8.1 TG trace of AP with 1% catalyst

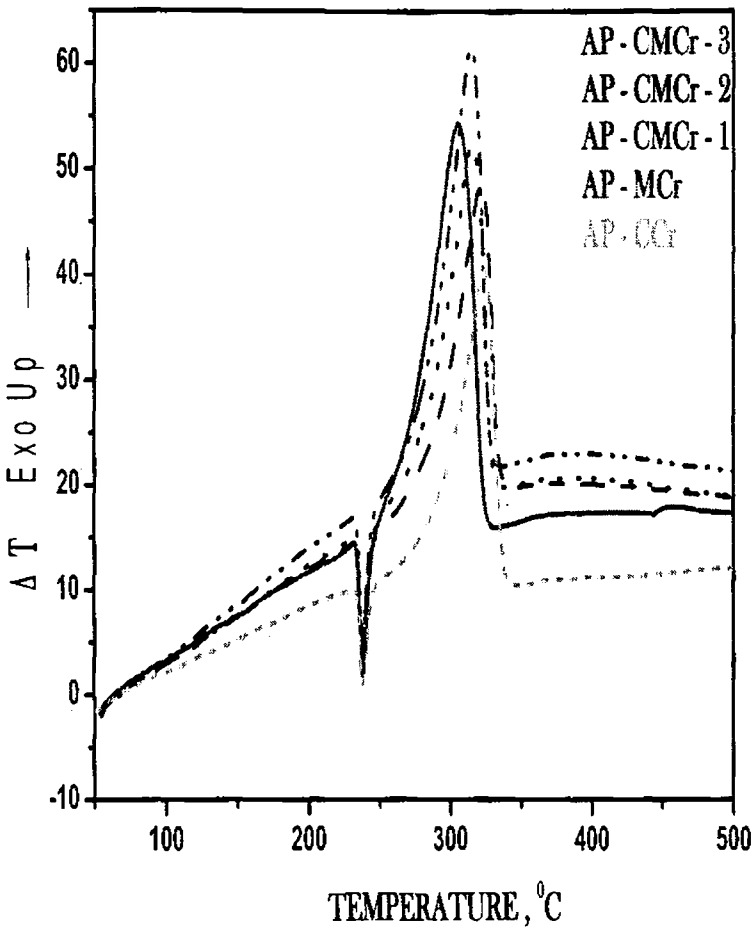

Fig.4.8.2 DTA trace of AP with 1% catalyst

CF and Cu-Fe series are inverse spinel whereas CCr and FCr are normal spinels. Therefore as the chromium is gradually replaced by Fe(III), one gets a gradual transition from a normal spinel to an inverse one. The tetrahedral coordination of the copper is replaced by octahedral, and the copper-oxygen bonds become more ionic [10]. This change in coordination and bond ionicity should alter the physicochemical properties of the spinel, in particular, the catalytic activity. All these additives catalyze the decomposition of the perchlorate, but the performance varies and has a regular relation to the composition. As Cr^{3+} is replaced by Fe^{3+}, there is a rise in the activity until the composition $CuFe_{1.5}Cr_{0.5}O_4$ is reached, after which the performance falls. FCr has the lowest activity among the studied systems.

The increased catalytic activity of CoCr, MCr, Cu-Co and Cu-Mn series, is due to the conversion of the spinel from the cubic form to the tetragonal one, which occurs because the lattice symmetry is reduced.

This study provides alternative choice of good burning rate catalysts for composite solid propellants in solid fuelled rockets.

Table 4.8 TG-DTA summary of the decomposition of AP with and without 1% catalyst.

Sample ID	DTG peak	% Mass loss	DTG peak	% Mass loss	DTA peak		
					Endo	Exothermic	
AP	307	11	370	81	242	-	370
AP-CCr	317	31	339	72	242	325	339
AP-CCoCr-1	-	-	332	75	237	-	330
AP-CCoCr-2	-	-	329	75	237	-	328
AP-CCoCr-3	-	-	315	64	237	-	315
AP-CoCr	-	-	329	94	241	-	324
AP-CFCr-1	-	-	336	78	239	-	330
AP-CFCr-2	-	-	337	78	240	-	331
AP-CFCr-3	-	-	329	72	238	-	328
AP-CF	312	32	338	81	243	319	339
AP-FCr	-	-	354	80	246	-	354
AP-CMCr-1	-	-	323	73	238	-	322
AP-CMCr-2	-	-	317	71	238	-	315
AP-CMCr-3	-	-	316	71	238	-	315
AP-MCr	-	-	306	62	238	-	305
AP-CNCr-1	-	-	329	89	239	-	328
AP-CNCr-2	-	-	319	68	238	-	318
AP-CNCr-3	-	-	316	76	239	-	315
AP-NCr	307	15	351	81	242	326	349

4.9 EFFECT OF SAMPLE MIXING

The samples were mixed physically by grinding AP and 1 % catalyst in a mortar. The sonicated mixture of sample was made by the following procedure. 0.010 g of catalyst was added into 10 mL of ethanol. After sonication for 15 min, the suspension was mixed with 1.0 g of ammonium perchlorate. The new suspension was then sonicated for another 15 min, to achieve a uniform dispersion. Then the sample was dried at vacuum condition. Finally, the powder mixture is ground carefully for 10 minutes and the mixtures were detected by simultaneous TG-DTA , under nitrogen flow of 200 mL/min with a heating rate of 10 °C/min from 50 to 550 °C.

From Table 4.9 we notice that there are two exothermic peaks on DTA curve of pure AP and AP-CF. These two peaks are denoted as low-temperature and high temperature exothermic peaks, respectively. Interestingly, the low-temperature exothermic peak of AP decomposition in the presence of catalysts other than CF (physically mixed) nearly disappeared. However, all of the high-temperature exothermic peaks of AP in the presence of different catalysts shifted to lower temperatures more or less, indicating that catalysts can promote the thermal decomposition of AP. The extent of lowering of exothermic temperature of physically (mechanically) mixed and that mixed by sonication is almost same except for CF and FCr. So sonication can improve the catalytic activity of CF and FCr catalysts to an appreciable extent. We understand that is no need of highly sophisticated techniques to prepare the homogeneously mixed sample. Practically it is difficult too.

Table 4.9 TG-DTA summary of the decomposition of AP and AP mixed with 1% catalyst by different methods.

Sl.No.	Sample ID	Mixing mode	DTA peak			DTG peak	% Weight loss	DTG peak	% Weight loss
			Endothermic	Exothermic					
1	AP	physical	239	321	348	319	28	350	90
2	AP	sonicated	240	-	348	-	-	351	18
5	AP-CCr	physical	238	-	327	-	-	329	75
6	AP-CCr	sonicated	238	-	319	-	-	320	69
7	AP-CoCr	physical	238	-	310	-	-	312	68
8	AP-CoCr	sonicated	238	-	307	-	-	308	74
9	AP- CF	physical	244	312	340	313	29	341	80
10	AP- CF	sonicated	240	-	318	-	-	322	66
11	AP- FCr	physical	245	-	354	-	-	355	83
12	AP- FCr	sonicated	238	-	307	-	-	320	82
13	AP-NCr	physical	238	-	327	-	-	329	60
14	AP-NCr	sonicated	238	-	319	-	-	319	65
15	AP-MCr	physical	238	-	312	-	-	313	60
16	AP-MCr	sonicated	238	-	308	-	-	309	73

4.10 EFFECT OF SIMPLE METAL OXIDES

Thermal decomposition of AP has been extensively studied by taking advantages of the catalytic activities of additives of transition metal oxides and metal powders [11,12].

The catalytic activities of CuO, Cr_2O_3, CoO and MnO crystals in the thermal decomposition of AP (150 μm) were also studied using the Pyris Diamond TG/DTA at a heating rate of 10°C min^{-1} in air atmosphere over the range of 50–550°C in an open platinum crucible. AP and simple metal oxide crystals were mixed at a mass ratio of 99:1 by sonicating to prepare the target

samples for thermal decomposition analyses. A total sample mass of 3 mg was used in all runs.

The decomposition of pure AP is generally centered at temperatures from 270 to 365°C. Addition of 1 % of each of CuO, Cr_2O_3, CoO and MnO, in AP led to a significant reduction of the ending decomposition temperature of AP (Table 4.10). For pure AP, an endothermic peak was observed at about 239°C, which is assigned to the crystallographic transition of AP from orthorhombic to cubic. With increasing the temperatures, AP underwent two complicated decomposition stages, i.e., a low temperature stage at 321°C and a high temperature stage at 348°C, which are followed by two exothermic peaks. All simple metal oxide crystals have no significant impacts on the phase transition of AP. The low-temperature decomposition stage and the high-temperature decomposition stage of AP overlaps and the decomposition temperature reduce to great extend when additives are used. We can see that Cr_2O_3 mainly promotes the decomposition of AP than other simple oxides studied. Simple metal oxides are better catalyst for thermal decomposition of AP but are less stable compared to spinel type mixed metal oxides. Spinel systems have rigid lattice, which makes them less active compared to simple metal oxides. Spinel system have rigid lattice and is amenable for electron exchange. Simple oxides decompose and result in metal formation. They are not reusable.

Table 4.10. TG-DTA data of the decomposition of AP with 1% of simple metal oxide catalyst

Sample ID	DTA Peak		DTG
	Endo	Exothermic	
AP – OXY	239	321 348	319 350
AP – CuO – OXY - SONICATED	238	325	326
AP – Cr_2O_3 – OXY - SONICATED	240	304	306
AP – CoO – OXY - SONICATED	238	311	311
AP – MnO – OXY - SONICATED	238	331	331

4.11 ELECTRICAL CONDUCTIVITY

The semiconducting properties of the simple oxides or their mixtures were found to play a major role in the decomposition of AP [13]. $CuCr_2O_4$ is a tetragonally distorted normal spinel oxide. The tetragonal distortion in this spinel is due to the cooperative Jahn-Teller effect of Cu^{2+} ion on the tetrahedral sites [14]. A number of spinel oxide semiconductors with co-operative Jahn-Teller distortion have been found to exhibit interesting electrical properties near the phase transition temperature [15]. $CuCr_2O_4$, which undergoes a phase transition at 853 K, is a p-type semiconductor in which conduction takes place by the hopping of charge carriers between the octahedral site cations [14] and shows considerable changes in its electrical transport properties near the tetragonal to cubic phase transition temperature [16]. These changes are due to a change in the cation-cation distance during phase transition.

Here, two-probe method was used for the conductivity study. Pellets of

AP and AP mixed with 1% catalyst were kept in the conductivity cell and the corresponding current across the sample was determined. The resistance (R) can be calculated from the value of voltage and current using Ohms law (R=V/I). Once R is known, resistivity (ρ) of the sample can be calculated by the formula, ρ=RA/I, where A is the area of the sample and I is the thickness of the sample. Conductivity measurements of all the systems were measured at room temperature. A voltage of 20V was applied across the pellet. The room temperature conductivity values of all the samples varied between 10^{-7} to 10^{-4} $S.m^{-1}$. This indicated the semi-conducting behaviour of all the compounds under investigation. The electrical conductivity data are collected in Table 4.11. The conductivity is least for pure AP pellet and increased by the addition of catalyst. Conductivity is highest for AP-MCr pellet. The direct correlation between the conductivity and catalyst activity towards thermal decomposition of AP is observed.

Table 4.11. The electron conductivity of pellets of AP and AP mixed with 1 %catalyst.

Sample ID	Conducivity ($S.m^{-1}$)
AP	$6.26*10^{-7}$
AP-CCr	$9.62*10^{-6}$
AP-CCoCr-1	$1.41*10^{-5}$
AP-CCoCr-2	$1.49*10^{-5}$
AP-CCoCr-3	$4.56*10^{-5}$
AP-CoCr	$1.64*10^{-5}$
AP-CFCr-1	$1.41*10^{-5}$

AP-CFCr-2	$1.39*10^{-5}$
AP-CFCr-3	$1.49*10^{-5}$
AP-CF	$9.62*10^{-6}$
AP-FCr	$8.20*10^{-6}$
AP-CMCr-1	$1.72*10^{-5}$
AP-CMCr-2	$4.55*10^{-5}$
AP-CMCr-3	$4.56*10^{-5}$
AP-MCr	$5.30*10^{-4}$
AP-CNCr-1	$1.49*10^{-5}$
AP-CNCr-2	$3.45*10^{-5}$
AP-CNCr-3	$4.55*10^{-5}$
AP-NCr	$8.40*10^{-6}$

4.12 TG-MS

The study of compound decomposition by thermogravimety (TG) can be greatly enhanced when evolved gas analysis is used. This can be achieved by combination of TG with other techniques capable of providing qualitative (evolved-gas detection ± EGD), or both qualitative and quantitative information (evolved-gas analysis ± EGA). It appears that the most popular technique used in combination with TG, is mass spectrometry (MS) on account of its sensitivity, versatility and fast analysis time.

TG-MS is a useful 'hyphenated' technique combining the direct measurement of weight loss as a function of temperature with the use of a

sensitive spectroscopic detector. The TG is coupled to the MS via a heated metal or quartz glass capillary tube. One end of the capillary is positioned close to the sample in the thermo balance. Part of the evolved gases is sucked into the capillary by the vacuum in the MS. The MS repeatedly measures the entire mass spectrum or monitors the intensity of characteristic fragment ions (m/z, the mass-to-charge ratio). TG-MS features are high sensitivity and high resolution, which allow extremely low concentrations of evolved gases to be identified, together with overlapping weight losses that can be interpreted qualitatively. In addition to the weight-loss information, MS permits temporal resolution of the gases that are evolved during thermal decomposition of ammonium perchlorate.

The catalytic activities and the decomposition products of a few representative samples (1%) were tested by TG-MS studies in argon atmosphere at a flow rate of 200mL/min for ammonium perchlorate.

Table 4.12 lists the different gaseous products obtained by the thermal decomposition of pure ammonium perchlorate and in the presence of 1% $CuCr_2O_4$ in argon atmosphere. It also lists the maximum mass spectrometric ion intensity values (*Im/z*). *Im/z* values are normalized to the ion current of H_2O^+, m/z=18, which is most intense among the evolved products. The following gaseous products of AP decomposition in Argon are identified on the basis of these relative *Im/z* values. The relative intensity of decomposition products of pure and catalyzed AP are almost the same.

Table 4.12: Assignments and intensities of the mass spectroscopic ions during the thermal decomposition of AP

Pure AP			AP + 1% $CuCr_2O_4$	
m/z	Assignment	Temperature ranges of peaks	Temperature ranges of peaks	Relative Intensity
1	H^+	300-380	300-380	0.650
14	N^+	300-350	290-350	66.70
16	O^+	290-380	300-380	24.90
18	H_2O^+	280-370	290-370	100.0
30	NO^+	310-400	290-370	8.970
35	Cl^+	350-440	-	3.900
36	HCl^+	-	290-370	0.280
44	N_2O^+	280-350	280-400	4.800
47	HNO_2^+	290-380	290-380	0.060
63	HNO_3^+	270-390	270-390	0.055
65	$NOCl^+$	270-360	270-360	0.059
67	ClO_2^+	300-350	300-350	0.056
71	Cl_2^+	300-350	300-350	0.055
81	$NClO_2^+$	270-380	270-380	0.058
100	$HClO_4^+$	250-390	250-390	0.055

Positive additives like $CuCr_2O_4$ influence both the temperatures at which AP decomposition begins and the extent of the subsequent reaction. At low temperature (< 300 ° C), the principal chlorine-containing product from the decomposition of AP is free chlorine, but with increasing temperature the amount of free chlorine is reduced as the concentration of HCl increases. At lower temperature the concentration of N_2O^+ is high whereas at higher temperatures NO^+ concentration increases tremendously as N_2O^+ is unstable at

higher temperatures.

The decomposition of pure AP proceeds in two steps. At low temperature, the products of thermal decomposition of pure AP are H_2O, N_2O^+ and a small amount of $NClO_2^+$ and $HClO_4^+$. During the high-temperature stage of AP decomposition, HCl^+, H_2O^+, N_2O^+, NO^+, O^+, and a small amount of ClO_2^+, Cl_2^+ are formed. Compared with the decomposition of pure AP, it can be seen that the products are formed in one step during the thermal decomposition of AP in the presence of 1 % of $CuCr_2O_4$. Similar TG-MS results are observed for the mixture of AP with CoCr, MCr, NCr, CF and FCr. A few representative TG-MS trace of AP with 1% CCr is shown in figure 4.12.1-4.12.5.

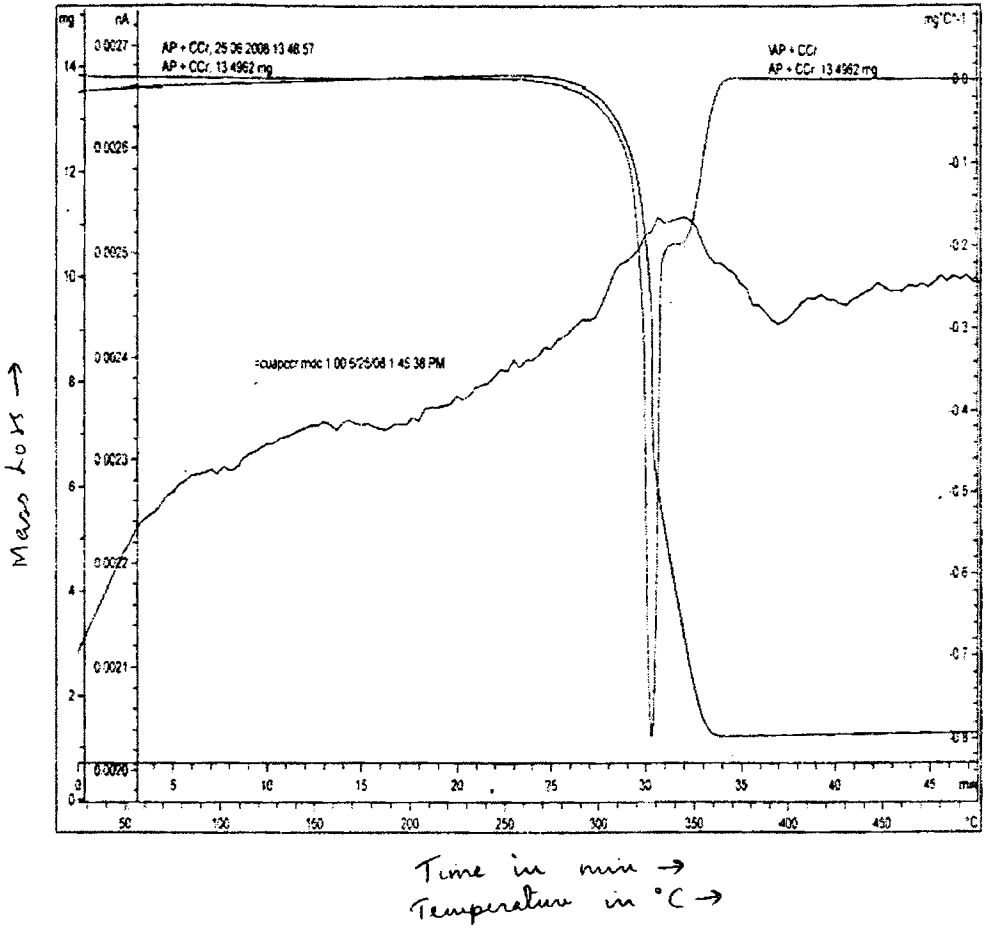

Figure 4.12.1 TG-MS trace of AP with CCr. Mass spectra corresponds to that of H^+ ion.

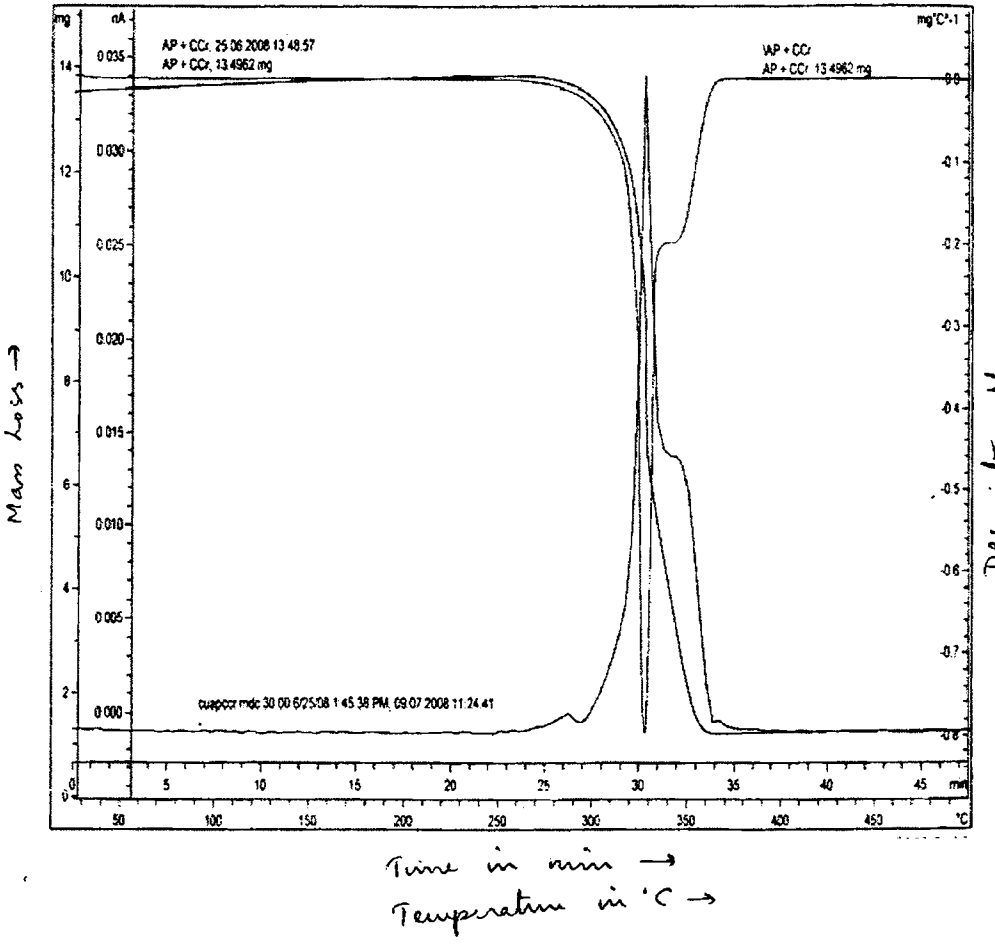

Figure 4.12.2 TG-MS trace of AP with CCr. Mass spectra corresponds to that of NO^+ ion.

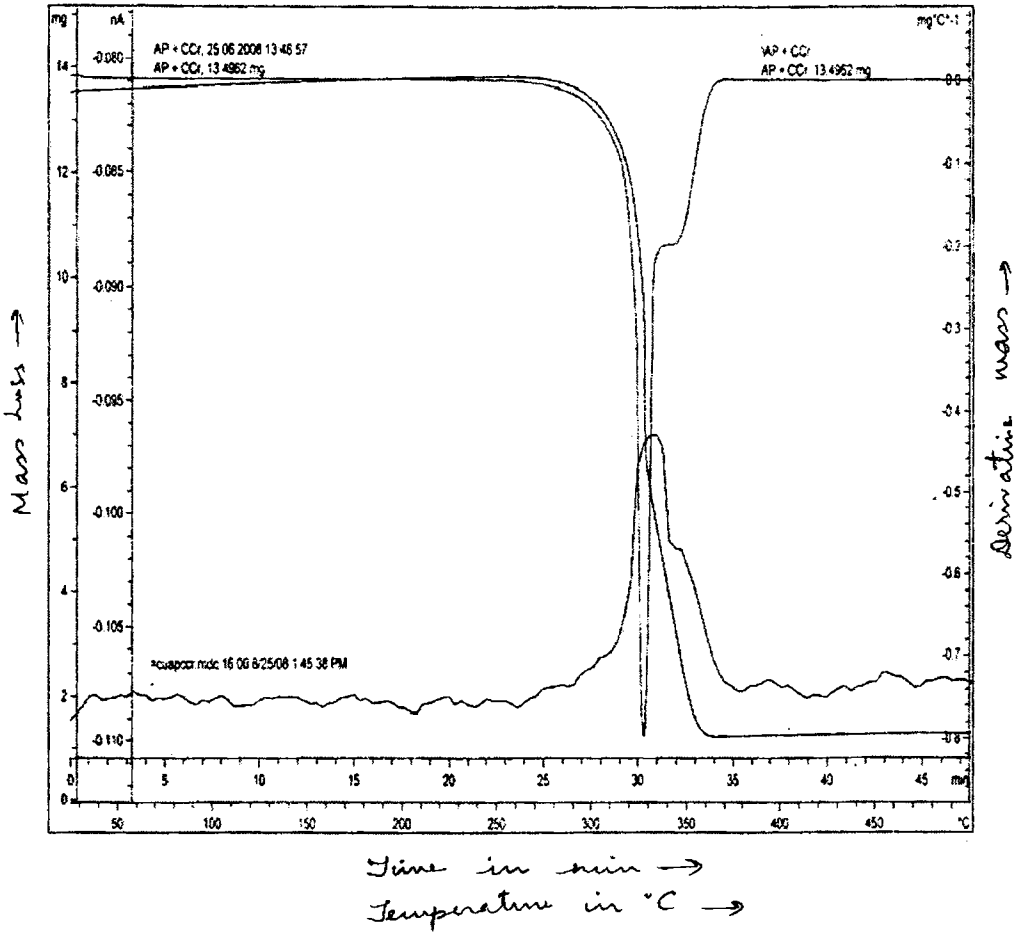

Figure 4.12.3 TG-MS trace of AP with CCr. Mass spectra corresponds to that of O^+ ion.

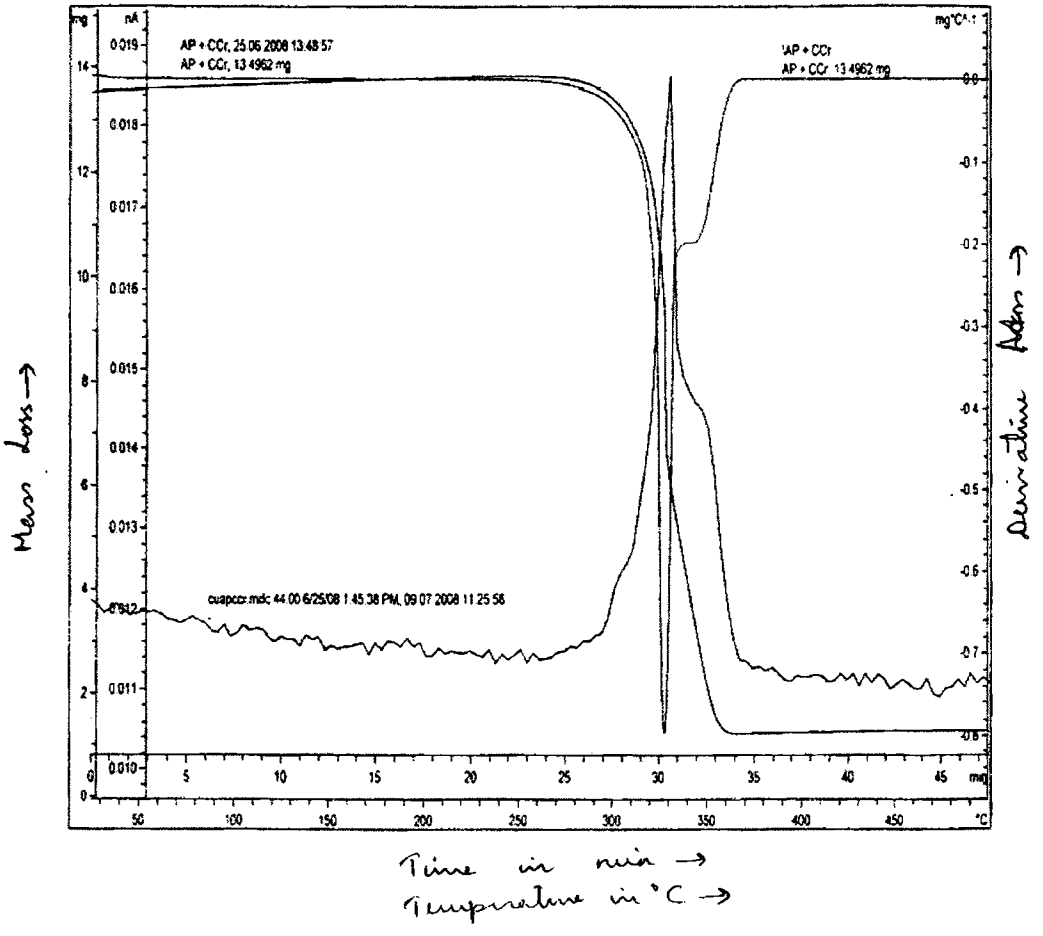

Figure 4.12.4 TG-MS trace of AP with CCr. Mass spectra corresponds to that of N_2O^+ ion.

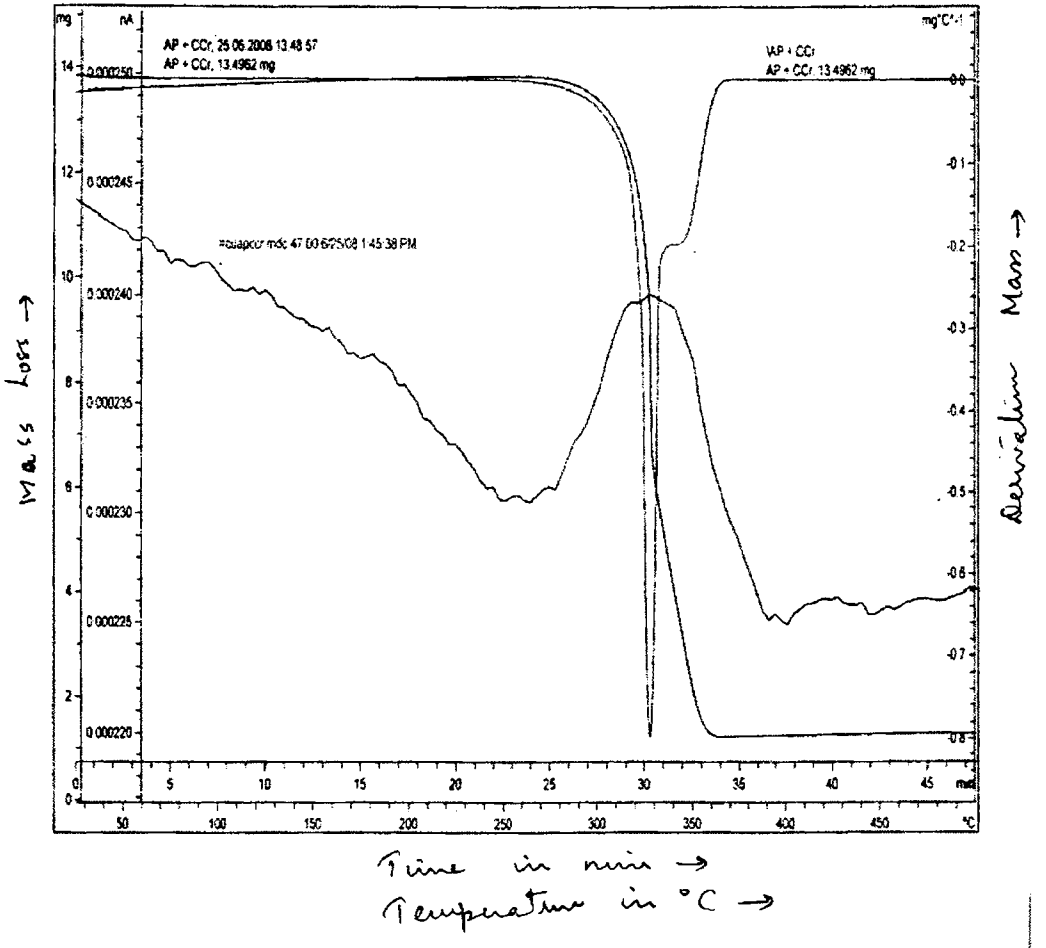

Figure 4.12.5 TG-MS trace of AP with CCr. Mass spectra corresponds to that of HNO_2^+ ion.

4.13 MECHANISM OF DECOMPOSITION OF AP

Our ultimate aim was to deduce, the reaction mechanisms and to determine how decomposition affects combustion phenomena involving AP.

Mechanism of decomposition of pure AP

AP decomposes by a proton transfer mechanism as shown in scheme of equation 4.13.1

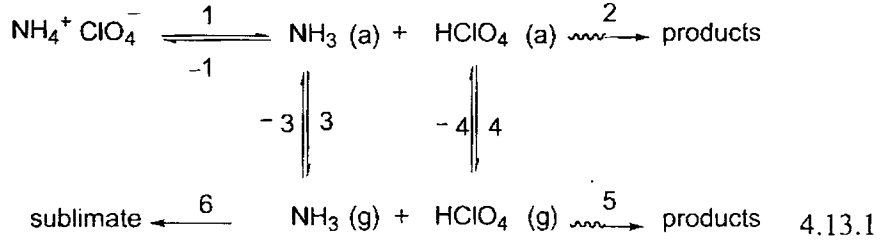

4.13.1

The fundamental step is proton transfer (1), which results in adsorbed ammonia and perchloric acid on the surface of the AP. Since the low temperature decomposition of AP is faster than the vacuum rate of sublimation [17,18], it must therefore involve the adsorbed species NH_3(a) and $HClO_4$(a). Furthermore, thermal decomposition reaction is unaffected by changes in the ambient pressure [17,19], whereas the sublimation process is pressure dependent [18]. These two sets of observations show that the low temperature reaction is initiated on the surface, although it may be completed in the gas phase. Since the reaction is catalyzed by $HClO_4$ and retarded by NH_3, it was

proposed [17,20] that decomposition at low temperatures proceeds *via* the bimolecular reaction of adsorbed perchloric acid molecules (4.13.2) followed by the rapid decomposition of the unstable chlorine oxides to yield O atoms and ClO radicals (4.13.3-4.13.5), which oxidize NH_3 (4.13.6-4.13.10), the reaction commencing in the adsorbed phase.

$2HClO_4(a) \rightarrow H_2O + [ClO_3] + [ClO_4]$ 4.13.2.

$[ClO_4] \rightarrow [ClO_2] + O_2$ 4.13.3

$[ClO_2] + [ClO_2] \rightarrow ClO^{\cdot} + [ClO_3]$ 4.13.4

$[ClO_3] \rightarrow ClO^{\cdot} + O_2$ 4.13.5

$NH_3 + ClO^{\cdot} \rightarrow NH_2^{\cdot} + ClOH$ 4.13.6

$NH_2^{\cdot} + O_2 \rightarrow NO + H_2O$ 4.13.7

$NH_2^{\cdot} + O_2 \rightarrow [HNO] + OH^{\cdot}$ 4.13.8

$2\,[HNO] \rightarrow H_2O + N_2O$ 4.13.9

$NH_2^{\cdot} + NO \rightarrow N_2 + H_2O$ 4.13.10

If the oxidation of ammonia proceeds with less than 100% efficiency, through desorption of the perchloric acid, of the chlorine oxides, or of the radicals performing the oxidation (O, ClO), then NH_3 will accumulate on the surface, thus suppressing the reversible proton-transfer process to the stage where this ceases altogether on an NH_3-covered surface. The failure of the low-temperature reaction to go to completion thus finds a rational basis in this mechanism. As the temperature is raised, desorption of NH_3 occurs, dissociation recommences, and a situation develops in which NH_3, and $HClO_4$

molecules are both desorbing into the gas phase rather than reacting on the surface (see eq 4.13.1). At low ambient pressures they diffuse sufficiently rapidly to get out of the heated zone of the reaction vessel before substantial decomposition of $HClO_4$ can occur. The NH_3 and $HClO_4$ then recombine on any cold surface to complete the sublimation process (step 6 in the reaction scheme represented by eq 4.13.1). As the ambient pressure increases, the rate of diffusion of NH_3, and $HClO_4$ through the gas phase decreases, and their residence time in the reactor is sufficiently long for decomposition of $HClO_4$ followed by oxidation of ammonia to occur.

Mechanism of decomposition of catalyzed AP

Here the decomposition of ammonium perchlorate takes place by the electron transfer mechanism [21]. By this mechanism the rate-determining step is the transfer of the electron of perchlorate ion to ammonium ion,

$NH_4^+ + ClO_4^- \leftrightarrow NH_4^{\cdot} + ClO_4^{\cdot}$ 4.13.11

ammonium and perchlorate radicals being formed.

In catalyzed AP decomposition, the rate-controlling step is the transfer of an electron from the perchlorate ion to the positive hole in p-type semiconducting additives [22-24]. According to our supposition, prepared catalyts promotes this electron transfer, i.e., the formation of radicals, so that on the one hand it embraces the electron of perchlorate by its defect electrons,

$ClO_4^- + {}^{\bullet}(M_{oxide}) \leftrightarrow ClO_4^{\cdot} + (M_{oxide})$ 4.13.12

perchlorate radical (positive hole) being formed, and on the other, it gives one electron to the ammonium ion , forming ammonium radical and a defect electron.

$$NH_4^+ + (M_{oxide}) \leftrightarrow NH_4^{\cdot} + {}^{\bullet}(M_{oxide}) \qquad 4.13.13$$

where ${}^{\bullet}(M_{oxide})$ represents a positive hole in the valence band of the oxide.

Padmanabhan et al [25] reported that $CuCr_2O_4$ is a p-type semiconductor and its conduction is due to charge hopping between the Cr^{3+} and Cr^{4+} ions. The greatest acceleration of reaction may be expected with catalysts having the greatest defect-electron density.

The effect of a metal oxide catalyst on the oxidation of NH_3 is twofold in that the electronic character of the metallic oxide can alter the activity, as well as the selectivity. In general, it appears that the order of increasing catalytic activity is p-type > n-type > insulators. Similarly, the selectivity of the reaction, in terms of N_2O yield, increases with increasing p-type character of the semiconductor.

4.14 POST CHARACTERIZATION OF CATALYSTS BY XRD AND SEM.

The XRD and SEM results of residue from the decomposition of ammonium perchlorate with 1 % catalyst are compared with that of fresh catalysts to understand the changes that happened in bulk and on the surface due to the reaction.

Diffractograms of the fresh and the residual catalysts are shown in Figure 4.14.1 and 4.14.2. The residual catalysts are crystalline and all the peaks are indexed. The 'd' values in both the fresh and residual catalysts are the same. It can be seen that the intensity of the peak turns out to be sharper with residual catalysts compared to that of fresh catalysts. This suggests the growth of the particle size and increase in crystallinity.

No significant changes in the XRD pattern of fresh and residual catalysts are observed. This is observed because the prepared spinel oxides are stable at higher temperature as compared to the simple metal oxides. The results obtained from the XRD of the fresh and residual catalysts are summarized in Table 4.14.1.

Table 4.14.1: XRD parameters of fresh and residual catalysts.

Sample	System	Average Crystallite size (nm)	Experimental data (theoretical)		
			2θ	d_{hkl} (Å)	hkl
CCr	Tetragonal	29.7	35.2 (35.2)	2.55	211
CCr-AP residue	Tetragonal	23.5	35.1(35.2)	2.55	211
CF	Tetragonal	33.9	35.5 (35.5)	2.51	311
CF-AP residue	Tetragonal	29.8	35.7	2.51	311
FCr	Tetragonal	27.3	33.7	2.65	311

FCr-AP residue	Tetragonal	26.6	33.5	2.65	311
MCr	Cubic	20.3	35.4(35.2)	2.68	311
MCr-AP residue	Cubic	28.5	35.5	2.68	311
CoCr	Cubic	10.1	35.7(35.7)	2.52	311
CoCr-AP residue	Cubic	9.4	35.9	2.52	311
NCr	Tetragonal	13.5	36.0 (36.0)	2.65	211
NCr-AP residue	Tetragonal	21.1	36.1	2.65	211

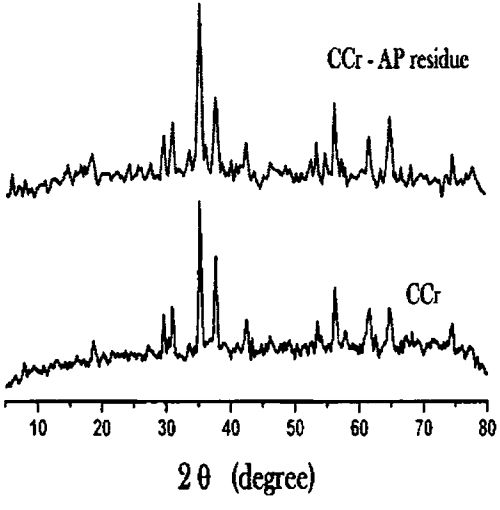

Fig. 4.14.1 XRD pattern of CCr and CCr-AP residue.

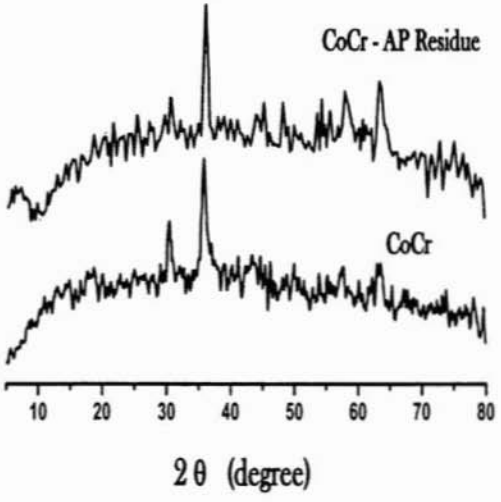

Fig. 4.14.2 XRD pattern of CoCr and CoCr-AP residue.

SEM techniques were used for a visual inspection of the combustion residues. SEM analysis seems to confirm, for the investigated systems and under the operating conditions used, that a decomposition reaction result in agglomeration of the catalysts and also it becomes more porous. According to the SEM microphotographs (Fig. 4.14.3), thermal decomposition commences at the outer crystal surface, yielding the ragged CCr, which surrounds the rest of tetragonal CCr crystal. Some of the surface crystal ruptures as a result of high temperature decomposition and in certain cases sintering take place. Spinel is stable even after decomposition but it becomes more porous. Figure 4.14.3 shows the SEM micrographs of some representative catalysts (fresh and residue).

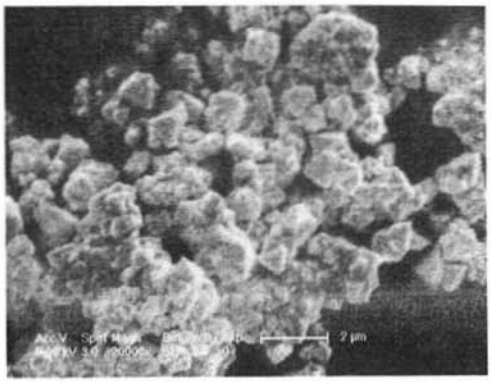

SEM micrograph of fresh CCr

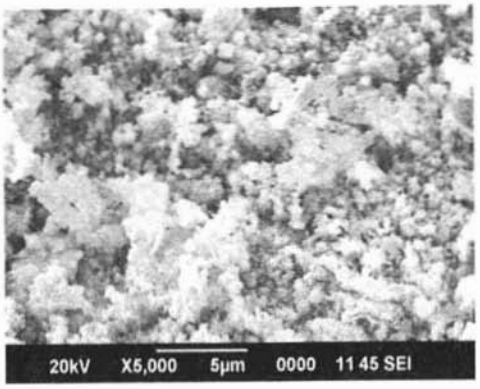

SEM micrograph of residual CCr

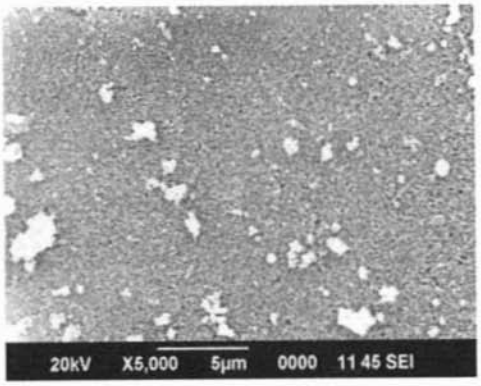

SEM micrograph of residual MCr

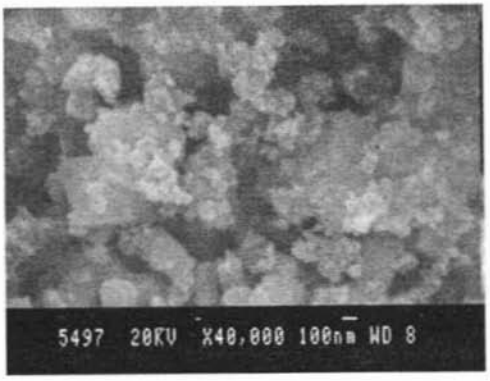

SEM micrograph of fresh MCr

Figure 4.14.3: SEM micrographs of fresh and residual catalysts.

REFERENCES

[1] T. Ganga Devi, M.P. Kannan, B. Hema, Thermochim. Acta 285 (1996) 269.
[2] A.A. Said, R. AI-Qusmi, Thermochim. Acta 275 (1996) 83.
[3] W.A. Rosser, S.H. Inami, Combust. Flame 12 (1968) 427
[4] P.W.M. Jacobsete, Combust. Flame 13 (1969) 419.

[5] T. Hatakeyama, Zhenhai Liu, "Handbook of Thermal Analysis", John Wiley & Sons Ltd, England (1998).

[6] R.C.Mackenzie, "Differential Thermal Analysis" , Vol.1, Academic Press, London (1970).

[7] Sutton, G. P.; Oscar, B. "In Rocket Propulsion Elements"; John Wiley & Sons: New York, 2001; Chapter 12. pp 474–519.

[8] Anuj A. Vargeese, Satyawati. S. Joshi and V. N. Krishnamurthy, *Crystal Growth & Design,* Vol. 8, No. 3, 2008.

[9] A.R. Hall and G.S. Pearson, *Oxidation Combust.* Rev., 3,No.1 (1968).

[10] A.V. Boldyrev *et al.,Fizika Goreniya i Vzryva,*Vol. 11,No. 5, pp 715-720 (1975).

[11] Y. L. Su, S. F. Li and D. H. Ding, *J. Therm. Anal. Cal.*, 86 (2006) 497

[12] J. Zhi, W. Tian-Fang, L. Shu-Fen, Z. Feng-Qi, L. Zi-Ru, Y. Cui-Mei, L. Yang, L. Shang-Wen and Z. Gang-Zhui, *J. Therm. Anal. Cal.*, 85 (2006) 315.

[13] A.A. Said, J.Therm.Anal.,37 (1991) 959.

[14] N. Padmanaban, B.N. Avasthi, and J. Ghose, *J. Solid State Chem.*81,250(1989).

[15] R. Metselaar, R.E.J.Vantol, and P.Piercy, *J. Solid State Chem.*38, 335 (1981).

[16] K.S.De, J.Ghose, and K.S.R.C. Murthy, *J. Solid State Chem.*43, 261 (1982).

[17] J. V. Davies, P. W. M. Jacobs, and A. Russell-Jones, *Trans. Faraday* SOC., 63,1737 (1967).

[18] P. W. M. Jacobs and A. Russell-Jones, *J. Phys. Chem.*, 72, 202 (1968).

[19] V. A. Strunin and G. B. Manelis, *Izv. Akad. Nauk, SSSR, Ser. Khim.*, 2226 (1964); *Bull. Acad. Sei. USSR, Diu. Chem. Sei.*, 2127(1964).

[20] P. W. M. Jacobs and A. Russell-Jones, *AIAA J.*, 5, 829 (1967).

[21] Galwey. A.K, Jacobs. P.W.M., *Proc.Roy.Soc.*(London) A254,455(1960)

[22] E.S.Freeman and A.D. Anderson, *Nature,*(London) 206 (1965)378.

[23] A.A. Said, E.A. Hassan and K.M. Abd El-Salaam, *Surf.Technol.*,20(1983)131.

[24] E.A. Hassan, A.A. Said and K.M. Abd El-Salaam, *Surf.Technol.*,21(1984)117.

[25] N.Padmanabhan, B.N. Avasthi, J.Ghose, *J.Solid State Chem.* 81 (1989) 250

CHAPTER 5

KINETICS OF THERMAL DECOMPOSITION OF AMMONIUM PERCHLORATE

Abstract

Interest in the reaction kinetics of solids was awakened in the early 20th century. At that time, the basic techniques known today as differential thermal analysis (DTA), thermogravimetry (TG) and evolved gas analysis (EGA) were developed. The earliest kinetic studies were performed under isothermal conditions. While non-isothermal methods were used to follow the reaction rates in solids, the results of these studies were not used for kinetic evaluations until the 1930s. The kinetic analysis of solid-state reactions from experimental thermoanalytical (TA) data recorded under non-isothermal conditions became very popular from the earlier proposals by Kissinger, Freeman and Carroll, Coats and Redfern, and Zako of formal kinetic equations to be used for this purpose. The popularity of the non-isothermal methods with regard to the isothermal ones rests on the assumption that the reaction kinetic parameters can be determined from a single non-isothermal experiment while isothermal methods require a set of experiments at different temperatures. The kinetics is usually followed either by weight loss or by pressure measurements.

5.1 INTRODCUTION

Many methods have been developed for studying solid-state kinetic data. These methods can be classified according to the experimental conditions selected and the mathematical analysis performed. Experimentally, either isothermal or non-isothermal methods are employed. The mathematical approaches employed can be divided into model-fitting and iso-conversional (model free) methods. Model-fitting methods were among the first and most popular methods to be used in evaluating solid-state kinetics, especially for non-isothermal experiments. Results obtained from different mathematical analysis methods have been viewed as conflicting rather than complimentary. Selection of the best model for experimental data is problematic because a statistical fit parameter (i.e., r^2) may be quite high for a number of fitted models [1]. The kinetic triplet (A, E_a and model) is essential for accurate kinetic description of any solid-state reaction since the reaction rate expression requires all the three .If only one or two of the triplet is known, an incomplete kinetic picture is generated [2-4].

The advantages of determining kinetic parameters by non-isothermal methods rather than by conventional isothermal studies are [5] (a) that considerable fewer data are required; (b) that the kinetics can be calculated over an entire temperature range in a continuous manner; (c) that when a sample undergoes considerable reaction in being raised to the required temperature, the results obtained by an isothermal method are often questionable; and (d) that only a single sample is required.

The kinetics of the thermal decomposition of the cubic ammonium perchlorate (AP) has been extensively studied. The reported effective activation energies vary from about 37 to 260 kJ mol^{-1} [6,7]. The mechanistic interpretation of the values is also different. The confusing character of the kinetic information is not surprising for the process that is known [8] to be a tangled interplay of various chemical (solid-state decomposition, reaction of gaseous products with the solid, gas-phase reactions) and physical (diffusion, sublimation, adsorption-desorption) processes. The effective activation energy of the thermal decomposition of AP is a composite value determined by the activation energies of these processes as well as by their relative contributions into the overall decomposition rate. If these processes have different activation energies, the effective activation energy shows a variation with the temperature. The kinetics of such multi-step processes cannot be characterized by a single constant value of the activation energy. The earlier kinetic evaluations of the activation energies of the thermal decomposition of AP were based on the assumption of constant activation energy.

The non-isothermal thermogravimetry with a linear temperature ramp is a convenient technique for studying the kinetics of processes involving solids, such as decomposition and gas-solid reactions, by following the mass loss of the samples with time/temperature [9].

5.2 THERMAL EXPERIMENTS

The decomposition reactions in nitrogen (of flow rate 200mL/min) were made with a Perkin Elmer Pyris Diamond TG/DTA model thermal analysis system. TG apparatus was calibrated via the melting points of indium (156°C) and tin (231°C) under the same conditions as for the sample. During the experiments, the weight loss (TG signal) and the rate of weight loss (DTG signal) as a function of time or temperature were recorded, while the samples (AP and AP mixed with 1% catalyst physically) were subjected to a computer-controlled temperature program. Approximately 3 mg of the sample was placed with a standard platinum crucible in the DTA cell. The decomposition reactions were investigated in the temperature range of 50 -550°C with a heating rate of 10°C/min.

5.3 KINETIC ANALYSIS

For the mathematical analysis, the TG-DTG data were preferred to the DTA-DSC data because the energy change manifestation sin these cases are rather complex, and the ΔT and ΔH values obtained are merely net values (depending on which step (endothermic or exothermic) dominates). Further the TG-DTG is intrinsically simpler as they relate to mass changes.

A full kinetic analysis of a solid-state reaction has at least three major stages:

1. experimental collection of data
2. computation of kinetic parameters using the data from stage 1.

3. prediction of the reaction progress for required temperature profiles applying determined kinetic parameters.

Using experimental DTG measurements performed on the examined samples (stage 1) Origin software determines kinetic characteristics of the reaction (stage 2). The calculated kinetic parameters are subsequently employed to predict the reaction progress of the investigated samples under any given temperature mode (stage 3).

5.4 RESULTS AND DISCUSSION.

The kinetic analyses of the TG-DTG data were carried out using a non-mechanistic (Coats-Redfern equation) and nine mechanistic equations.

The non-mechanistic employed is:

(1) The Coats-Redfern (CR) [10] equation

$$CR = \ln [g(\alpha)/T^2] = \ln [(AR/\varphi E)(1-2RT/E)]-E/RT$$

where T is the temperature in K, A is the pre-exponential factor, φ is the heating rate in °C/min, E is the energy of activation and R is the gas constant. In the above equations, the g (α) term for n=1 is defined as

$$g(\alpha) = [\, 1-(1-\alpha)^{1-n}]/(1-n)$$

where $\alpha = m_t/m_\infty$ and n is the order parameter; m_t is the mass loss at time t and m_∞ is the mass loss at the completion of the reaction in TG experiments. A graph is plotted between ln $[g(\alpha)/T^2]$ and 1/T. The slope of the resultant straight line is –E/R. The intercept of the line is ln (AR/φE). So from slope and intercept we get the value of A and E. It has been stated that only n values of 0, 1/3, 2/3, 1, and 2 have any chemical basis and hence rate laws are examined for the values of these n. Some workers also include the value of 1/2 in the list of possible values.

The mechanistic equations used are based on g (α) values corresponding to different mechanism for solid-state reactions, as listed in Table 5.4.1.

Table 5.4.1 Mechanism based equations

Equation	Form of g (α)	Rate controlling process
I	α^2	One-dimensional diffusion (D1)
II	$\alpha+(1-\alpha)\ln(1-\alpha)$	Two-dimensional diffusion (D2)
III	$[1-(1-\alpha)^{1/3}]^2$	Three-dimensional diffusion, spherical symmetry; Jander equation (D3)
IV	$(1-2/3\ \alpha)-(1-\alpha)^{2/3}$	Three-dimensional diffusion, spherical symmetry; Ginstling-Brounshtein equation (D4)
V	$-\ln(1-\alpha)$	Random nucleation; one nucleus on each particle; Mampel equation (first order) (F1)

VI	$[-\ln(1-\alpha)]^{1/2}$	Random nucleation; one nucleus on each particle; Avrami equation I (A2)
VII	$[-\ln(1-\alpha)]^{1/3}$	Random nucleation; one nucleus on each particle; Avrami equation II (A3)
VIII	$1-(1-\alpha)^{1/2}$	Phase boundary reaction, cylindrical symmetry (R2)
IX	$1-(1-\alpha)^{1/3}$	Phase boundary reaction, spherical symmetry (R3)

Kinetic parameters from non-mechanistic equation are listed in Table 5.4.2. Table 5.4.3 presents the kinetic parameters evaluated from mechanistic based equations. The kinetic parameters are calculated for all the exothermic decomposition stages. Of the nine mechanistic equations examined, the equation that gives kinetic plots with the highest linearity (highest coefficients) is used to calculate the kinetic parameters. The kinetic parameters calculated for mechanistic equation V show closest agreement with those evaluated from non-mechanistic equation. Therefore, the rate controlling process would be a random nucleation; one nucleus on each particle (Mampel equation-first order). Nuclei may be present initially or they may grow in at certain locations by a process that is usually considered to be first-order.

The activation energy obtained from both the mechanistic and non-mechanistic equation (Table 5.4.2 and 5.4.3) is found to vary catalytic activity of the system. The activation energy of pure AP calculated using non-mechanistic equation is found to be 580 kJ mol^{-1} and that of the mixture (AP-

catalyst) is found to be in the range 558 -173 kJ mol $^{-1}$. AP-MCr mixture shows the minimum activation energy (173 kJ mol $^{-1}$) and also MCr reduces the decomposition temperature to the greatest extent. No such correlation is obtained from the frequency factor. The problem of interpretation of experimentally determined Arrhenius parameters is often associated with the problem of applicability of the Arrhenius equation in solid-state kinetics [11]. A practical problem in the interpretation of experimentally determined values of E and A does exist, and it lies in the very nature of the experiments. Standard experimental techniques (TG, DTA) as well as more sophisticated methods [12,13] generally do not allow the isolation of elementary reactions. Rather, they provide a global measure of the rate or extent of a process that usually involves several steps with different activation energies. For this reason, experimentally derived Arrhenius parameters of a solid-state process must be interpreted as effective values unless mechanistic conclusions can be justified by ancillary data.

Table 5.4.2 Kinetic parameters for the decomposition of catalysed and uncatalysed AP using non-mechanistic equation from TG data.

Sample ID	DTG peak	% Mass loss	Order (n)	E / kJ mol^{-1}	A / s^{-1}	DTG peak	% Mass loss	Order (n)	E / kJ mol^{-1}	A / s^{-1}
AP	307	11	1	157	$7.0*10^{10}$	370	81	1	580	$2.1*10^{46}$
AP-CCr	317	31	1	292	$1.1*10^{24}$	339	72	1	558	$3.0*10^{46}$
AP-CCoCr-1	-	-	-	-	-	332	75	1	240	$2.1*10^{19}$
AP-CCoCr-2	-	-	-	-	-	329	75	1	241	$5.3*10^{19}$
AP-CCoCr-3	-	-	-	-	-	315	64	1	237	$3.2*10^{19}$
AP-CoCr	-	-	-	-	-	329	94	1	234	$1.4*10^{19}$
AP-CFCr-1	-	-	-	-	-	336	78	1	240	$2.3*10^{19}$
AP-CFCr-2	-	-	-	-	-	337	78	1	244	$7.2*10^{19}$
AP-CFCr-3	-	-	-	-	-	329	72	1	252	$2.9*10^{20}$
AP-CF	312	32	1	444	$1.7*10^{39}$	338	81	1	283	$1.6*10^{23}$
AP-FCr	-	-	-	-	-	354	80	1	190	$2.3*10^{14}$
AP-CMCr-1	-	-	-	-	-	323	73	1	180	$1.9*10^{14}$
AP-CMCr-2	-	-	-	-	-	317	71	1	178	$3.0*10^{14}$
AP-CMCr-3	-	-	-	-	-	316	71	1	174	$1.0*10^{14}$
AP-MCr	-	-	-	-	-	306	62	1	173	$1.1*10^{14}$
AP-CNCr-1	-	-	-	-	-	329	89	1	360	$1.2*10^{27}$
AP-CNCr-2	-	-	-	-	-	319	68	1	357	$3.0*10^{27}$
AP-CNCr-3	-	-	-	-	-	316	76	1	350	$2.8*10^{27}$
AP-NCr	307	15	1	292	$2.2*10^{24}$	351	81	1	346	$4.7*10^{27}$

Table 5.4.3 Kinetic parameters for the decomposition of catalysed and uncatalysed AP using mechanistic equations from TG data.

Sample ID	DTG peak	% Mass loss	Order (n)	E / kJ mol^{-1}	A / s^{-1}	DTG peak	% Mass loss	Order (n)	E / kJ mol^{-1}	A / s^{-1}
AP	307	11	1	157	$7.4*10^{10}$	370	81	1	586	$2.8*10^{46}$
AP-CCr	317	31	1	292	$1.5*10^{24}$	339	72	1	562	$3.5*10^{46}$
AP-CCoCr-1	-	-	-	-	-	332	75	1	244	$2.8*10^{19}$
AP-CCoCr-2	-	-	-	-	-	329	75	1	243	$5.7*10^{19}$
AP-CCoCr-3	-	-	-	-	-	315	64	1	240	$3.6*10^{19}$
AP-CoCr	-	-	-	-	-	329	94	1	236	$1.2*10^{19}$
AP-CFCr-1	-	-	-	-	-	336	78	1	242	$2.6*10^{19}$
AP-CFCr-2	-	-	-	-	-	337	78	1	247	$7.0*10^{19}$
AP-CFCr-3	-	-	-	-	-	329	72	1	253	$2.8*10^{20}$
AP-CF	312	32	1	450	$1.5*10^{39}$	338	81	1	282	$1.5*10^{23}$
AP-FCr	-	-	-	-	-	354	80	1	194	$2.3*10^{14}$
AP-CMCr-1	-	-	-	-	-	323	73	1	182	$1.8*10^{14}$
AP-CMCr-2	-	-	-	-	-	317	71	1	181	$3.2*10^{14}$
AP-CMCr-3	-	-	-	-	-	316	71	1	176	$1.2*10^{14}$
AP-MCr	-	-	-	-	-	306	62	1	172	$1.0*10^{14}$
AP-CNCr-1	-	-	-	-	-	329	89	1	362	$1.4*10^{27}$
AP-CNCr-2	-	-	-	-	-	319	68	1	360	$3.2*10^{27}$
AP-CNCr-3	-	-	-	-	-	316	76	1	356	$2.8*10^{27}$
AP-NCr	307	15	1	294	$2.4*10^{24}$	351	81	1	350	$5.1*10^{27}$

The way in which the analysis is performed is to determine a series of values for the fraction of the reaction complete, α, at a series of temperatures,

T. Then the functions represented by the left-hand side of the equation are computed for each pair of (α, T) values for various values of n. The values for the functions are then plotted against 1/T, and the series that gives the most nearly linear plot is presumed to correspond to the ' 'correct' ' reaction index, n. Table 5.4.4 shows values of α and T for AP decomposition reaction. In keeping with the usual practice, n values of 0, 1/3, 2/3, 1, and 2 were chosen, and the values calculated for the functions when these values were used are also shown in Table 5.4.4. In this decomposition reaction, the best fit is provided when n=1, so the index of reaction is 1.

Figure 5.4.4 shows plots of the values of the functions versus 1/T. As can be seen from the figure, the line corresponding to n=1 provides the best fit to the data (highest correlation coefficient and minimum standard error – Table 5.4.5). Of course, that is the value used to generate the α values at different temperatures, so it should provide the best fit.

While this procedure may certainly give an ' 'optimum' ' value of n with respect to the linearity of the f (α, T) versus 1=T plot, the ' 'order' ' determined may have no relationship to the molecularity of a transition state in the usual kinetic sense. The n value is usually called the index of reaction. In most cases, the results obtained from this type of analysis are similar to the kinetic parameter determined by conventional isothermal means, and in many cases the agreement is excellent.

Table.5.4.4. Values of α and f (α) for various trial values of n.

T (K)	$10^3/T$	α	n=0	n=1/3	n=1/2	n=2/3	n=1	n=2
548	1.825	0.000	-	-	-	-	-	-
558	1.792	0.004	-18.29	-18.29	-18.29	-18.29	-18.29	-18.29
568	1.760	0.011	-17.23	-17.23	-17.23	-17.23	-17.23	-17.22
578	1.730	0.023	-16.50	-16.49	-16.49	-16.49	-16.48	-16.47
588	1.700	0.043	-15.89	-15.88	-15.88	-15.88	-15.87	-15.85
598	1.672	0.069	-15.46	-15.45	-15.44	-15.44	-15.43	-15.39
608	1.644	0.101	-15.11	-15.10	-15.09	-15.08	-15.06	-15.01
618	1.618	0.141	-14.81	-14.78	-14.77	-14.76	-14.73	-14.66
628	1.592	0.204	-14.48	-14.44	-14.42	-14.40	-14.36	-14.25
638	1.567	0.295	-14.14	-14.08	-14.05	-14.02	-13.97	-13.79
648	1.543	0.390	-13.89	-13.81	-13.77	-13.73	-13.65	-13.40
658	1.520	0.505	-13.66	-13.56	-13.50	-13.44	-13.33	-12.958
668	1.497	0.642	-13.45	-13.31	-13.23	-13.15	-12.98	-12.42
678	1.475	0.785	-13.28	-13.08	-12.97	-12.85	-12.61	-11.74
688	1.453	0.926	-13.14	-12.86	-12.69	-12.51	-12.11	-10.54
698	1.432	1	-13.10	-12.70	-12.40	-11.99	-	-

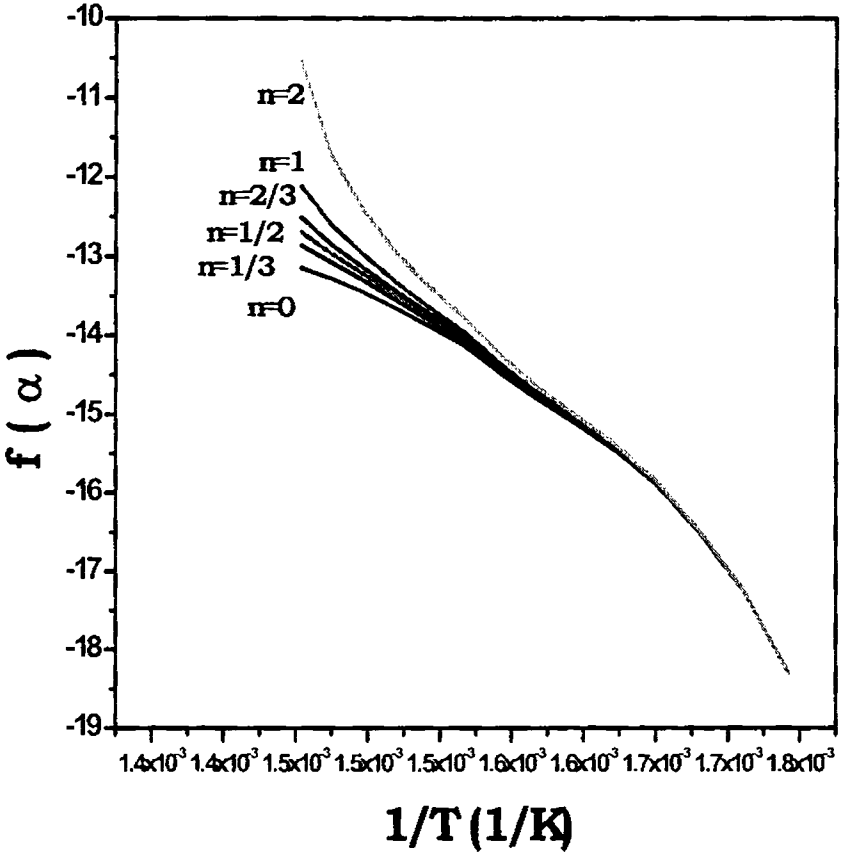

Figure.5.4.4 Coats and Redfern analysis of AP decomposition reaction for which n=1.

Table. 5.4.5 Variation in standard error and correlation coefficient for AP with different values of n (Coats-Redfern model).

n	Correlation coefficient	Standard error
0	0.978	0.340
1/3	0.984	0.305
1/2	0.986	0.286
2/3	0.989	0.268
1	0.992	0.240
2	0.989	0.334

As we cannot represent the reaction rate in terms of concentrations, we must use some other approach. For reactions in the solid state, the fraction of the sample reacted, α, is frequently chosen as the reaction variable. It should be apparent that if α is the fraction of the sample reacted, $(1 - \alpha)$ is the fraction of the sample that has not reacted. The rate of the reaction may be expressed as being equal to $d\alpha/dt$, and the reaction has gone to completion when $\alpha = 1$.

Table 5.4.6. Values of α as a function of time for a reaction following a first order rate law (AP and AP-MCr decomposition).

AP-bulk		AP-MCr	
Time (min)	α	Time (min)	α
23.6	0.000	22.1	0.000

24.6	0.004	22.5	0.025
25.6	0.011	23.0	0.060
26.5	0.023	23.4	0.102
27.5	0.043	23.9	0.158
28.4	0.069	24.3	0.225
29.4	0.101	24.7	0.311
30.3	0.141	25.1	0.411
31.3	0.204	25.6	0.534
32.2	0.295	26.0	0.666
33.2	0.390	26.5	0.811
34.2	0.505	27.1	0.935
35.2	0.642	27.7	1
36.1	0.785		
37.1	0.926		
38.2	1		

Having a set of (α, t) data available, a graph was prepared to illustrate the type of plot that can be expected when a reaction follows a first order rate law. The result is shown in Figure 5.4.6, and the sigmoidal curve is characteristic of a reaction that follows a nucleation rate law. For reactions in the solid state, sigmoidal plots are more likely to indicate that some type of nucleation process controls the reaction.

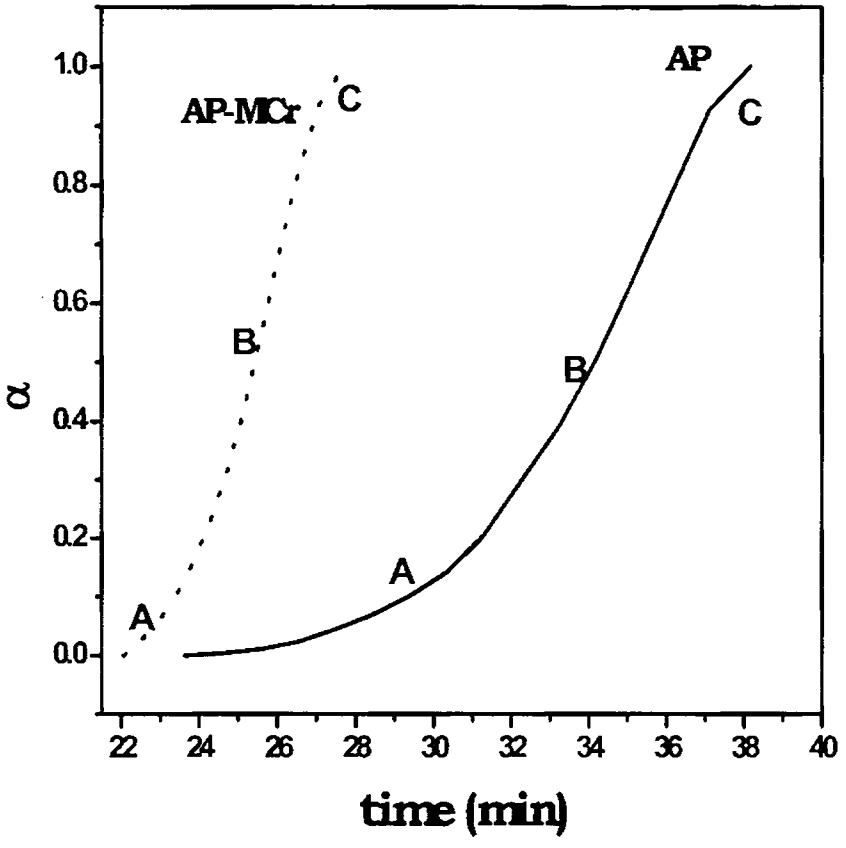

Fig. 5.4.7. A plot of α versus time for the data shown in Table 5.4.4

The region of the curve (Fig.5.4.5) labeled as A represents an induction period where the rate is beginning to accelerate. MCr shortens the length of the induction period that precedes decomposition. The region of the curve represented as B corresponds to the part of the reaction where it is progressing

at the maximum rate. For most reactions in the gas phase or in solution, the initial rate is the maximum rate because that is the time when the concentration of the reactant is highest. However, many reactions in solids do not begin at the maximum rate. The reaction may proceed from particular sites (usually referred to as active sites or nuclei), and these may require some time to become fully developed. Region C is called the decay region, and it represents a stage where the reaction is starting to slow down markedly as the reaction approaches completion. A reaction that takes place in the solid phase may never actually progress to $\alpha = 1$ for several reasons. First, the retention of a gaseous product in the reactant or solid product can occur. Retention is regarded as the adsorption (or chemisorption) of a volatile product by the solid. Because of the nature of the forces between particles that make up the solid (depending on the solid, they may be atoms, molecules, or ions), there is a tendency for a given amount of material to be arranged so as to give a minimum surface area. When heated, particles in a solid become more mobile and may rearrange to give a smaller surface area by forming rounded corners and edges. This process, known as sintering, tends to increase the likelihood of retention of volatile products because the surface area becomes smaller thus hindering the escape of a volatile product. Also, cracks, pores, and other imperfections in the crystal tend to be annealed out to produce a more compact and regular structure, which also hinders the escape of a gas. The coalescence of particles due to sintering is not a factor in all reactions involving solids, but it may be important in certain cases [14].

Critical Review

Physical meaning of activation energies in solid-state reactions:

- Solid state kinetics are completely described by g(α), A and E (kinetic triple), in a strict sense activation energies can only be compared if the other two parameters are coincidently equal.

- E has been observed to vary with α in solid-state reactions (change of reactivity, complex mechanism).

- E of isothermal and non-isothermal experiments are usually not in agreement for solid state reactions.

If carefully used and complemented with other techniques the analysis of solid-state kinetics can give indications on the reaction mechanism and yields valuable information on the reactivity that can be very helpful for the development of preparative strategies.

REFERENCES

[1] S. Vyazovkin, C.A. Wight, *J.Phys.Chem.A.*,101 (1997) 8279.

[2] Macienjewski.M, Reller.A, *Thermochim.Acta,* 110 (1987) 145.

[3] Macienjewski.M, *Thermochim.Acta,* 355 (2000) 145.

[4] Sewry. J.D.,Brown. M.E., *Thermochim.Acta,* 390 (2002) 217.

[5] Duval .C, "Inorganic Thermogravimetric Analysis", 2nd ed., Elsevier, Amsterdam (1963).

[6] Brill, T. B.; Brush, P. J.; Patil, D. G. *Combust. Flame* 1993, 94, 70.

[7] Kishore, K; Pai Verneker, V. R.; Krishna Mohan, V. *Thermochim. Acta* 1975, 13, 277

[8] Jacobs, P. W. M.; Whitehead, H. M. *Chem. Rev.* 1969, 69, 551.

[9] S. Vyazovkin, C.A. Wight, *Thermochim.Acta*, 340-341, 53-68 (1999).

[10] A.W. Coats and J.P.Redfern, Nature, 201 (1964)68.

[11] Sergey Vyazovkin, Charles. A. Wight, *International Reviews in Physical Chemistry,*Vol.17, No.3 (1998) 407-433.

[12] Delmon. B, *Introdition a la Cinetique Heterogene,* Paris:Editions Technip. (1969).

[13] Barret. P, *Cinetique Heterogene,* Paris: Gauthier-Villars (1973).

[14] James E. House, "Principles of Chemical Kinetics", 2nd ed., Elsevier, Amsterdam (2007).

CHAPTER 6

SUMMARY AND CONCLUSION

The various conclusions drawn based on the work are summarized in this chapter.

Chapter 1 presents a general introduction to catalysis and various types of catalysis. It mainly describes the published literature on the structure, preparation and catalytic aspects of spinels with special emphasize on chromites. The necessity of using XPS being a surface science technique in catalysis is described. The role played by spinel catalyst in thermal decomposition of ammonium perchlorate is described. This chapter provides important foundation materials for the next four chapters.

Chapter 2 describes the procedure for the syntheses of various composition of the $CuCr_{2-x}Fe_xO_4$ (x=0.5,1.0,1.5,2.0) and $Cu_{1-x}M_xCr_2O_4$ (M is a transition metal cation like Ni, Co, Mn and x=0,0.25,0.5,0.75 and 1.0) were prepared by sol-gel thermolysis method and the various instrumental techniques adopted for the characterization of all the catalysts prepared. This method is technically simpler, more effective and more time and energy efficient than other techniques in terms of the application of the catalysts. Theory and experimental procedure for each technique is described briefly under the respective technique.

Chapter 3 described in detail the results of various characterization methods applied for the surface as well as bulk characterization. The spinel phase formation at the calcinations temperature 550°C has been ascertained by the XRD data. The crystalline size characterized from the XRD broadening is in the range 10 – 34 nm. The XRD patterns show that the spinel powders are pure and crystalline in nature. Crystallize sizes roughly below 100 nm can accurately be evaluated using powder diffraction techniques. The stoichiometries of the compositions checked by the XRF and EDX analysis were found to be in good agreement with the theoretical values. TEM analysis confirms the nano nature of the samples. Most nanoparticles are very small, in the range of 5-16 nm. The selected area for electron diffraction pattern has many widen rings made up of many diffraction spots which indicate the relatively wide size distribution of nanoparticles prepared by sol-gel thermolyzed method. The spinel chromites prepared by sol-gel thermolysis method possess sufficiently large surface area except in the case of CF. The spinel phase formation is further confirmed by the appearance of two strong infrared bands ν_1 and ν_2 below 1000 cm^{-1}. XPS data suggests that Cu, Ni, Co and Mn are in +2 oxidation state and Cr and Fe are in +3 oxidation state. Oxygen shows -2 oxidation states. The tetragonal distortion for the NCr and Cu-Ni chromites is due to the simultaneous influence of A-site Ni^{2+} ions (spin-orbit coupling) and tetrahedral Cu^{2+} ions (the Jahn-Teller effect). Thermal analysis, TGA/DTA was confirmed the thermal stability. Surface morphology was collected on scanning electron microscope. Information regarding the coordination and oxidation state of the prepared catalysts metal ions is

obtained from UV-vis DRS. The desorption studies of pyridine adsorbed samples well supported the NH_3-TPD results.

Chapter 4: The nanometric metal oxide particles have been proved effective to improve the decomposition of ammonium perchlorate a key energetic material and the most common oxidizer in the rocket propellant. The thermal decomposition of ammonium perchlorate occurs in two processes: the endothermic process and the exothermic process. The endothermic process of all the catalyzed and uncatalyzed AP occurs at about 240°C. The exothermic process of AP-bulk completes in three steps (320, 361 and 411°C) while that of AP-150μm completes in a step (350°C). The exothermic process of AP catalyzed by CCr, CF and NCr completes in two steps and rest of the catalysts enables the AP exothermic process to complete in a step. The exothermic temperature is reduced in presence of catalysts. Among the metal chromites, MCr showed significant activity. During the exothermic process, the exothermic decomposition temperature of AP with CoCr contents of 1%, 2%, 3%, 4% and 5% are 334,327,326,323 and 317°C respectively. As the content of CoCr increases, its catalytic activity reaches to maximum. As the heating rate increased, the exothermic peak shifted toward higher temperatures.

Morphology-controlled AP particles were synthesized by using a water-soluble PVA polymer as a crystal-habit modifier. Although the exact mechanism of the nucleation and growth control of the crystals is not clear, the observed formation of rectangular wedge shaped particles of AP in PVA matrices with different concentrations may be attributed to the steric control exerted by the

PVA matrix and the adsorption of the hydroxyl group onto the growing faces of the AP crystals. Decomposition has found to be more effective for ammonium perchlorate of rectangular wedge shape.

As the oxygen balance of ammonium perchlorate is found to be high (+34) the furnace atmosphere has little significance in the decomposition. The transport studies revealed that the different series of chromites are semiconductors. The particle size of AP does not any effect on the reaction pathway.

The overlap in thermal decomposition traces can result in large variations of the activation energy with the extent of conversion. Altering the experimental conditions of the measurements like heating rates can influence the degree of overlap and thus, the dependence of the activation energy on the extent of conversion. The use of slow heating rates allows one to narrow the temperature range of a non-isothermal experiment.

The catalysts are found to be a mixed conductor; the total conductivity involves both electronic and ionic conductivity terms, due to the presence of holes and oxygen vacancies. The conductivity mechanism can be attributed to the hopping of p-type small polarons. In addition, the conductivity measurement revealed that the maximum conductivity is for AP-MCr pellet, which is in accordance with the activity of the catalyst towards thermal decomposition of AP. The changes in the electronic structure of the catalyst would affect the catalyzed decomposition. The building in of foreign ions in

simple metal oxides, largely affects the electronic structure and hence the conductivity of it.

Combining with associated literature, we proposed the probably catalytic mechanism of the prepared spinel oxides on the AP thermal decomposition. There are lattice defects in the as-burnt catalysts, and many positive holes and electrons exist in it. In the decomposition process of AP, the prepared catalysts provide a bridge for the transfer of electrons from the perchlorate ions to the ammonium ions. The catalysts promote the transfer of electrons, which makes the activation energy of thermal decomposition of AP reduced, so the decomposition of temperature of AP depresses and the decomposition rate of AP accelerates. When the content of catalyst exceeds an optimum amount, the positive hole and electrons emerge partial annihilation, so the catalytic activity depresses. The uncatalysed decomposition of AP proceeds by proton transfer mechanism. The physical characterization of decomposition product of the investigated process was analyzed by the SEM and X-ray diffraction experiments.

Chapter 5: Kinetics of solid-solid reactions are much more complicated if reactants are polycrystalline. The activation energy was calculated in KJ/mol for the decomposition of pure and catalyzed AP using Coats-Redfern method. AP-MCr is found to have low activation energy calculated using both the methods.

AP is found to have high activation energy calculated using this method. Since high decomposition activation energy is associated with high thermal stability,

AP is considered to be more thermally stable than catalyzed AP. The decomposition reactions followed first order reaction kinetics. The activation energy and frequency factor obtained by fitting non-isothermal kinetic data depend strongly on the model to which the data are fitted.

With all of the features that may be exhibited in a reaction of a solid, it should not be surprising that it is frequently observed that no one rate law will describe the entire course of the reaction. Furthermore, it should come as no surprise to find that the rate laws often appear to have mathematical forms that are quite different from those that successfully describe gas and solution phase reactions. Although a large body of information and well-established principles exist, the study of reactions in solids is still largely an empirical science. Common features between reactions are often found, but many reactions in solids are often highly individualistic.

Chapter 6 illustrates the summary, conclusion and future outlook of the present thesis work.

6.1 FUTURE OUTLOOK

ISRO's Polar Satellite Launch Vehicle (PSLV-C11) was chosen for launching Chandrayaan-1 spacecraft into space. The first and third stages as well as the strap-ons of PSLV use solid propellants (fuel-oxidiser combination). Whereas, it's second and fourth stage use liquid propellants. The solid propellant stages and strap-ons of PSLV use aluminium powder as fuel, HTPB as fuel binder, ammonium perchlorate as the oxidizer and copper chromite as burning rate catalyst. So the significance of AP and the burning rate catalyst remains same or increases. Ammonium Dinitramide (AND) is an energetic material, which is a potential replacement for AP in composite propellants. Since ADN does not contain chlorine, a composite rocket propellant containing ADN and a polymer binder will produce minimal smoke, and will be more environmentally friendly compared with propellants based on AP. However, there are some drawbacks: ADN is relatively shock sensitive, and is also sensitive to light and moisture. The problem is how to get the material pure enough and how to stabilize it in storage. In addition, ADN is detonable, even as a propellant mixture. That is certainly a risk, especially with large rockets. Further research is needed to overcome these drawbacks of eco-friendly ADN. Extensive studies can be made in field of ADN chemistry and the potential use of the prepared catalysts can be done.

PAPERS PRESENTED IN INTERNATIONAL/NATIONAL CONFERENCES

1. Bolie Therattil and S. Sugunan, "Thermal decomposition of ammonium perchlorate based mixture with metal oxides", MATCON 2010 - International Conference on Materials for the Millennium by Applied Chemistry Department, CUSAT (11-13 January 2010, Cochin).

2. Bolie Therattil and S. Sugunan, "Thermal decomposition studies of sonicated metal oxide-ammonium perchlorate mixtures", Indian Analytical Science Congress 2009 on Analytical Science for Industrial Development and Technological Progress by Indian Society of Analytical Scientists (12-13 November 2009, Lonavala).

3. Bolie Therattil and S. Sugunan, "Evolved gas analysis of catalytic decomposition of ammonium perchlorate using TG-MS", The Workshop on Applications of Mass Spectrometry and Related Hyphenated Techniques in Analytical Science by Indian Society of Analytical Scientists (25 April 2009, Cochin, Kerala).

4. Bolie Therattil and S. Sugunan, "Synthesis of nano-copper chromites and evaluation of their catalytic activity in thermal decomposition of ammonium perchlorate, National Conference on Advances in Physical and Theoretical Chemsitry (APTChem -2009) by Department of Chemistry, Calicut University (19-20 March 2009, Calicut, Kerala).

5. Bolie Therattil and S. Sugunan, "Thermal Decomposition of Ammonium Perchlorate Using Nano Copper Chromite Catalyst" The International Conference on Materials for the Millenium (MatCon 2007, March 1-3, 2007), Department of Applied Chemistry, Cochin University of Science and Technology, Cochin-22, India.

6. Bolie Therattil and S. Sugunan, "Catalytic Thermal Decomposition Studies of Modified Ammonium Perchlorate", 19th National Symposium on Catalysis, Catalysis for Sustainable Energy and Chemical (CATSYPM -19, January 18-21, 2009) NCL,Pune.

7. Bolie Therattil and S. Sugunan, "Thermal Decomposition Studies of Modified Ammonium Perchlorate and Manganese Chromite" 2nd International Symposium on Advanced Materials and Polymers for Aerospace and Defense Application (SAMPADA-2008, December 8-12,2008), Yashada MD Center,Pune.

8. Bolie Therattil and S. Sugunan, "Synthesis, Characterization and Thermal Activity Studies of Nano-$MnCr_2O_4$", Indian Analytical Science Congress 2008: Analytical Sciences for Sustainable Development (November 21-23, 2008, ISAS, Munnar).

9. Bolie Therattil and S. Sugunan, "The Thermal Decomposition of Ammonium Perchlorate by Cobalt- Chromium Oxides", National Workshop on Catalysis (CATWORKSHOP-2008, February 18-20, 2008) IMMT, Bhubaneswar).

10. Bolie Therattil and S. Sugunan, "Catalytic Thermal Decomposition Studies of Ammonium Perchlorate" DAE-BRNS 16th National Symposium and Workshop (THERMANS 2008, February 4-8, 2008), Indira Ghandhi Centre for Atomic Research Kalpakkam, India).

11. Bolie Therattil and S. Sugunan, "Effect of Particle Size on Thermal Decomposition of Ammonium Perchlorate", CTRIC 2008, Cochin University of Science and Technology, Cochin.

12. Bolie Therattil and S. Sugunan, "Nickel Modified Copper Chromite – A Better Catalyst in Ammonium Perchlorate Based Rocket Propellants", International Conference on Advanced Materials and Composites (ICAMC-2007, October 24-26,2007), Trivandrum.

13. Bolie Therattil and S. Sugunan, "Synthesis and Characterization of Copper Chromite prepared from Modified Sol-Gel Method", Catalysis for Future Fuels: 18th National Symposium and Indo-US Seminar on Catalysis (April 16-18, 2007, IIP, Dehradun).

14. Bolie Therattil and S. Sugunan, "Nano-Copper Chromite Systems of High Surface Area and Porosity –A Better Catalyst", CMET, March 2007, Thrissur.

15. Bolie Therattil and S. Sugunan, "Role of Chromites in the Thermal Decomposition of Ammonium Perchlorate", 5th National Symposium and Conference on Solid State Chemistry and Allied Areas (ISCAS-2007, November 16-18, 2007, Nagpur).

16. Bolie Therattil and S. Sugunan, "Homogeneous Copper Chromite Preparation by Modified Sol-Gel Process", National Conference in Chemistry, Central College, Bangalore (September 27-29, 2006).

17. Bolie Therattil and S. Sugunan, National Conference on Women Scientists/Technocrats Challenges and Opportunities, (June 2006, Cochin-22).

WORKSHOPS/CONEFERNCES/PRE-SCHOOLS ATTENDED

1. "Seminar on Spectroscopy" organized by Dept. of Chemistry, St. Paul's College, Kalamassery and co-sponsored by M.G. University, Kottayam on 20th May 2009.

2. "The User Awareness Programme on Access to E-resources" under the UGC INFONET Digital Library Consortium organized by the INFLIBNET and CUSAT in association with Kerala Library Association, Ernakulam region at CUSAT on 21st April, 2009.

3. TA Instruments: Material Characterisation by Thermal, Rheology and Microcalorimeters, Taj Residency, Ernakulam.

4. "Women in Science: A Career in Science" an initiative of Indian Academy of Sciences: Women in Science conducted in CUSAT on 5th April, 2008.

5. "Workshop on Thermal Analysis (THERMANS-2008)" held in Indhira Gandhi Centre for Atomic Research Kalpakkam, February 7-8, 2008.

6. Tutorial on "Temperature Programmed Techniques (TPX) in Catalysis", February 15-16, 2008 at IMMT, Bhubaneswar.

7. Pre-conference school on "X-ray Spectroscopic Techniques in Catalysis", January 16-17, 2009, NCL, Pune.

8. "Nanomaterials Technology, Characterisation and Application (Nanomaterials 2006)", December 9, 2006, ISAS Kochi Chapter, Cochin.

9. "National Workshop on Catalysis", February 8-10, 2007, (Catalysis Society of India), Bangalore Institute of Technology, Bangalore.

10. "National Conference on Emerging Trends in the Application of Plasma in Materials Science and Technology 2007 (APIMSAT-07)", December 7-8, 2007, ISAS Kochi Chapter, Cochin.

11. "National Conference on the Role of Analytical Chemistry in Materials Science and Technology (ACIMSAT-2006)", April 30-May1, 2006, ISAS, Munnar.

12. "Orientation Programme for Research Scholars in Catalysis", November 17-December 7, 2006, National Centre for Catalysis Research (NCCR), IIT, Madras.

AWARDS

1. Best Poster Award – Consolation Prize in the 2nd International Symposium on Advanced Materials and Polymers for Aerospace and Defense Applications (SAMPADA-2008), 8-12th December 2008 at Yashada MD Center, Pune.

2. Best Paper Award in Indian Analytical Science Congress 2008 (Theme: Analytical Sciences for Sustainable Development) held at Munnar, Kerala during 21-23rd November 2008.

3. Hindustan Platinum Award for the Best Poster presentation in the CATWORKSHOP 2008 held at the Institute of Minerals and Materials Technology, Bhubaneswar during February 18-20, 2008.